INTEGRATED DEPOSITIONAL MODEL AND HYDROCARBON POTENTIAL OF DISTAL RAMP DEPOSITS, AGRIO FORMATION, NEUQUÉN BASIN, ARGENTINA

by

Shawn A. Moore

A thesis submitted to the faculty of
The University of Utah
in partial fulfillment of the requirements for the degree of

Master of Science

in

Geology

Department of Geology and Geophysics

The University of Utah

August 2018

The University of Utah Graduate School

STATEMENT OF THESIS APPROVAL

The thesis of **Shawn A. Moore**

has been approved by the following supervisory committee members:

Lauren Birgenheier	, Chair	**04-25-2018** Date Approved
Kathleen Ritterbush	, Member	**04-13-2018** Date Approved
Matthias Greb	, Member	**04-02-2018** Date Approved

and by **Thure E. Cerling** , Chair of

the Department of **Geology and Geophysics**

and by David B. Kieda, Dean of The Graduate School.

ABSTRACT

The mudstone-dominated Early Cretaceous Agrio Formation is the youngest marine source rock interval of the hydrocarbon prolific Neuquén Basin, Argentina, yet its unconventional hydrocarbon potential remains relatively understudied. A northern section of the entire Agrio Formation and a southern composite section of the lower Pilmatué and middle Avilé Members, totaling ~1,200 m of outcrop, were measured. From these measured sections, programmed pyrolysis, X-ray diffraction (XRD), and thin section analyses were conducted on subsets of 441 samples and a high-resolution facies scheme and depositional model were established. The facies scheme and depositional model indicate distinctly more dynamic sedimentation in the substorm wave base, basinal to outer ramp portion, of this homoclinal ramp than previously described.

Characterization of such heterogeneity allows for recognition of stratigraphic packaging and correlative relationships with established updip stratigraphy. Utilizing TOC, S2, and HI value cutoffs, this study identifies discrete stratigraphic packages totaling ~140 m thick within the upper Agua de la Mula and lower Pilmatué Members with the highest source rock potential. Based on regional correlation, source intervals within the Pilmatué Member lie within Retrogradational to Aggradational Parasequence Sets. This study provides a novel integration of macro and microfacies analysis, stratigraphy, and a geochemical analysis to define a new offshore depositional model and source potential of the Agrio Formation. The model presented here provides an analog for

carbonate-dominated mudstone successions of interest as unconventional reservoirs worldwide.

TABLE OF CONTENTS

LIST OF TABLES

Tables

LIST OF FIGURES

Figures

ACKNOWLEDGMENTS

Sponsorship for this project was provided by Shell. I would like to thank Daniel Minisini, Fernando Sanchez-Ferrer, Pedram Zarian, and Orlando Ortega from Shell for their discussions. I thank Adolfo Giusiano, the director, Minister of the Hydrocarbon Secretariat of Neuquén Province, Argentina for sharing his expertise on the Neuquén basin and the Agrio Formation, as well as helping the authors design and carry out a field campaign. David Thul, Maísa Tunik, Julieta Omarini, Alex Koch, and Jessica Page were also key to the successful field work carried out for this project. I thank Chris Carlson, Clay Jones, and Joe Moore for allowing us to use the Energy and Geoscience Institute (EGI) XRD lab and for quantifying the XRD data. Dhrupad Beti performed critical quality control on programmed pyrolysis data and helped oversee use of the HAWK at EGI. Matthias Greb provided key incites for the geochemical portions of this work. David Watkins, University of Nebraska-Lincoln, provided key identifications and descriptions of nannofossil species. Additional student research grants were received to support the study from the Society for Sedimentary Geology (SEPM) Foundation Research Grant (2014, S.A. Moore), and the American Association of Petroleum Geologists (AAPG) Grants-in-Aid Harry and Joy Jamison Named Grant (2014, S.A. Moore). I would especially like to thank my advisor Lauren Birgenheier.

INTRODUCTION

Unconventional hydrocarbon resources are projected to account for 60% of total U.S. crude oil production and two thirds of total U.S. natural gas production by 2040, largely due to production from shale plays (U.S. EIA 2017). A basic, early understanding of unconventional plays purports that, in contrast to conventional plays, the source, reservoir and seal rock are synonymous and defined within the same stratigraphic interval. However, a closer inspection at the bed or even pore scale indicates that hydrocarbon generation should be considered separately from hydrocarbon storage and production in unconventional systems. For instance, many leading carbonate-rich unconventional plays, including the Eagleford and Niobrara, display organic-rich intervals with source rock or hydrocarbon generation potential as well as reservoir intervals that display increased porosity and permeability, and/or brittle behavior conducive to hydraulic fracturing and production (Sonnenberg 2011; Taylor and Sonnenberg 2013; Breyer 2016).

In contrast to previous models that depict mud-dominated systems as recording quiet depositional conditions with mud settling slowly out of suspension, these systems are now considered to be current-dominated with a broad range of sedimentation rates and more variable energy conditions (Bhattacharya and MacEachern 2009; Schieber and Yawar 2009; Macquaker et al. 2010a; Zeller et al. 2015; Schieber 2016). Along with this change in sedimentation style, there has been an accompanying change in our

understanding of the stratigraphy of mudstone-dominated formations: from internally homogenous and laterally extensive to heterogeneous with internally complex stratigraphic stacking patterns that lend to lateral facies changes (Macquaker et al. 2007). This complex variability in sedimentary geologic characteristics and composition both laterally and vertically poses technical challenges in effectively developing unconventional resources through hydraulic fracturing. High resolution offshore facies models that consider the dynamic nature of mudstone deposition and diagnose depositional mechanisms along with their resultant products in the sedimentary record are only recently emerging in the literature (e.g., Kietzmann et al. 2014, 2016; Zeller et al. 2015; Birgenheier et al. 2017; Comerio et al. 2018; Schwarz et al. 2018). Furthermore, sedimentary and organic geochemical investigations of unconventional systems have developed in parallel, and most organic geochemical investigations lack a detailed and sedimentary context and vice versa (Nawratil et al. 2012; Kietzmann et al. 2014; Stinco and Barredo 2014). Proper detailed geologic characterization considering geochemical proxies for source quality and geomechanical analyses to categorize reservoir quality and brittleness, within a facies and stratigraphic context, is essential to predicting favorable response to hydraulic fracturing and prioritizing zones for responsible and more sustainable development. The former of which, source quality, is addressed herein. The Agrio Formation is an ideal field area in which to conduct a detailed, integrated sedimentologic, stratigraphic and organic geochemical study due to the availability of thick, well-exposed mudstone deposits, the combination of which are unique for mudstone-dominated successions.

Despite the importance of the Agrio Formation as one of three marine source

rocks within the Neuquén Basin, the unconventional hydrocarbon potential of this unit remains relatively understudied. Though extensive biostratigraphic, sedimentary, and stratigraphic studies have been performed on the formation, there has been little integration of these analyses with multiproxy geochemical and geomechanical assessments. It is well established that the Agrio Formation represents a marine ramp environment with siliciclastic deposits dominating in the southern Neuquén region and carbonate sediments dominating in the northern Mendoza area (Legarreta and Uliana 1991, 1999; Sagasti 2002, 2005; Lazo et al. 2005). Previous studies indicate that throughout the basin the upper and lower members of the Agrio formation record shoreface to basinal deposits within an open marine ramp (Legarreta and Uliana 1991, 1999; Spalletti et al. 2001a, 2001b; Lazo et al. 2005; Lazo 2006, 2007a, 2007b). Older more general stratigraphic studies and several more recent sedimentary facies studies (e.g., Spalletti et al. 2011; Comerio et al. 2018; Schwarz et al. 2018) provide a comprehensive description of the current facies models for the Agrio Formation throughout the Neuquén Basin, based largely on studies located between 30 and 75 km south of this study's southernmost locality. In this study, we focus on describing in more detail the facies specifically present in the more distal carbonate-rich portion of the Neuquén province. This distal, northern portion of the basin is also where the highest potential organic richness is predicted (Legarreta and Uliana 1991; Uliana and Legarreta 1993; Cruz et al. 1996; Kozlowsky et al. 1998; Uliana et al. 1999). The most distal facies within the Agrio Formation are underrepresented in many facies studies and are usually described as interbedded shales, marls, and limestones (Spalletti et al. 2001a, 2001b; Lazo et al. 2005; Spalletti et al. 2011). Due to high variability in the descriptions used for

fine-grained sedimentary rocks between various studies, these terms can be problematic and do not best capture the heterogeneity of these deposits.

The goals of this study are (1) categorize facies variability in the distal portion of the Agrio system by integrating macrofacies, microfacies, and geochemical analyses, (2) utilize this understanding of facies heterogeneity to define a depositional model that recognizes the complexities inherent in dynamic distal marine environments and mixed carbonate-siliciclastic ramp systems with lateral shoreline variability, (3) utilize this high-resolution depositional environment assessment to define stratigraphic stacking patterns and relate them to updip stratigraphy to the south established by Schwarz et al. (2018), and (4) establish the source rock potential of these distal deposits within the context of facies and depositional models and stratigraphic framework. These are important steps in developing a working model that better informs the play prospectivity of the unconventional Agrio Formation. Establishing the relationship between depositional environment and source, reservoir, and seal characteristics at a high resolution will provide valuable input data for modeling the subsurface behavior of the Agrio Formation. More broadly, this study provides an integrated method of defining depositional models and hydrocarbon potential that is analogous to carbonate-dominated mudstone successions of interest worldwide, particularly those of Mesozoic age.

GEOLOGIC BACKGROUND AND STUDY AREA

The retroarc Neuquén Basin (35-39°S lat. to 69-70°W long.) was initiated as a rift basin and is the thickest rift fill of a linked system of northwest-southeast trending extensional basins in west-central Argentina (Urien et al. 1995; Aguirre-Urreta et al. 1999; Ramos and Folguera 2005) (Fig. 1a). From the Early Jurassic through the Early Cretaceous, the basin was characterized by widespread protracted thermal subsidence related to marine plate subduction below the western margin of Gondwana. During this time fluctuations in relative sea-level resulted in the deposition of marine and continental, carbonate, siliciclastic, and evaporitic deposits. By the Early Cretaceous, continued thermal subsidence lead to marine inundation, transforming a preexisting Late Triassic to Early Jurassic intraplate extensional half graben into the 120,000 km^2 marine embayment in which the Agrio Formation was deposited (Fig. 2). This embayment is described as triangular in shape with a low-gradient depositional surface and a shallow water depositional environment (Legarreta and Gulisano 1989; Legarreta and Uliana 1991, 1999; Lazo et al. 2008). Sedimentation during the Late Jurassic and Early Cretaceous was affected by widespread transgressive-regressive cycles of varying magnitude, which were the result of a combination of eustatic oscillations and, to a lesser extent, tectonic factors such as local uplift and changes in subsidence rates (Legarreta and Uliana 1991; Vergani et al. 1995). Subduction led to the formation of a magmatic arc, which bordered the western margin of the basin where the embayment connected to the proto-Pacific Ocean

(Fig. 2). From the Late Cretaceous to the Cenozoic, acceleration of plate convergence along the western margin of South America resulted in compression and uplift within the Neuquén Basin, closing the embayment. Throughout the basin's formation, its expansion was limited to the northeast by the Sierra Pintada System and to the south by the North Patagonia Massif (Vergani et al. 1995; Howell et al. 2005; Ramos and Folguera 2005).

The Agrio Formation is part of a large Mesozoic sedimentary cycle known as the Ándico Cycle supersequence and makes up the majority of the middle and upper Mendoza Group mesosequences (Legarreta and Gulisano 1989) (Fig. 3). The Early Cretaceous Agrio Formation was deposited over a maximum of ~10 Ma from 136 to 126 Ma (Aguirre-Urreta et al. 1999; Sagasti and Ballent 2002) and is the youngest of the three main source rocks of the Neuquén Basin. The remaining two are the Early-Middle Jurassic Los Molles Formation and the Late Jurassic Vaca Muerta Formation, the latter of which is the most prolific hydrocarbon source rock in the basin (Villar et al. 1998; Legarreta et al. 2005; Legarreta and Villar 2012). The underlying contact of the Agrio Formation with the terrigenous Mulichinco Formation is gradational, but the base of the first thick marine black shale unit is typically taken to mark the diachronous lithostratigraphic contact between the two formations (Aguirre-Urreta and Rawson 1997). The Agrio Formation is unconformably overlain by the siliciclastic and evaporitic beds of the Huitrín Formation, which mark the end of marine influenced sedimentation in the Neuquén Basin during the Barremian (Urien et al. 1995; Aguirre-Urreta et al. 1999). There are three members identified within the Agrio Formation. The lower Pilmatué Member and upper Agua de la Mula Member, formally named by Leanza et al. (2001), are generally associated with accumulation during transgressive periods in a slowly

subsiding marine ramp environment, and the central Avilé Member, named by Weaver (1931), is associated with a sudden rapid regression that occurred in the mid-Hauterivian (Legarreta and Gulisano 1989; Legarreta and Uliana 1991; Spalletti et al. 2011).

In general, during the deposition of the Agrio Formation, the Neuquén Basin was dominated by coastal to lower shoreface siliciclastic deposits in the southern to southeastern portions of the basin with a complex carbonate and siliciclastic shoreline forming the eastern margin of the basin (Legarreta and Uliana 1991, 1999; Sagasti 2002, 2005; Lazo et al. 2005; Spalletti et al. 2011) (Fig. 2). Distal marine deposits were restricted to the central and northwestern portions of the basin (Sagasti 2005; Spalletti et al. 2011). The study area of this work is located near Chos Malal (Fig. 1a, b) where the most distal carbonate-rich deposits of the Pilmatué and Agua de la Mula Members with the highest predicted organic richness are found within the Neuquén province (Legarreta and Uliana 1991; Uliana and Legarreta 1993; Uliana et al. 1999; Sagasti 2005; Spalletti et al. 2011; Aguirre-Urreta et al. 2017). The Avilé Member is fairly well studied in this area (Rossi 2001; Veiga et al. 2011).

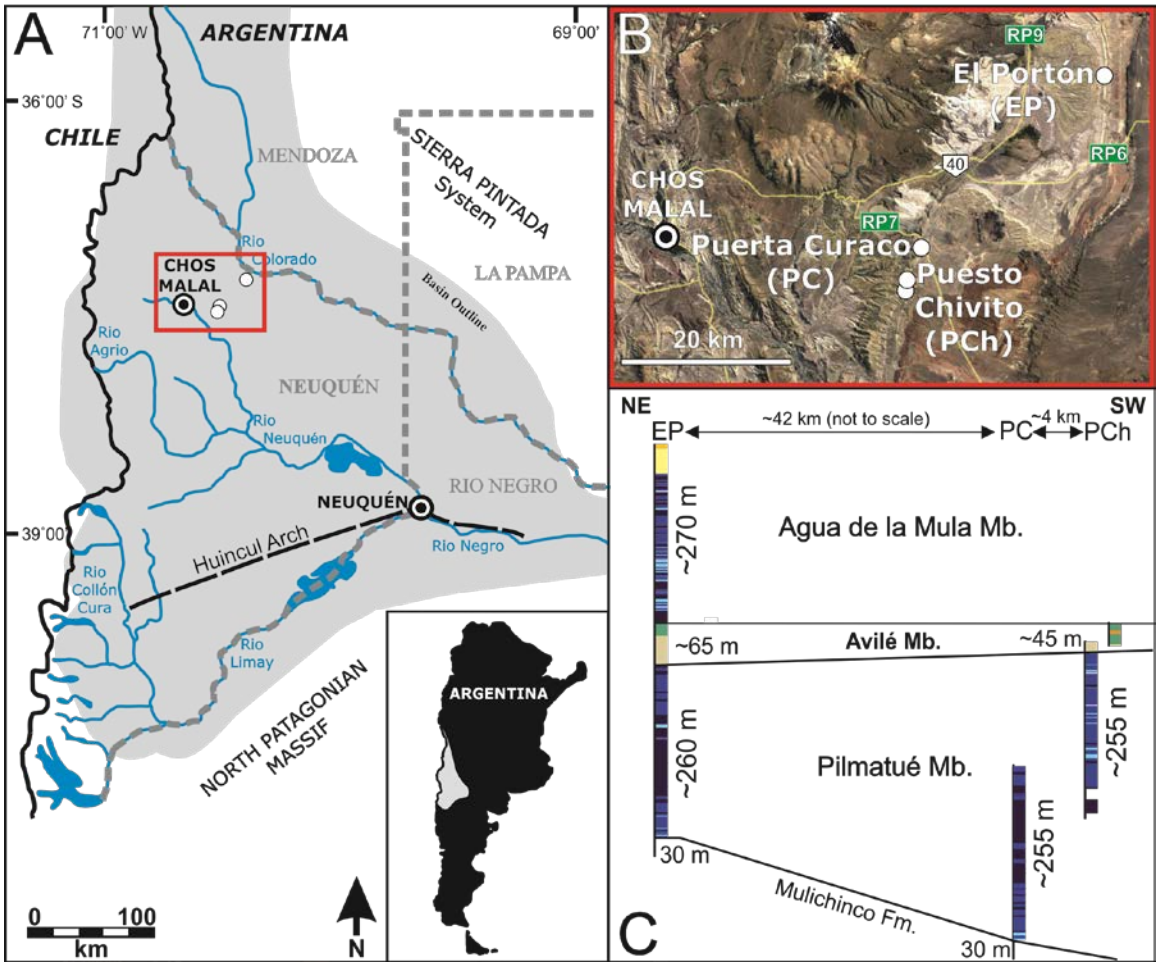

Figure 1. Map of the Neuquén basin, and map and cross-section of the study area. (A) Location map of the Neuquén Basin (grey polygon) with the study area in a red box. Province borders are dashed grey lines. Adapted from Vergani et al. (1995) and Kietzmann et al. (2016). (B) Google Earth image of the study area with major towns and roads marked and this studies' localities labeled. (C) Stratigraphic correlation of the outcrops measured within this study showing the members present and thicknesses measured at each locality. Outcrop sections are represented by their depositional environment designations (see Fig. 16 for key). The contact between the Avilé and Agua de la Mula Members is the datum horizon.

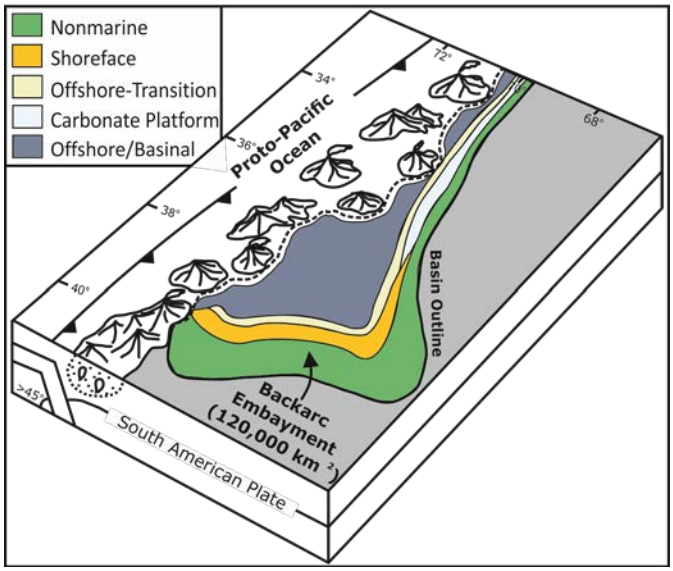

Figure 2. Paleogeographic reconstruction of the Neuquén Basin during the Early Cretaceous at the time of Agrio Formation deposition. Adapted from Howell et al. (2005). Depositional environment overlays adapted from Spalletti et al. (2011) and Schwarz et al. (2018).

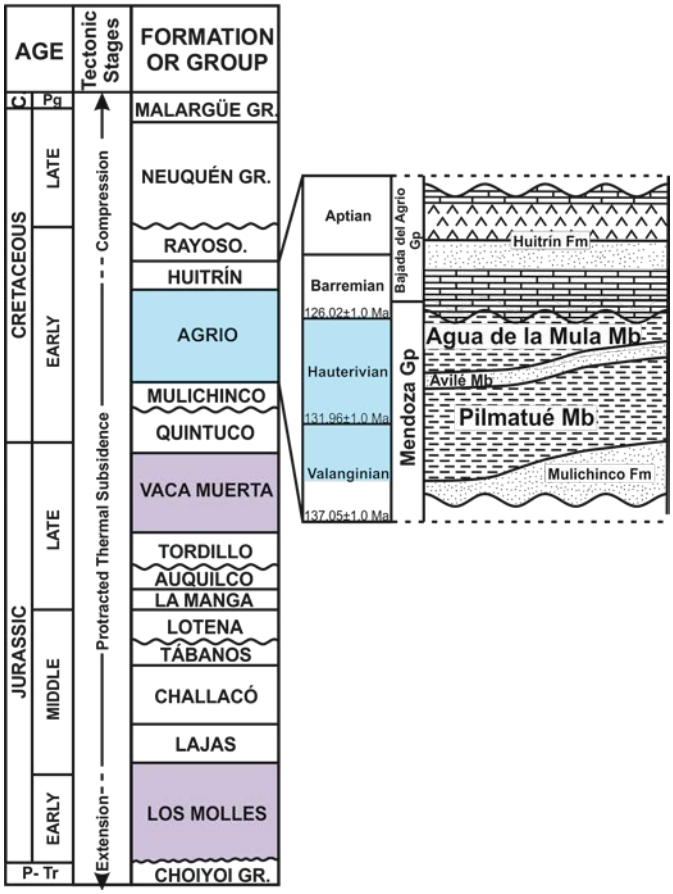

Figure 3. Stratigraphic column of the Neuquén Basin including major tectonic stages and a schematic stratigraphic section of the Early Cretaceous units. Study interval highlighted in blue and older marine source rock formations of the Neuquén Basin highlighted in purple. Adapted from Urien & Zambrano (1994), Aguirre-Urreta & Rawson (1997), Howell et al. (2005), and Veiga et al. (2005). Age dates for the base of the Valanginian, Hauterivian, and Barremian from Aguirre-Urreta et al. (2017).

DATA SET AND METHODS

In order to construct a depositional model for the Agrio Formation and to assess its source potential, this study combines field data from over 1200 m of measured sections, petrographic analysis of 69 thin sections (~20 μm), X-ray diffraction (XRD) analysis on 69 samples, and programmed pyrolysis data from 339 samples.

Four outcrop sections from three localities were measured at the centimeter scale with particular emphasis placed on sedimentary structures, bedding style, trace fossils, and stratigraphic stacking patterns. Moving from north to south, these localities are El Portón, Puerta Curaco and Puesto Chivito (Fig. 1b, c). Grain composition, fossil content, bioturbation and diagenetic features were described in thin section, allowing for a comparison to the outcrop based macrofacies. An adaptation of the Lazar et al. (2015) facies naming scheme was utilized both in the analyses of outcrop facies and thin section facies. Carbonate mudstone and wackestone terminology is used following Dunham (1962). Modifiers indicate the dominant grains present in each facies, even where grains are rare. The Bioturbation Index (BI) is based on Taylor and Goldring (1993). The combination of macrofacies and microfacies observations allows for a unified facies scheme presented herein.

Whole-rock and clay XRD analyses were performed using a Bruker D8 Advance X-ray diffractometer at the Energy & Geoscience Institute, University of Utah. When analyzing both the clay-sized fraction and the bulk samples, the following calibration

parameters were used: Cu-K-α radiation at 40 kV and 40 mA, 0.02º2θ step size, and 0.4 and 0.6 seconds per step, for clay and bulk samples, respectively. Clay samples were examined from beam diffraction angles 2 to 45º2θ and the bulk samples from 4 to 65º2θ. At a minimum, three analyses were conducted on each sample, two or more on the clay-sized fraction and one on the bulk sample.

Programmed pyrolysis analysis was performed on the HAWK instrument at Energy & Geoscience Institute at University of Utah. All samples were hand crushed using a mortar and pestle in order to avoid degradation of hydrogen through the frictional heating involved with mechanized crushing methods. An empty crucible, a Wildcat Technologies rock standard and an internal standard were placed in 25 sample intervals in the run sequence to assure that acceptable percent error was maintained. A large benefit to conducting programmed pyrolysis using the HAWK instrument is that acid preparation of samples is unnecessary even in samples containing high percentages of carbonate. To ensure that carbonate content did not skew the data produced by the HAWK instrument, a subset of 15 samples were treated with acid and analyzed following "Bulk-rock/basic" method/cycle procedure on a Rock-Eval 6 device at the Stratochem Labs in Cairo, Egypt. Analyses from both methods yielded nearly identical results providing a high confidence in the data derived from the HAWK.

The main programmed pyrolysis proxies of interest for evaluating source potential and thermal maturity are total organic carbon (TOC), S2 (the remaining generative potential), hydrogen indices (HI), oxygen indices (OI), and Tmax (the temperature of peak hydrocarbon generation during pyrolysis). TOC informs the quantity of organic

material, S2 is a proxy for the quality of organic material, and HI and OI are proxies for the type of organic material. Tmax acts as a proxy for thermal maturity.

SEDIMENTARY FACIES AND PROCESSES

Analyses of outcrops, thin section microscopy, and XRD were used to establish seven facies within the Pilmatué and Agua de la Mula Members (Table 1; Fig. 4 to 11), four facies specific to the upper 45 m of the Agua de la Mula Member at El Portón (Table 2), and eight facies within the Avilé Member of the Agrio Formation (Table 3). Other studies have focused more directly on describing the siliciclastic-dominated facies of the upper Agua de la Mula Member at El Portón (Veiga et al. 2005; Tunik et al. 2009; Spalletti et al. 2011), and Avilé Member (Legarreta et al. 1981; Veiga and Vergani 1993; Veiga et al. 2002, 2007, 2011) with results consistent with the facies presented herein (Table 2, 3). This study focuses on distinguishing mudstone-dominated facies and environments, and, even though seven facies were identified (Table 1), there are four key facies that make up the highest volume of the Pilmatué and Agua de la Mula Members in the distal ramp portion of the basin. Thus, only these four calcareous micritic facies are detailed below. Supplemental information provides outcrop measured sections (Appendices A, B, C) and detailed descriptions of the three Pilmatué and Agua de la Mula Member facies not presented herein (Appendix D).

Facies 1: Detrital Silt-Bearing Fine Mudstone (fMs)

Detrital silt-bearing fMs, facies 1, is the most volumetrically abundant facies within the Pilmatué and Agua de la Mula Members at all localities within this study. In

outcrop, facies 1 appears black to gray in color and is recessed with a fissile weathering appearance (Fig. 4a, d). Beds of this facies can be up to 13 m thick, but most commonly they are only a few centimeters thick due to high-frequency interbedding with facies 2, 3, and 7 and to a lesser degree, facies 4, 5, and 6 (Table 1; Appendix D). No sedimentary structures, bioclastic material, or trace fossils are visible in outcrop other than rare ammonite casts.

In thin section (*n = 27*) detrital silt-bearing fMs is dominated by micritic matrix. The grain fraction accounts for ~11% of this facies on average and is dominated by subangular, medium silt-sized, dispersed detrital quartz grains (Fig. 4b, 5). The silt fraction also includes dispersed bioclastic shell material and rare radiolaria and foraminifera. The shell material is largely on the microfossil scale, but some samples include identifiable gastropods, bivalves, echinoid spines, and ostracod macrofossil fragments (Fig. 4c). All bioclastic and biogenic material has been recrystallized, if originally aragonite or calcite, or replaced, if originally siliceous, by drusy and/or blocky spar calcite cement. The recrystallization could have occurred as aggrading neomorphism, indicative of late diagenesis. The sand fraction accounts for less than 3% of the composition of this facies on average but consists largely of partially degraded plagioclase grains (Fig. 4b, 5). Though definitive outlines of individual burrowers are difficult to identify in thin section, visible clotted organic-rich and dispersed detrital silt-rich domains in thin section suggest heavy bioturbation characterizes this facies (Fig. 4e). Cryptobioturbation has admixed the sediment and destroyed original sedimentary structures completely (Fig. 4b, e).

XRD analyses on 28 samples of facies 1 indicate that the matrix within the detrital silt-bearing fMs is composed of calcite and detrital illite with minor amounts of other detrital clay minerals (Fig. 6). For all facies, the XRD calcite content represents both carbonate mud and the calcite cement recrystallizing/replacing all bioclastic and biogenic material. On average clay minerals, feldspars, and silica constitute over 55% of facies 1. Only minor amounts of dolomite, pyrite and other accessory minerals are present.

Programmed pyrolysis results on 155 samples of facies 1 (Table 4) show TOC content ranging from 0.31 to 10.66 wt.% with an average of 1.57 wt.% (Fig. 7a). S2 values range from 0.04 to 70.28 mg HC/g rock with an average of 3.44 mg HC/g rock (Fig. 7b), and HI values ranging from 6 to 709 mg HC/g TOC with an average of 153 mg HC/g TOC (Fig. 7c). Kerogen types inferred from these geochemical proxies ranges widely from terrigenous- to marine-dominated, with many samples showing a mixed terrigenous and marine signature (Type II/III) (Fig. 8).

Facies 2: Radiolarian-Bearing Calcareous fMs

Radiolarian-bearing calcareous fMs, facies 2, is the second most volumetrically abundant facies within the Pilmatué and Agua de la Mula Members at all localities within this study. Facies 2 is resistant in outcrop creating thin to thick (0.03-1.1 m), laterally continuous beds with sharp nonerosive bases. These beds are interbedded with facies 1 and are either discrete or grouped in packages, which amalgamate laterally in some cases (Fig. 9a, b). They commonly display a white weathering appearance but are dominantly black beneath on a fresh surface (Fig. 9b). Though largely structureless, rare beds show either continuous planar parallel, discontinuous wavy parallel, or discontinuous wavy

nonparallel laminations (Fig. 9c). Bioclastic material is not visible in outcrop, but ammonite casts are common. *Planolites* and *Thalassinoides* trace fossils are uncommonly visible on the upper bedding planes of this facies in outcrop, commonly where it is overlain by facies 7 (Table 1; Fig. 9d). BI is most commonly 1, but ranges from 1 to 4 in outcrop.

Radiolarian-bearing fMs is dominated by micritic matrix in thin section (*n = 21*). The grain fraction accounts for ~9% of this facies on average and is heavily dominated by very fine sand-sized radiolaria that have been completely replaced by blocky spar calcite cement (Fig. 9e, f). The remainder of the sand fraction consists of foraminifera, some unidentifiable macrofossil shell material, identifiable macrofossil bivalves, gastropods, and echinoderm plates, and rare degraded feldspar grains (Fig. 9g, h, i). The silt fraction consists of approximately equal percentages of medium silt-sized, subangular detrital quartz grains and dispersed microfossil shell material. Rare sponge spicules are also present in some cases. As in facies 1, all bioclastic and biogenic material has been recrystallized or replaced by drusy and/or blocky spar calcite cement, possibly through aggrading neomorphism. Though detrital silt is not as abundant as in facies 1, it also is completely dispersed in thin sections of facies 2, indicating that the sediment was admixed through heavy cryptobioturbation.

XRD analyses on 24 samples of facies 2 indicates that the matrix of facies 2 is composed primarily of calcite with minor detrital clay minerals, the most common of which is illite (Fig. 6). On average clay minerals, feldspars, and silica account for less than 30% of facies 2. Facies 2 has a relatively high percentage of dolomite at ~15% as compared to other facies, with very minor amounts of pyrite and other accessory

minerals.

Programmed pyrolysis results on 107 samples from facies 2 (Table 4) show TOC content ranging from 0.25 to 3.8 wt.% with an average of 1.20 wt.% (Fig. 7a). S2 values range from 0.06 to 21.29 mg HC/g rock with an average of 3.97 mg HC/g rock (Fig. 7b), and HI values range from 14 to 637 mg HC/g TOC with an average of 262 mg HC/g TOC (Fig. 7c). Kerogen types inferred from these geochemical proxies show a similar variability and range to that of facies 1. However, facies 2 shows a distinct trend of more marine-dominated organic material (Type II) (Fig. 8).

Facies 3: Detrital Silt and Shell-Bearing Calcareous fMs

Detrital silt and shell-bearing calcareous fMs, facies 3, is slightly less volumetrically abundant than facies 2 within the Pilmatué and Agua de la Mula Members and is commonly interbedded with facies 1 in outcrop and rarely with facies 2. In outcrop this facies forms semiresistant, relatively thin (0.03-0.5 m) beds that are generally laterally continuous but are commonly too weathered to distinguish easily from facies 1 (Fig. 4d). No trace fossils, sedimentary structures or bioclastic material are visible in outcrop.

Detrital silt and shell-bearing calcareous fMs is dominated by micritic matrix in thin section ($n = 8$) with the grain fraction accounting for ~14% on average. The grain fraction is dominated by a slightly more mixed percentage of bioclastic material and subangular, medium silt-sized, dispersed detrital quartz grains than present in facies 1(Fig. 4e, 5). The bioclastic material is primarily unidentifiable microfossil shell fragments with some gastropod, bivalve, ostracod, and echinoderm plates macrofossil

fragments (Fig. 4g, h). Facies 3 also contains elevated percentages of very fine sand-sized radiolaria and foraminifera compared to facies 1 (Fig. 4h, 5). As in facies 1 and 2, all bioclastic and biogenic material has been recrystallized or replaced by drusy and/or blocky spar calcite cement, possibly through aggrading neomorphism. Additionally, syntaxial overgrowths are apparent on some echinoderm plates (Fig. 4h). Similar to facies 1, thin sections of facies 3 show visible clotted organic-rich and dispersed detrital silt-rich domains suggesting cryptobioturbation destroyed original sedimentary structures.

XRD analyses of two samples of facies 3 indicate the matrix of facies 3 is composed almost entirely of calcite with only very small amounts of detrital illite (Fig. 6). The high concentration of calcite recrystallized or replaced bioclastic and biogenic material within the grain fraction of this facies also attributes to a high average calcite content. On average clay minerals, feldspars, silica, dolomite, pyrite, and other minerals account for less than 25% of facies 3.

Programmed pyrolysis results on 13 samples of facies 3 (Table 4) show TOC content ranging from 0.46 to 15.9 wt.% with an average of 2.67 wt.% (Fig. 7a). S2 values range from 0.12 to 106.32 mg HC/g rock with an average of 13.02 mg HC/g rock (Fig. 7b), and HI values show a range from 21 to 673 mg HC/g TOC with an average of 272 mg HC/g TOC (Fig. 7c). Kerogen types inferred from these geochemical proxies show a bimodal trend of terrigenous-dominated (Type III) and marine-dominated samples (Type II) (Fig. 8).

Facies 4: Calcareous Wackestone

Calcareous wackestone, facies 4, displays a similar outcrop expression to facies 2 in that it is resistant, tabular, and thinly to thickly bedded (0.03-1.1 m) with a white weathering surface and sharp nonerosive bases. Similarly, beds are either discrete or amalgamated in packages. Rare continuous wavy nonparallel laminations and trace fossils are apparent in outcrop. This facies differs from facies 2 in that it contains a higher percentage of silt to sand-sized grains, thus it is categorized as a wackestone. Grains are composed primarily of reworked shell debris of variable size and/ or disarticulated bivalves (Fig. 10a, b, c, d). Beds contain between 5 and 15% bioclastic material and ammonite casts are common. Identifying specific taxa and genera is beyond the scope of this work but has been the focus of a number of other studies on the Agrio Formation (Lazo 2004, 2006, 2007a, 2007b; Lazo et al. 2005, 2008; Aguirre-Urreta et al. 2008). *Thalassinoides* and *Planolites* trace fossils were only observed in outcrop in one bed at the Puesto Chivito locality (Fig. 10e).

Though calcareous wackestone is dominated by micritic matrix in thin section (*n = 5*), the grain fraction accounts for ~30% on average. The grain fraction is dominated by sand- to silt-sized shell material, consisting of bivalve, gastropod, ostracod, and unidentifiable fragments (Fig. 5, 10f, g, h, i). The majority of the shell material is dispersed but some larger shell fragments show parallel to subparallel orientation (Fig. 10h). The grain fraction also contains medium silt-sized dispersed detrital quartz grains in similar quantities as seen in facies 1, relatively high concentrations of medium sand-sized foraminifera, and minor radiolaria, dolomite, feldspar, and pyrite. All bioclastic and biogenic material has been recrystallized or replaced by drusy and/or blocky spar calcite

cement, possibly through aggrading neomorphism. Some micritization is also visible (Fig. 10i). Similar to facies 2, intense bioturbation is inferred from the dispersed nature of the detrital silt within facies 4.

XRD analyses on five samples of facies 4 indicate that the matrix of the facies is composed primarily of calcite with minor detrital clay mineral composition, the most common of which is illite (Fig. 6). Similar to facies 3, the high concentration of calcite recrystallized or replaced bioclastic and biogenic material within the grain fraction of facies 4 attributes to a high average calcite content. On average clay minerals, feldspars, and silica account for around 40% of facies 4, which is dominated by ~55% calcite. Facies 4 contains minor amounts of dolomite, pyrite, and other accessory minerals.

Programmed pyrolysis results on 14 samples of facies 4 (Table 4) show TOC content ranging from 0.54 to 4.14 wt.% with an average of 1.77 wt.% TOC (Fig. 7a). S2 values range from 1.42 to 24.73 mg HC/g rock with an average of 8.86 mg HC/g rock (Fig. 7b), and HI values range from 261 to 682 mg HC/g TOC with an average of 474 mg HC/g TOC (Fig. 7c). Kerogen types inferred from these geochemical proxies are marine-dominated (Type II) to mixed terrigenous and marine (Type II/III) (Fig. 8).

Facies Interpretations: Proximal to Distal Trends

The main constituents of the four most volumetrically abundant facies of the Pilmatué and Agua de la Mula Members in this distal portion of the basin can be separated into three groups: detrital material, pelagic and benthic biogenic material, and carbonate mud (micrite). The mud-dominated nature of these facies indicates that they were deposited in a relatively low energy environment, below storm wave base (Morris et

al. 2006; Wilson and Schieber 2014; Schwarz et al. 2018) The presence of pervasive cryptobioturbation in thin section, horizontal trace fossils in outcrop within facies 2 and 4, and a lack of scouring and other storm deposit indicators (e.g. HCS) support a low energy environment (Burchette and Wright 1992; MacEachern et al. 2010).

The detrital material component consists of siliciclastic detrital silt, detrital argillaceous mud (clay), and bioclastic shell material. This detrital material was transported offshore from a siliciclastic-dominated shore proximal zone and could have been transported by either 1) hyperpycnal flows, 2) hypopycnal plumes, or 3) wave and/or current-enhanced sediment gravity flow remobilization of siliciclastic shallow marine deposits (Bhattacharya and MacEachern 2009; Wilson and Schieber 2014; Denommee et al. 2016; Schieber 2016; Birgenheier et al. 2017). The shallow ramp, low angle gradient supports these three possible depositional mechanisms for detrital material (Schieber 2016). The highly fragmented nature of the bioclastic shell material indicates a long transport distance from more shore proximal zones (Egenhoff and Fishman 2013), likely through the same mechanism responsible for the transport of the detrital silt and argillaceous mud. The presence of radiolaria indicates some pelagic production of biogenic material that was likely deposited by suspension settling. Benthic foraminifera indicate some benthic production of biogenic material with the possibility of further transport via traction currents (Egenhoff and Fishman 2013). Possible sources for carbonate mud commonly described for Cretaceous marine systems are pelagic calcareous nannofossils or detrital carbonate produced in shallow water environments (Bornemann et al. 2003).

Based on the processes indicated above and an understanding of the typical

homoclinal ramp morphology, grain population trends within these facies can be utilized to establish proximal to distal trends (Fig. 11). Facies 4 has the highest percentage of grains at ~30%, and the dominant grain populations are shell fragments, primarily macrofossils, and detrital quartz grains (Fig. 5). This relatively high percentage of macrofossils and detrital silt indicate that facies 4 is the most proximal facies, with the highest input of detrital material transported from a siliciclastic-dominated shore proximal zone (Fig. 11). The high carbonate percentage compared to quartz and argillaceous clay minerals from XRD is a function of high percentage of calcite derived from recrystallized or replaced macro and microfossil bioclastic material and biogenic material, which dilutes the detrital quartz and clay signal. Facies 3 displays very similar XRD percentages and similar normalized grain population percentages as facies 4; yet with a markedly lower percentage of grains at ~14%, a dominance of microfossil shell fragments as opposed to macrofossils, and a lower abundance of benthic forams (Fig. 5). Therefore, facies 3 represents a slightly more distal environment than facies 4 (Fig. 11). Facies 1 contains slightly less grains than facies 4 and 3, at ~11%, with a marked shift in grain population from mixed bioclastic and quartz-dominated to strongly quartz-dominated (Fig. 5). This is apparent in the XRD data that display a relatively high percentage of detrital argillaceous clay minerals, and a calcite dilution of detrital components is lacking (Fig. 6). The relatively high percentage of detrital silt and detrital argillaceous mud in facies 1 (though lower absolute detrital silt percentages than facies 4 and 3), along with a slightly lower microfossil abundance compared to facies 3, is interpreted as representing slightly more distal deposition than facies 3 (Fig. 11). Facies 2 has the lowest percentage of grains at 9%, the lowest absolute abundance of detrital

quartz grains, and is dominated by pelagic biogenic produced radiolaria (Fig. 5). As such, it is interpreted as representing the most distal deposits (Fig. 11).

Based on the model for the distribution of grain populations presented here, it would be expected that radiolaria would be more abundant in the distal facies than in the more proximal facies, which is not what is seen in the overall compositional trends by facies (Fig. 5). The similar overall high abundance of radiolaria in the most proximal (facies 4) and most distal (facies 2) facies may be a result of increased winnowing out of mud in the more proximal zones leading to concentrations of radiolaria. Conversely this trend could be a function of the difference in thin section sample size by facies.

Facies 2 displays the highest marine-dominated organic matter (Fig. 8). Thus, the organic geochemical data support facies 2 as the most distal facies. Similarly, facies 1, which is interpreted as more proximal with a higher detrital component compared to facies 2, displays a mixed terrestrial and marine organic matter signal (Fig. 8).

Figure 4. Examples of key feature in facies 1 (Detrital silt-bearing fine mudstone) and facies 3 (Detrital silt and shell-bearing fine mudstone). (A) Outcrop view with facies 1 with a few isolated interbeds of facies 3 and facies 4. Scale bar = 4 m (~13 ft). (B) Thin section of facies 1 with dispersed detrital quartz silt *(Qtz)*, bladed shell fragments *(SF)*, and rare plagioclase grains *(P)*. (C) Bivalve shell fragment recrystallized by blocky spar calcite cement. (D) Outcrop view of the fissility of facies 1. Hammer is 33 cm (13 in). (E) Thin section of facies 1 showing darker clotted organic-rich and lighter dispersed detrital silt-rich domains. (F) Outcrop with facies 3 (marked by white arrows) interbedded with facies 1. (G) Thin section of facies 3 showing higher concentration of thin shell fragments and lower concentrations of detrital silt than seen in facies 1. (H) Echinoderm plates in the center and radiolarian to the right recrystallized by spary calcite cement and showing signs of compaction. The echinoderm plate shows evidence of a syntaxial overgrowth.

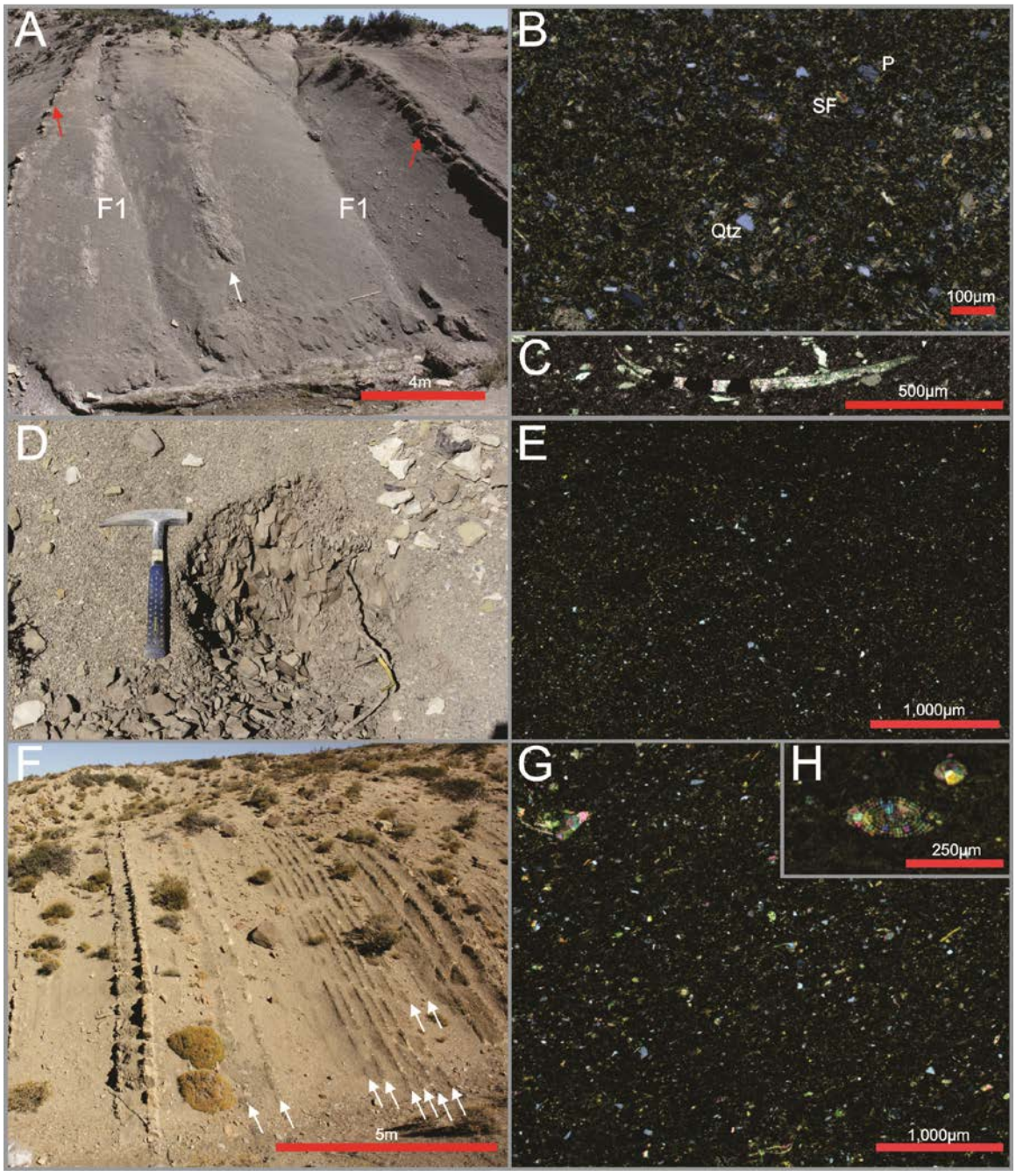
A
F1
F1
4m
B
P
SF
Qtz
100µm
C
500µm
D
E
1,000µm
F
5m
G
1,000µm
H
250µm

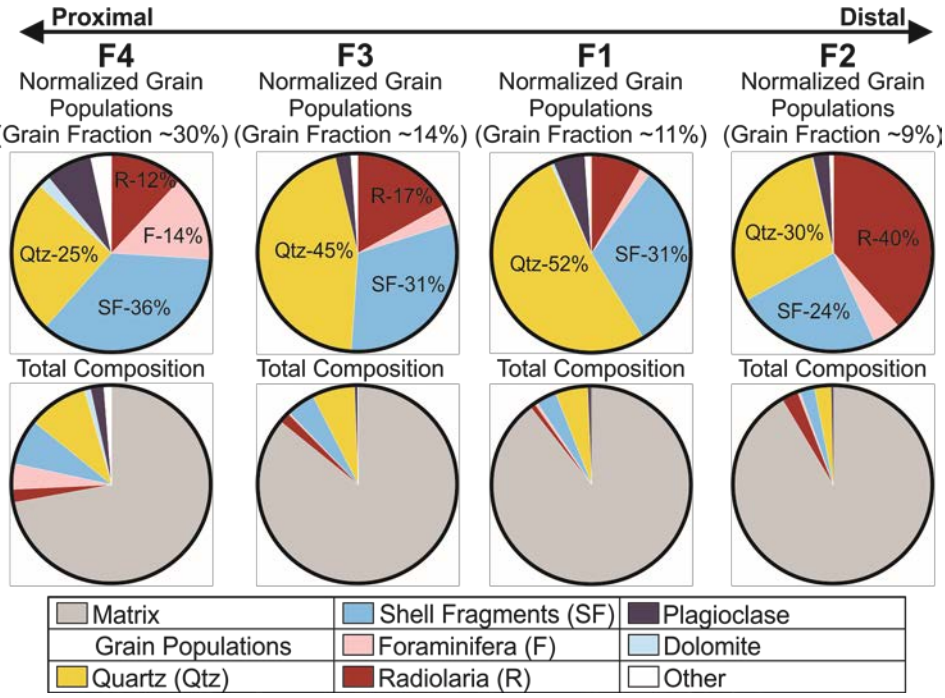

Figure 5. Proximal to distal trends by facies based on normalized grain populations and total compositions established through thin section microscopy.

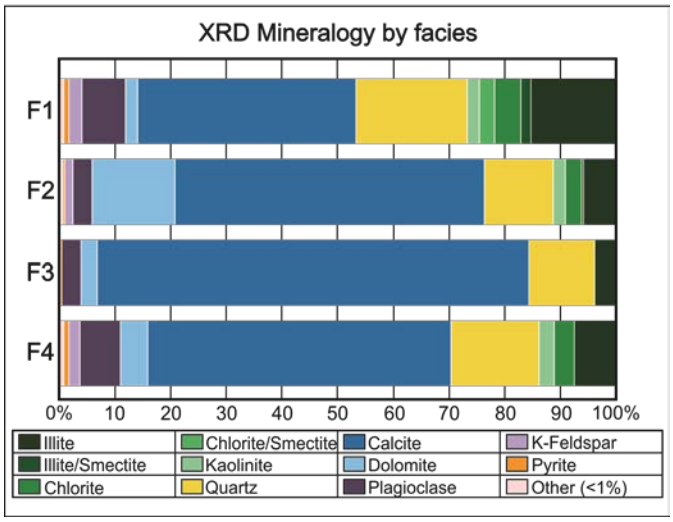

Figure 6. Mineralogy by facies based on x-ray diffraction.

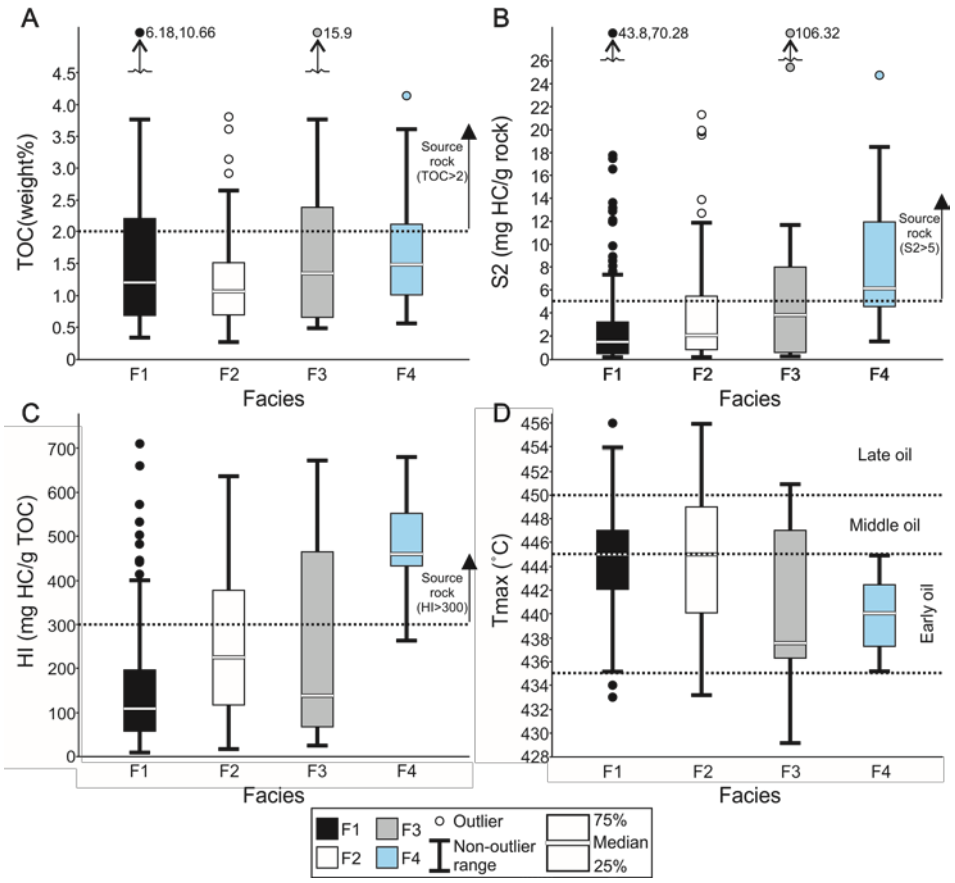

Figure 7. Variations in geochemical properties by facies based on programmed pyrolysis. Box plots show median, distribution quartile, nonoutlier range, and outliers of each parameter.

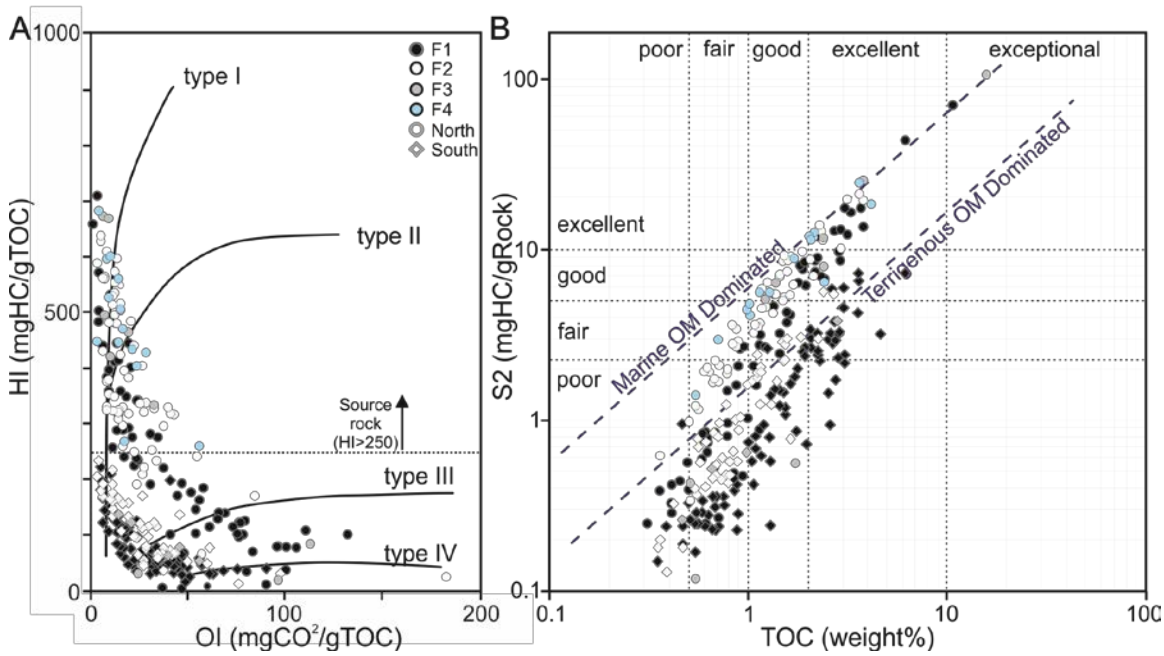

Figure 8. Geochemical plots based on programmed pyrolysis data. (A) Hydrocarbon index versus oxygen index (pseudo van Krevelen diagram). (B) S2 versus total organic carbon. Both colored by facies with shapes denoting location.

Figure 9. Examples of key feature in facies 2 (Radiolarian-bearing fine mudstone). (A) Outcrop with resistant facies 2 thinly interbedded with recessed facies 1. Hammer is 33 cm (13 in). (B) Close up of facies 2 showing the white weathering appearance. (C) Facies 2 showing discontinuous, wavy, nonparallel laminations. (D) Bedding plane of facies 2 with orange tuff stained *Thalassinoides* trace fossils visible. Pencil is 14.5 cm (5.70 in). (E) Thin section of facies 2 showing blocky spar calcite replaced radiolarians. (F) Spary calcite replaced radiolarian with preserved spine (red arrow). (G) Blocky spar calcite recrystallized gastropod. (H-I) Blocky spar calcite recrystallized or replaced benthic foraminifera with some of its original test morphology preserved (H: possibly agglutinated, I: possibly *Nodosaridae*).

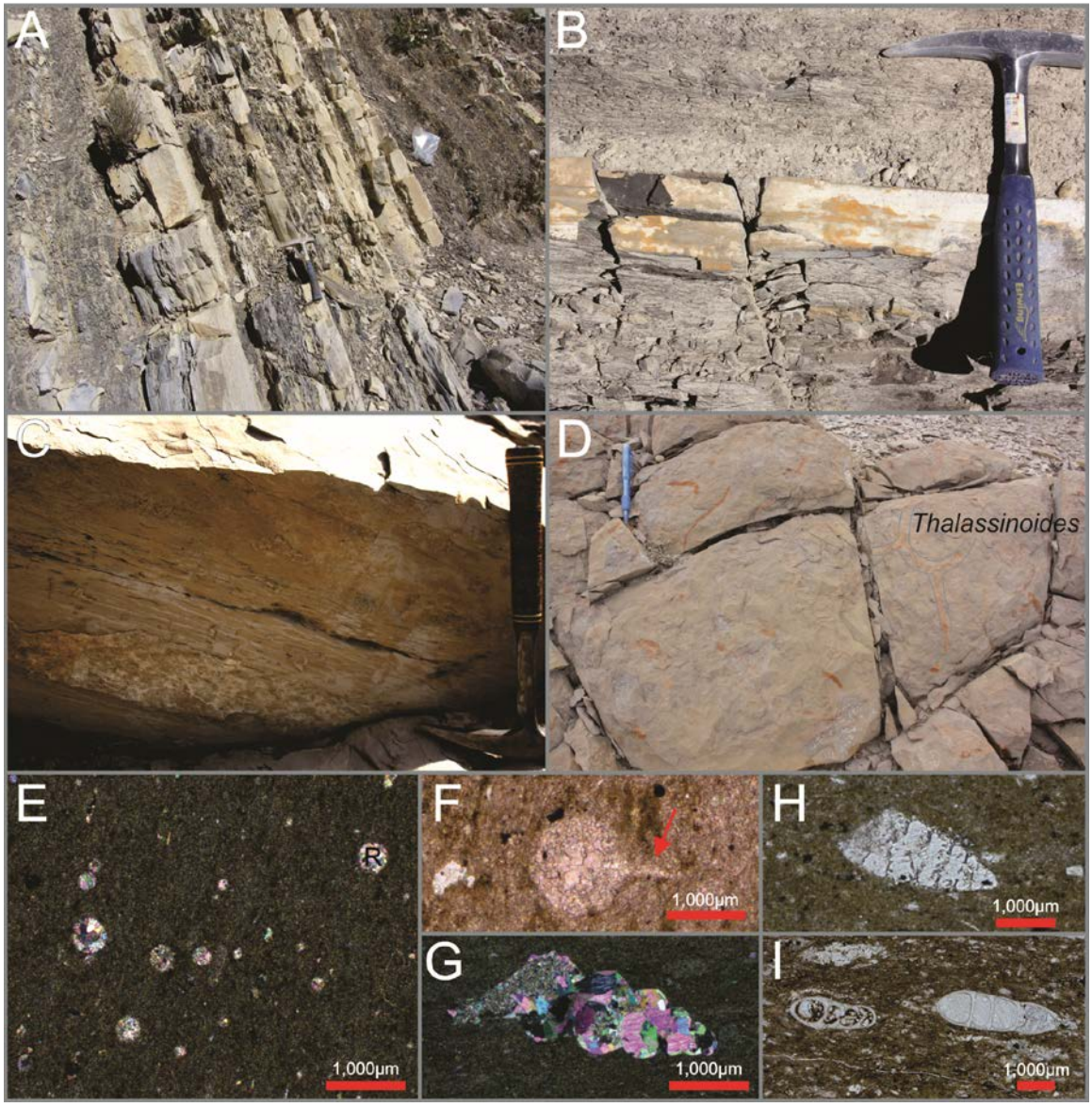
A
B
C
D
Thalassinoides
E
R
1,000µm
F
1,000µm
H
1,000µm
G
1,000µm
I
1,000µm

Figure 10. Examples of key feature in facies 4 (Calcareous wackestone). (A) Outcrop with facies 4 showing a large bivalve shell, (B) a cast of an articulated bivalve, (C) a gastropod fragment, (D) millimeter scale dispersed shell fragments (white arrows), and (E) abundant *Thalassinoides* and rare *Planolites* trace fossils visible on top of bedding plane. (F) Dual carbonate stained thin section showing wackestone with *Epistomina* benthic foraminifera *(F)*, shell fragments *(SF)*, detrital silt (red arrow), and plagioclase crystals *(P)*. (G) Thin section showing a wackestone with shell fragments *(SF)*, gastropods *(G)*, forams (*F)*, possibly agglutinated), and radiolaria *(R)*. (H) Thin section showing wackestone displaying blocky spar calcite recrystallized shell fragments oriented subparallel to lamination. Replaced radiolaria visible. (I) Blocky spar calcite recrystallized articulated shell, note micrite in the cell center. (J) A slightly compressed, calcite recrystallized ostracod.

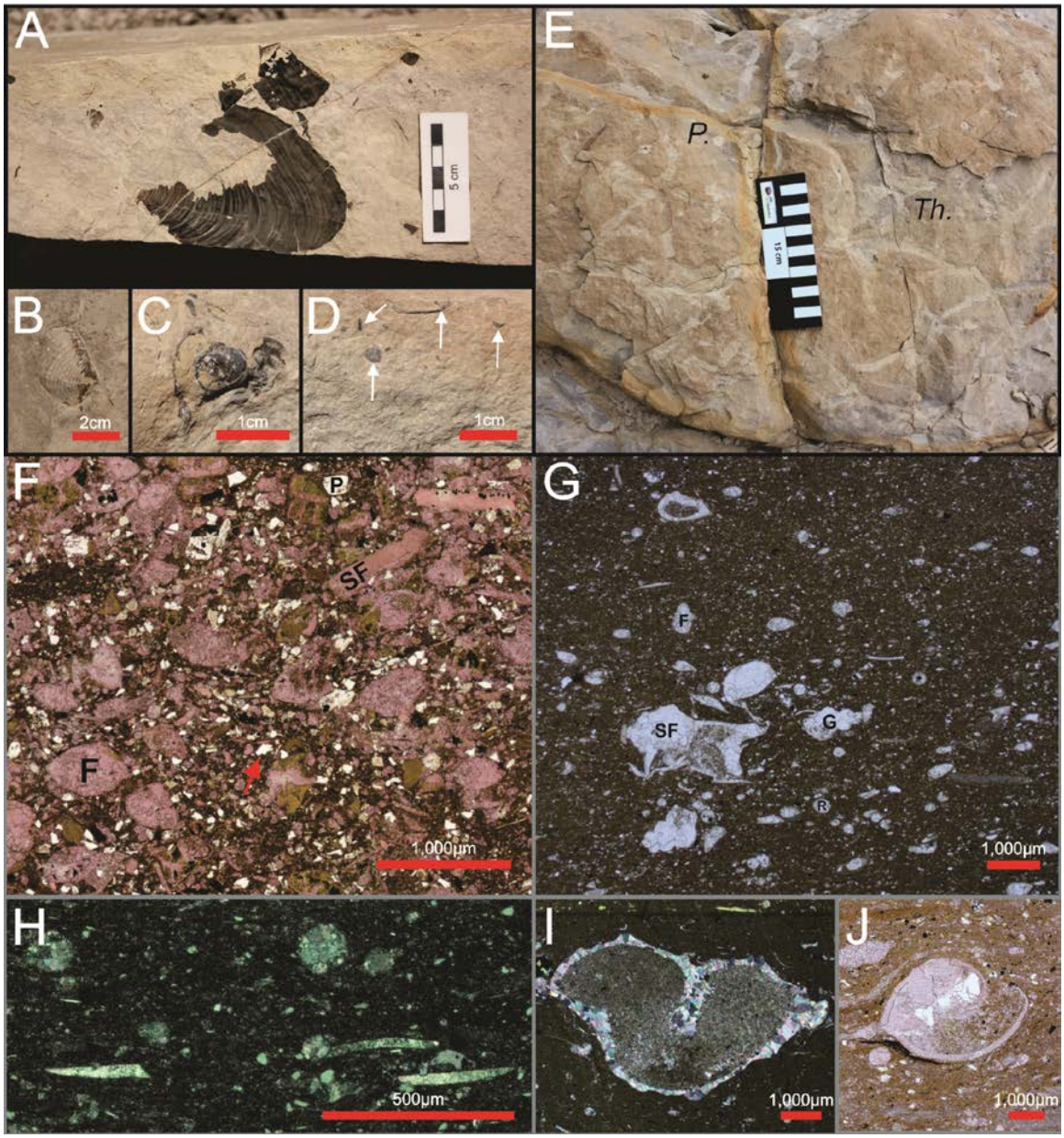
A
5 cm
B
2cm
C
1cm
D
1cm
E
P.
Th.
F
P
SF
F
1,000µm
G
F
SF
G
R
1,000µm
H
500µm
I
1,000µm
J
1,000µm

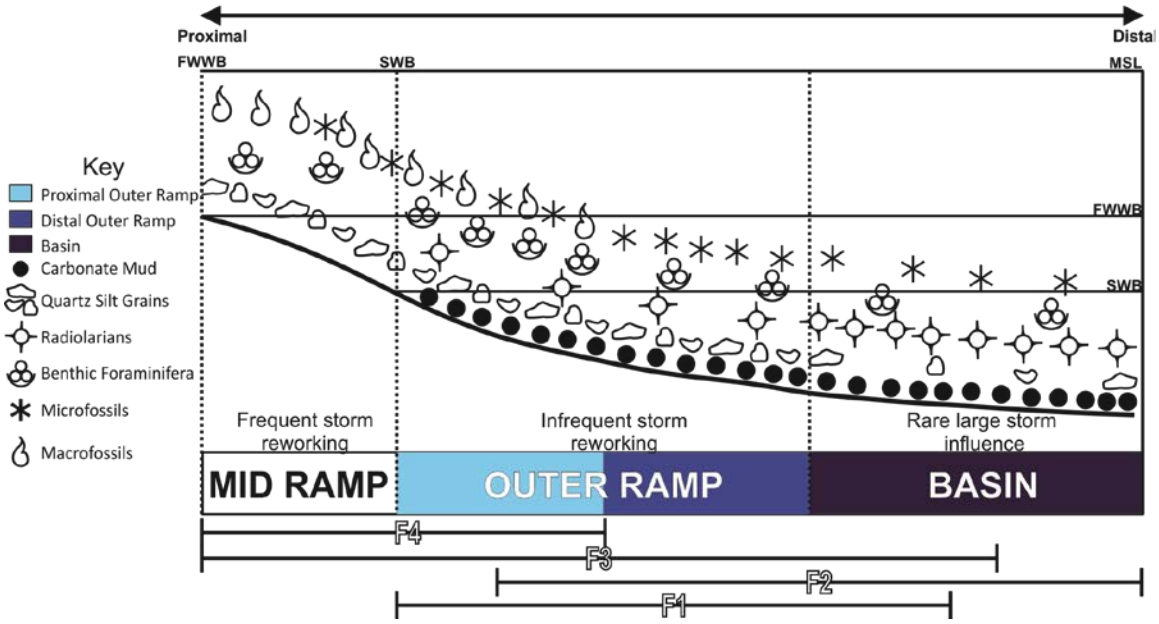

Figure 11. Summary diagram showing the distribution of grain populations. Interpreted ranges of distal carbonate ramp facies denoted. Interpreted subdepositional environments from the sections measured within this study are shown.

Table 1. Facies of the Pilmatué and Agua de la Mula members within this study area

Facies #	Facies name	Grain population	Mineralogical composition	Outcrop expression	Bioturbation index	Process interpretation	Depositional environment
1	Detrital silt-bearing fine mudstone	Micrite dominated; Grain fraction ~11% on average and dominated by detrital quartz grains	Calcareous to argillaceous; micritic matrix composed mainly of calcite and illite; detrital clay minerals, feldspars, and silica constitute >55% on average	Black to gray; recessed, fissile; beds up to 13 m, but commonly centimeter scale; interbedded with all other facies; no sedimentary structures, bioclastic material, or trace fossils visible in outcrop	5 to 6; crypto-bioturbation in thin section	Shallow marine contourites, enhanced sediment gravity flows, minor suspension settling of pelagic material	Present from proximal outer ramp to basinal environments, but characteristic of the distal outer ramp
2	Radiolarian -bearing calcareous fine mudstone	Micrite dominated; Grain fraction ~9% on average and dominated radiolaria	Calcareous; micritic matrix composed mainly of calcite; detrital clay minerals, feldspars, and silica constitute <30% on average; ~15 % dolomite on average	Black with white weathering face; resistant; beds 0.03-1.1 m, laterally continuous, sharp non-erosive bases; may be discrete or grouped; amalgamating; largely structureless, with rare laminations; bioclastic material not visible in outcrop	5 to 6; crypto-bioturbation in thin section; *Planolites* and *Thalassinoides* trace fossils visible in outcrop	Shallow marine contourites & suspension settling of pelagic material, minor enhanced sediment gravity flows	Present from proximal outer ramp to basinal environments, but characteristic of the basinal setting
3	Detrital silt and shell-bearing calcareous fine mudstone	Micrite dominated; Grain fraction ~14% on average and dominated by shell fragments and detrital silt	Calcareous; micritic matrix composed mainly of calcite; detrital clay minerals, feldspars, and silica constitute <25% on average	Gray; semi-resistant; 0.03-0.5 m laterally continuous beds; no sedimentary structures or bioclastic material visible in outcrop.	5 to 6; crypto-bioturbation in thin section	Shallow marine contourites, enhanced sediment gravity flows, minor suspension settling of pelagic material	Present from proximal outer ramp to basinal environments
4	Calcareous wackestone	Micrite dominated; Grain fraction ~30% on average and dominated by shell fragments and/or foraminifera	Calcareous; micritic matrix composed mainly of calcite; detrital clay minerals, feldspars, and silica constitute ~40% on average	Black with white weathering face; resistant; 0.03-1.1 m, laterally continuous beds with sharp non-erosive bases; discrete or grouped; amalgamating; largely structureless, with rare laminations; contains between 5 and 15% bioclastic material	5 to 6; crypto-bioturbation in thin section; *Planolites* and *Thalassinoides* trace fossils visible in outcrop at Puesto Chivito	Shallow marine contourites, enhanced sediment gravity flows, minor suspension settling of pelagic material	Characteristic of the proximal outer ramp

Table 1. Continued

Facies #	Facies name	Grain population	Mineralogical composition	Outcrop expression	Bioturbation index	Process interpretation	Depositional environment
5	Calcareous intraclastic packstone	Micrite dominated; Grain fraction ~60% on average and dominated by micritic intraclasts	Calcareous; micritic composed mainly of calcite; Detrital clay minerals, feldspars, and silica constitute ~15% on average	Rare (only seen at El Portón); tabular, laterally continuous beds ~0.4 m thick; flaggy laminar appearance; densely packed, round sand-sized "grains" visible on the tops of beds; no shell material or trace fossils visible in outcrop	0	Transgressive erosion (?)	N/A
6	Calcareous floatstone	N/A	N/A	Rare (only several beds in the upper portion of the Pilmatué member at Puesto Chivito); semi-resistant; laterally discontinuous over more than 10 m; 5-15 cm beds; contains both abundant shell debris (mm-5cm scale bivalve and gastropod fragments) and large articulated and disarticulated bivalve shells	0; no thin sections available to identify crypto-bioturbation	Storm related enhanced sediment gravity flows & *in situ* colonization	Characteristic of the more proximal portion of the distal outer ramp
7	Tuff	N/A	N/A	Orang-ish weathering color; friable; 0.01-0.15 m beds; commonly heavily altered by gypsum	0; no thin sections available to identify crypto-bioturbation	Distal ash fall/ suspension settling	N/A

Table 2. Facies of the upper 45 m of the Agua de la Mula Member at El Portón

Facies name	Grain size	Sedimentary structures/ featured	General composition	Process interpretation	Depositional environment
Detrital silt-bearing fine mudstone	Clay dominated; Grain fraction dominated by detrital quartz grains	None visible in outcrop; no thin sections available for further analysis	XRD (*n=1*) mineralogical percentage: 41% Illite, 5% Chlorite, 4% Kaolinite, 11% Plagioclase, 9% K-Feldspar, 30% Quartz	Hyperpycnal flows	Outer ramp
Silty very fine sandstone	Very fine sand; <50% silt	Reddish weathering color; in places displays distinctly tabular weathering pattern with planar partings		Deposition below storm wave base related to storm flows	Offshore transition
Thinly bedded very fine sandstone	Very fine sand	mm scale tabular ripple cross laminated beds; ripples are unidirectional; rare beds appear hummocky		Deposition above storm wave base related to storm flows	Lower-shoreface
Very fine sandstone	Very fine sand	cm-m scale beds; trough and planar crossbedding; low angle to plane parallel laminations; soft sediment deformation; symmetrical oscillation ripples; cross laminations commonly display carbonaceous material	XRD (*n=1*) mineralogical percentage: 7% Illite, 2% Kaolinite, 17% Plagioclase, 13% K-Feldspar, 52% Quartz, 9% dolomite	High energy and high sedimentation conditions under oscillatory flow conditions above storm wave base	Upper-shoreface

Table 3. Facies of the Avilé Member within this study area

Facies name	Grain size	Sedimentary structures and featured/general composition	Process interpretation	Depositional environment
Mudstone	Coarse Silt to clay; between 10-20% very fine sand	None visible in outcrop; thin section analysis was not conducted on this facies	Wave, tide, or current enhanced sediment gravity flows	Mudbelt
Structureless very fine silty sandstone	Very fine sand; ~30% admixed medium silt to clay	XRD (*n=1*): 24% Illite, 8% Chlorite, 18% Plagioclase, 6% Kspar, 37% Quartz, 7% calcite; Folk classification: medium silt, course sandstone, bimodal, submature, quartz rich calcarenite; massive or mottled likely due to bioturbation, admixed grain size populations	Rapid deposition under storm conditions above storm wave base with subsequent burrowing. May have also been impacted by enhanced sediment gravity flows	Distal Prodelta
Structureless fine sandstone	Fine sand	Structureless; may contain large (0.2 x 0.5 m) globular concretion packages (laterally continuous)	Sediment gravity flow most likely from collapsing banks coupled with dewatering	Fluvial
Laminated Sandstone	Fine to medium sand	Plane parallel to low angle laminations; Folk classification: medium sandstone, submature	Antidunes created by upper flow regime unidirectional flow	Fluvial
Rippled Sandstone	Fine sand	Current ripple laminations and/or climbing ripples	Lower flow regime (under high sedimentation rate if climbing ripples present)	Fluvial
Planar crossbedded sandstone	Very fine to medium sand	Planar crossbeds ranging in scale from 10-40 cm; cross laminations display carbonaceous material; occur isolated and in sets	Bedform migration under lower flow regime flow (2-D dunes)	Fluvial
Trough crossbedded sandstone	Very fine to medium sand	Trough crossbeds; cross laminations display carbonaceous material; rare in outcrop	Bedform migration under lower flow regime flow (3-D dunes)	Fluvial
Large scale crossbedded sandstone	Fine to medium sand	Crossbedds ranging in scale from 0.8-2.1 m; third order reactivation surfaces seen in foreset packages; upper and lower boundaries are truncated; cross laminations display carbonaceous material	Accumulation of grainflow and grainfall deposits on the base of leeslopes	Eolian dune field

Table 4. Programmed pyrolysis data by facies with averages bolded

Facies	TOC (wt. %)	S2 (mg HC/g rock)	HI (mg HC/g TOC)	Dominant organic matter type
Facies 1 (*n=155*)	0.31-10.66 (**1.57**)	0.04-70.28 (**3.44**)	6-709 (**153**)	Type III/II
Facies 2 (*n=107*)	0.25-3.8 (**1.20**)	0.06-21.29 (**3.97**)	14-637 (**262**)	Type II
Facies 3 (*n=13*)	0.46-15.9 (**2.67**)	0.12-106.32 (**13.02**)	21-673 (**272**)	Type II / Type III
Facies 4 (*n=14*)	0.54-4.14 (**1.77**)	1.42-24.73 (**8.86**)	261-682 (**474**)	Type II

DEPOSITIONAL MODEL

Facies 1 through 4 of the Pilmatué and Agua de la Mula Members are dominated by calcareous micrite by more than 84% on average (Fig. 5), making for a thick accumulation (~500 m) of interbedded carbonate mud deposits. The interpretation that the majority of the Pilmatué and Agua de la Mula Members were deposited below storm wave base is consistent with the placement of storm wave base in a paleo-updip study conducted by Schwarz et al. (2018). Previous depositional models of the Agrio Formation have called upon suspension settling of mud as the dominant, if not sole, depositional mechanism below storm wave base (Sagasti 2005; Veiga and Schwarz 2017; Schwarz et al. 2018). One marked exception is the work of Comerio et al. (2018), which highlights evidence of dynamic sedimentation in the basal portion of the Aqua de la Mula member in deposits south of this study. Our detailed study of the mudstone-dominated facies of the Agrio Formation indicates the substorm wave base system was much more dynamic than simple suspension settling throughout the deposition of the unit.

Depositional Mechanisms

There are three main depositional mechanisms that resulted in distinct features in the offshore facies record including 1) wave and/or current-enhanced gravity flows delivering siliciclastic fluvial and shallow marine sediments from areas paleodepositionally updip (Veiga and Schwarz 2017; Schwarz et al. 2018) to the offshore

realm, 2) along-shore and oblique shallow water contour current-transported carbonate mud, sourced from the shallow marine carbonate platform portion of the shoreline, and 3) production of pelagic and benthic tests, both calcareous and siliceous (i.e., nanno- and micro-fossils) (Fig. 12).

Wave and/or current-enhanced sediment gravity flows. There are three possible depositional mechanisms that could be responsible for transporting fine-grained siliciclastic detrital silt, detrital argillaceous mud, and siliciclastic shoreline related bioclastic material offshore in this system: hyperpycnal flows, hypopycnal plumes, and wave and/or current-enhanced sediment gravity flows (Bhattacharya and MacEachern 2009; Birgenheier et al. 2010; Wilson and Schieber 2014; Denommee et al. 2016; Schieber 2016). Though these sedimentary processes are typically distinguished using characteristic sedimentary structures, cryptobioturbation obliterated these in the Agrio Formation, preventing a definitive interpretation in this way. However, through the established understanding of the Neuquén Basin's paleogeography, namely distance from the shoreline and estimated slope angles, we interpret that wave and/or current-enhanced sediment gravity flows are responsible for transporting fine-grained detrital material offshore. Units in this study were deposited ~20 km from the nearest siliciclastic paleoshorelines, which were dominated by longshore drift processes, but were at least 200 km away from the southern fluvial-deltaic point source that could have produced hyperpycnal flows and hypopycnal plumes (Sagasti 2005; Schwarz et al. 2018). Additionally, previous assessments indicate inner ramp to middle ramp slope angles ranging from 0.1 to 0.01 for the Neuquén Basin during deposition of the Agrio Formation (Sagasti 2005), and our own observed clinoform geometries from the field area indicate a

slope angle ≤0.38°. Wave and/or current-enhanced sediment gravity flows are the only documented process capable of transporting detrital silt over 200 km from the deltaic-dominated shoreline, particularly at this low slope angle (Schieber 2016), independent of any mechanism that was responsible for initial nearshore transport of such material (Fig. 12).

Though several offshore marine depositional models infer detrital silt sourced from eolian or volcanic input (Werne et al. 2002; Sageman et al. 2003; Gabbott et al. 2010; Egenhoff and Fishman 2013), evidence in the four facies presented in detail herein do not support these interpretations. The dominance of subangular grains, rather than euhedral quartz grains, suggests volcanic input is unlikely. Additionally, previous studies of altered tuffs in the Agrio Formation indicate that they primarily consist of volcanic glass shards with very little quartz and plagioclase present (Aguirre-Urreta et al. 2015, 2017; Schwarz et al. 2016). Eolian input is also unlikely as it fails to account for the transport of the detrital argillaceous mud, since clay particles cohesively form and act like larger particles that generally aren't transported by wind (Nichols 2009). The cohesive behavior of mud sized particles over a wide range on compositional variations and experimental conditions is well established (i.e., Schieber et al. 2007; Aplin and Macquaker 2011). Additionally, updip siliciclastic shoreface and offshore deposits documented by Schwarz et al. (2018) favor a siliciclastic shoreline over eolian origin. Though an in-depth investigation of paleogeography, paleoclimate, and paleowind patterns would be needed to exclude the presence of a large eolian source region, periods of high sea level, such as during the deposition of the Pilmatué and Agua de la Mula Members, are inconsistent with desert formation (Schieber 2016).

It has been suggested that in shallow (≤ 300 m), ancient epeiric seas the development of seasonal, thermal stratification related dysoxic to anoxic periods would be likely, particularly under greenhouse conditions such as those that characterize the Early Cretaceous (Tyson and Pearson 1991; Sageman et al. 2003). *Thalassinoides* traces and cryptobioturbation occur in environments with oxygen levels ranging from dysoxic to oxic and suboxic to oxic respectively. This model of fluctuating oxygenation in basins such as the Neuquén Basin, along with the presence of *Thalassinoides* burrows seen in outcrop and cryptobioturbation seen in thin section, suggests oxygenated to suboxic conditions existed at the sediment water interface during the entire time span of the deposition of the Agrio Formation. Yet, clearly, a subset of samples preserves a high amount of organic material (Fig. 7). Most established geochemical models would assert this defined subset of samples preserve evidence of anoxic conditions to promote organic matter preservation and deter biodegradation (Demaison and Moore 1980; Pedersen and Calvert 1990; Ingall et al. 1993; Calvert et al. 1996; Tyson 2001; Van Dongen et al. 2006). However, the preservation of organic material within an oxygenated water column may also be explained by the encapsulation of organic matter into “marine snow” (Macquaker et al. 2010b) that reached the sea floor during periods of relative calm when weak bottom currents slightly buried it in an anoxic and reduced sea floor, thus preserving it (Comerio et al. 2018; Minisini et al. 2018). Furthermore, the preservation of organic material within an oxygenated sediment water interface that supports burrowing infauna may be explained by a rapid deposition of the marine snow when algal blooms outpaced the rate of organic-carbon decay (Macquaker et al. 2010).

Origin of carbonate mud. The origin of carbonate mud in modern and ancient environments remains somewhat enigmatic. Models of shallow marine Cretaceous systems commonly assert that the bulk of micrite is composed of calcareous nannofossils that lived in the water column and then settled to the sea floor (Bornemann et al. 2003). Though there have been a number of studies that have identified nannofossils within the Agrio Formation, primarily for biostratigraphic assessments, but no study has attempted to quantify what percentage of a given sample they account for (Aguirre-Urreta et al. 1999, 2005, 2017; Comerio et al. 2018). Slide smear analyses reveal that the matrix contains rare, barely identifiable nannofossil test of the most dissolution resistant Cretaceous nannofossil species, *Watznaueria barnesiae* (Fig. 13), but severe burial and weathering diagenesis makes quantifying the original volume of nannofossils present impossible (Watkins, personal communication). Typical modern sedimentation rates for pelagic environments range from 0.2-3 cm/ky suggesting that nannofossil sedimentation rates would be of a similar magnitude (Bornemann et al. 2003). Rough, decompacted sedimentation rates, based on extensive biostratigraphic studies and available U-Pb age dates, indicate a sediment accumulation rate of ~18 cm/ky for the Agua de la Mula Member and an average sediment accumulation rate of ~14 cm/ky for the Pilmatué Member in this portion of the basin (Martinez et al. 2012, 2015, Aguirre-Urreta et al. 2015, 2017; Schwarz et al. 2016). Because the sediment accumulation rates in the distal portion of the Agrio Formation are an order of magnitude greater than those explained by nannofossil accumulation alone, and because the dominant component of the facies is carbonate mud, it suggests an additional depositional source for carbonate mud was operating.

Additional micritic carbonate may have been derived from siliciclastic poor, shallow carbonate-rich regions of the shoreline, where the fine-grained fraction winnowed out of shallow carbonate periplatform ooze and transported laterally and obliquely and deposited offshore as a drift (Betzler et al. 2013, 2014). Existing paleogeographic reconstructions document a siliciclastic shoreline to the south and a shallow carbonate platform to the east and northeast (Spalletti et al. 2011; Schwarz et al. 2018). As such, we propose the carbonate platform derived mud was transported offshore from the shallow marine carbonate platform in the east and northeastern portion of the basin and deposited along, and oblique to the shoreline by offshore to oblique to shore currents (Fig. 2, 12). These inferred shallow water contour currents formed a shoreline parallel carbonate mudbelt. Contour currents may have originated from palaeoceanographic circulation patterns driven by a combination of thermohaline and wind-driven currents (Stow et al. 2002; Frébourg et al. 2016). These currents were likely modified by interaction with the seafloor topography and deflected to the south offshore by the Coriolis force. Sediment accumulation rates associated with carbonate platform marginal environments, ~14 cm/ky, are more in line with the magnitude of sediment accumulation calculated for the sections in this study (McNeill 2005; Phelps et al. 2015). Thus, a combination of pelagic nannofossil production and shallow water contour currents account for the carbonate mud in the Agrio system, as nannofossil test production alone is unlikely to account for the documented high sedimentation rates (Fig. 12). A higher proponent of shallow platform derived micrite than pelagic calcareous production has been briefly suggested by Sagasti (2005) and is further supported by the dataset herein.

The paleogeographic juxtaposition of a siliciclastic-dominated shallow marine system to the south and east of the offshore study area, and a carbonate-dominated shallow marine system to the north and east of the study area created an offshore environment that reflect the mixed siliciclastic-carbonate mud sources and facies described herein (Sagasti 2002, 2005; Schieber et al. 2007; Betzler et al. 2014; Rebesco et al. 2014; Schwarz et al. 2018) (Fig. 2). The high concentration of carbonate mud within all facies described in the study area, with the exception of facies 6, indicates that the carbonate mudbelt was a prominent feature of all depositional environments on the carbonate ramp below storm wave base.

Pelagic and benthic deposition. Pelagic biogenic calcareous and silica test production in this system resulted in the deposition of calcareous nannofossils and dispersed radiolaria through suspension settling (Fig. 12). Note that radiolaria tests that were originally siliceous have been dissolved and replaced with blocky spar calcite cement, a significant diagenetic event. The lack of preservation of nannofossil tests also indicated extensive diagenesis. Benthic biogenic production in this system resulted in the deposition of benthic foraminifera (Fig. 12). Where concentrations of these benthic forams in the succession are high and rather monotypic, such as high concentrations of *Epistomina* within facies 4, they represent a local population, with limited secondary transport (Sagasti and Ballent 2002). Since other lines of evidence suggest active currents characterized the system, where the foraminifera assemblages are more mixed and are admixed with other transported shell material, microfossils may have experienced entrainment, transport in active currents, and subsequent redeposition.

Depositional Environments

The relative influence of each of the three depositional mechanisms outlined above within each facies indicates subdepositional environments within the distal offshore realm of a mixed siliciclastic to carbonate shoreline. The offshore realm is characterized by a homoclinal ramp divided into three sectors: basinal ramp, distal outer ramp, and proximal outer ramp (Fig. 11, 12, 14).

Basinal outer-ramp. Lithology is dominated by packages of facies 2 (radiolarian-bearing fMs) interbedded with volumetrically minor amounts of facies 1 and 3 (Fig. 14). Environment is dominated by micrite, derived from a combination of pelagic nannofossils and shallow water contour current-transported carbonate derived from the east/carbonate platform-dominated shoreline (Fig. 2, 12), but it is characterized by deposition of biogenic pelagic tests (typical of facies 2) and low concentration of transported detrital material (Fig. 11).

Distal outer-ramp. Lithology is dominated by facies 1 (detrital silt-bearing fMs) interbedded with rare facies 2 and 3 (and facies 7 in the southern-most location) (Fig. 14). The environment is also dominated by micrite, derived from a combination of pelagic nannofossils and shallow water contour current-transported carbonate derived from the east/northern carbonate platform-dominated shoreline (Fig. 2, 12). However, it is characterized by relatively high dilution from detrital material derived from gravity flows moving northward and westward from the siliciclastic-dominated southern shoreline, and deposition of relatively minor biogenic pelagic input compared to the basinal ramp environment (Fig. 11). In the upper Pilmatué Member, facies 1 (4 samples) show an increase in illite and decrease in carbonate. At the same stratigraphic positions the

southernmost locality contains isolated, discontinuous floatstone beds, which are interpreted herein as local bioherms, suggesting a more proximal environment within the distal outer-ramp. Analogous outer-ramp buildups have been documented in similar cratonic basin (Burchette and Wright 1992).

Proximal outer-ramp. Lithology is dominated by facies 4, wackestone, interbedded with volumetrically minor amounts of facies 1 and 3, and even less amounts of facies 2 (Fig. 14). The environment is also dominated by micrite, derived from a combination of pelagic nannofossils and shallow water contour current-transported carbonate derived from the east/northern carbonate platform-dominated shoreline, though to a lesser degree than the basinal and distal outer ramp environments (Fig. 2, 12). Additionally, the proximal outer ramp is characterized by the highest dilution by sediment gravity flows of detrital material, and by coarser-grained macrofossil shell debris, both sourced from the siliciclastic-dominated southern shoreline and suggesting a more proximal location compared to the distal outer ramp, but just below storm wave base (Fig. 11).

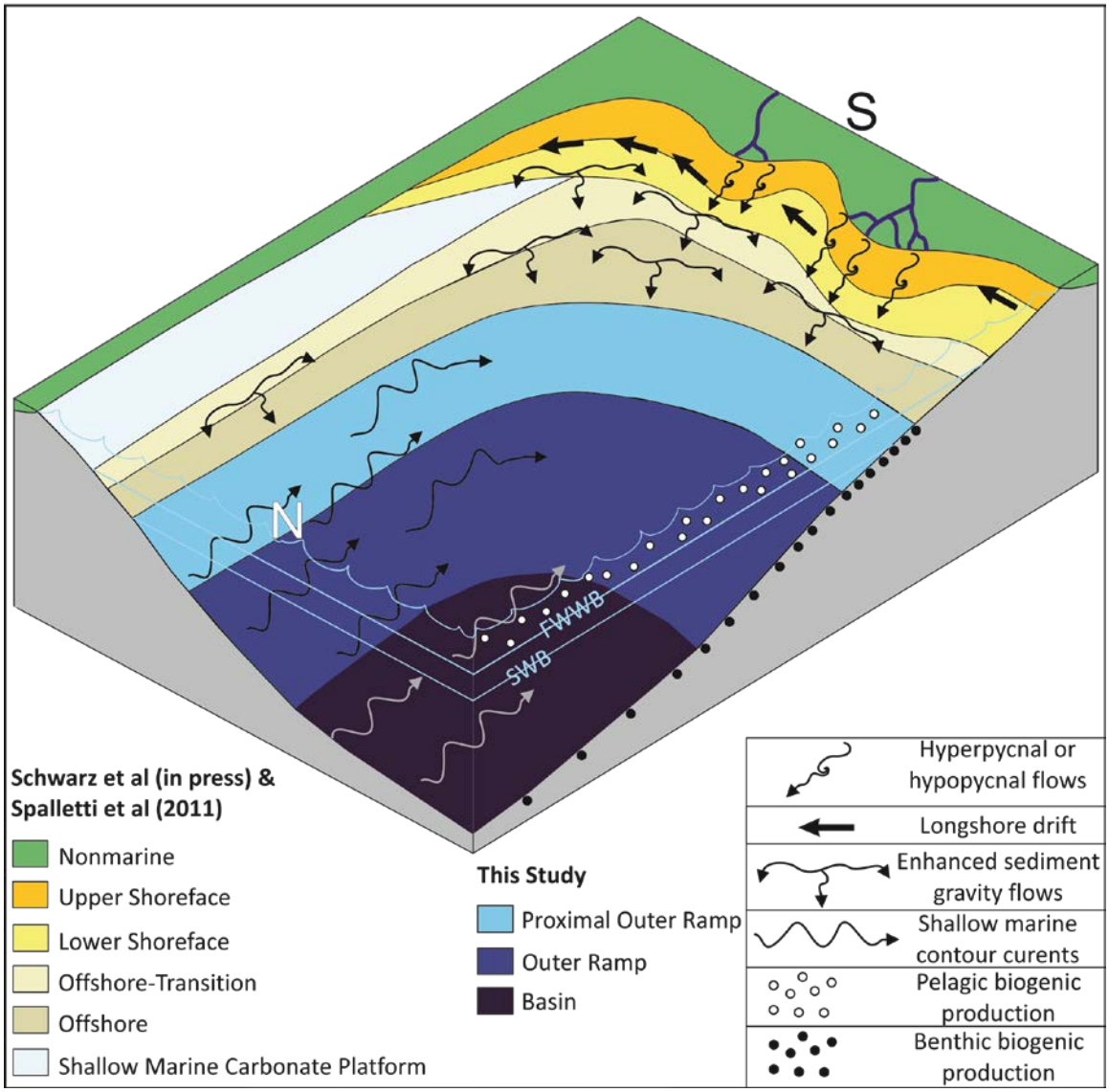

Figure 12. Schematic illustration of interpreted distal environments of deposition from the sections measured within this study. Depositional mechanisms outlined. The southern siliciclastic shoreline is modified from Schwarz et al. (2018), and the northern carbonate and siliciclastic shoreline is modified from Spalletti et al. (2011).

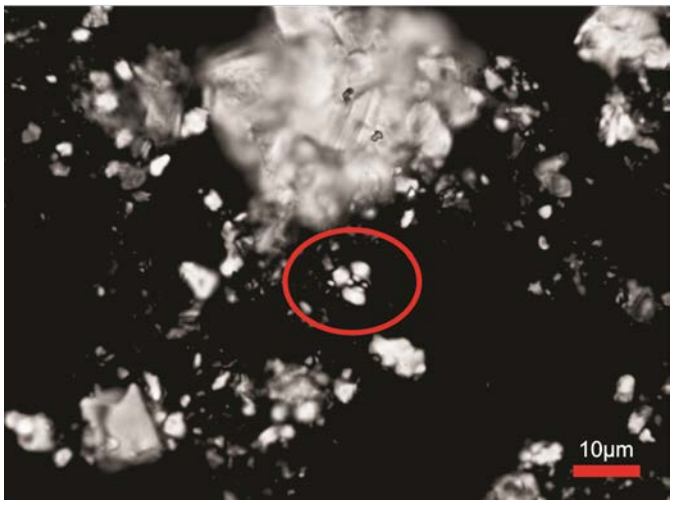

Figure 13. Smear slide of facies 2 showing a Watznaueria barnesiae calcareous nannofossil. Advanced diagenetic alteration including breakage is exhibited (red circle).

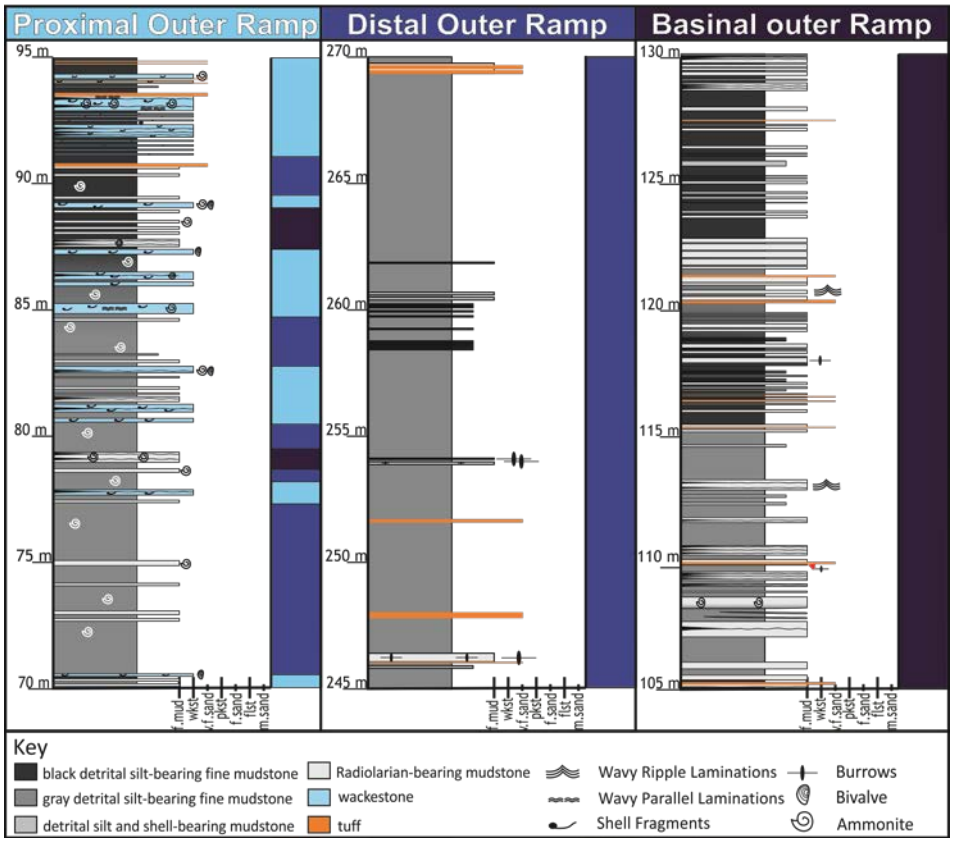

Figure 14. Lithologic logs characteristic of the three subdepositional environments established in this study.

STRATIGRAPHIC STACKING PATTERNS

Parasequences and Parasequence Sets

Utilizing proximal to distal trends established by the proposed depositional model, local scale parasequences and parasequence set stacking patterns were established and correlated to the stratigraphic framework of Schwarz et al. (2018) from localities to the south of the study area (Fig. 15, 16). A parasequence was identified in this study as a shallowing upwards stratigraphic package overlain by a flooding surface. The shallowing upward trend of a parasequence was interpreted where distal facies transitioned to proximal facies upwards, which could be the result of fluctuation in relative sea level or climatic oscillations. Flooding surfaces that top each parasequence were identified by a stratigraphically abrupt basinward shift in facies (i.e., proximal to distal depositional environment). Parasequence sets were identified based on observed progradational, aggradational, or retrogradational stacking patterns of multiple parasequences. A progradational stacking pattern of parasequences was identified by multiple, stacked parasequences (consisting of a parasequence set) that display a progressive, stepwise shallowing upward expression with the stacking of each parasequence. In contrast, a retrogradational stacking pattern was identified by multiple, stacked parasequences that display a progressive, stepwise, deepening upward expression with the stacking of each parasequence. As such, parasequence sets (or systems tracts) were assigned using the following terminology (*sensu* Neal and Abreu 2009): aggradational to progradational

parasequence set (APPS), progradational to aggradational parasequence set (PAPS), and retrogradational to aggradational parasequence set (RAPS) terminology. The stacking of each parasequence set type together in turn represents one sequence, bound by a sequence boundary (SB), and containing a maximum flooding surface (MFS) and transgressive surface (TS) (*sensu* Neal and Abreu 2009).

Eight parasequence sets were identified spanning from the proximal zones described by Schwarz et al. (2018) to the most distal deposits of this study (Fig. 16). Since interval one is interpreted as an APPS, and the overlying interval two as a RAPS, the surface between them is interpreted as a combined sequence boundary and transgressive surface (SB/TS). Combined SB/TS are also found at the top of intervals three, five and seven (APPS). The sequence boundaries never express subaerial exposure. Vice versa, since interval two is a RAPS and interval three is an APPS, the surface between them is interpreted as a maximum flooding surface (MFS). MFS are also found at the top of intervals four, six and eight (RAPS). These eight parasequence sets and their key stratigraphic surfaces constitute four full composite sequences that correlate basin wide (Fig. 16).

Absolute ages both from the proximal and the distal sectors (Schwarz et al. 2016, 2018; Aguirre-Urreta et al. 2017) support that the units analyzed are coeval (i.e., parasequence set 4 in the proximal area report 130.0 +- 0.8 Ma, whereas in the distal area it reports 130.34 +-0.03 Ma) (Fig. 16). The stratigraphic correlation datum chosen, the top of the Avilé Member, is a known regionally extensive chronostratigraphic surface, thought to represent flooding following the deposition of the Avilé Member during lowstand (Spalletti et al. 2011; Schwarz et al. 2018). Additionally, possible

chronostratigraphic tie points include altered tuffs, though detailed tuff correlation was not in the scope of this study. A prominent zone of concretions in the basal portion of the Pilmatué Member in both study localities act as an additional stratigraphic marker supporting the correlation zones established herein.

In general, downdip stacking patterns follow updip stacking patterns (Fig. 16). This is particularly evident in the prominent retrogradational stacking (i.e., back-stepping) visible in both the distal and proximal zones of parasequence set 4 (Fig. 16). This age correlation and stacking pattern consistency in the stratigraphic framework from both this study and Schwarz et al. (2018) provides an independent test of the validity of the depositional model developed herein (Fig. 16). In the distal portion of the system, retrogradational and aggradational packages are expanded relative to the proximal portion (e.g., interval four), as the system was likely not accommodation limited in the distal portion. Similarly, the aggradational phase of APPS intervals three and seven is more pronounced in the distal portion of the system with the progradational phase more pronounced in the proximal portion. Most notable is the lack of PAPS in the entire analyzed stratigraphic unit. In general, PAPS form when sedimentation rate is outpacing accommodation (Neal and Abreu 2009). It is not surprising that this particular stacking pattern is not present in a distal mudstone deposit, where accommodation was relatively high and sediment input (or sedimentation rates) are relatively low in the offshore marine setting. Under these high accommodation, low sediment supply conditions, only a major drop in relative sea level would deliver high amounts of sediment to this portion of the ramp. The variation in accommodation between the shore-proximal and offshore distal

ramp settings suggests erosional unconformities may be significant in shore-proximal successions of the Agrio Formation.

Figure 15. Google Earth image showing this studies localities and localities from Schwarz et al. (2018) that are utilized for a stratigraphic correlation of the Pilmatué Member.

Figure. 16. Stratigraphic correlation of the Pilmatué Member from this study to the stratigraphic cross-section to the south, as presented by Schwarz (2018). The contact between the Avilé and Agua de la Mula Members is the datum horizon. Eight parasequence set intervals are numbered, labeled as aggradational to progradational (APPS) or retrogradational to aggradational (RAPS), and separated by dashed white lines indicating maximum flooding surfaces (MFS) or combined sequence boundaries and transgressive surfaces (SB/TS).

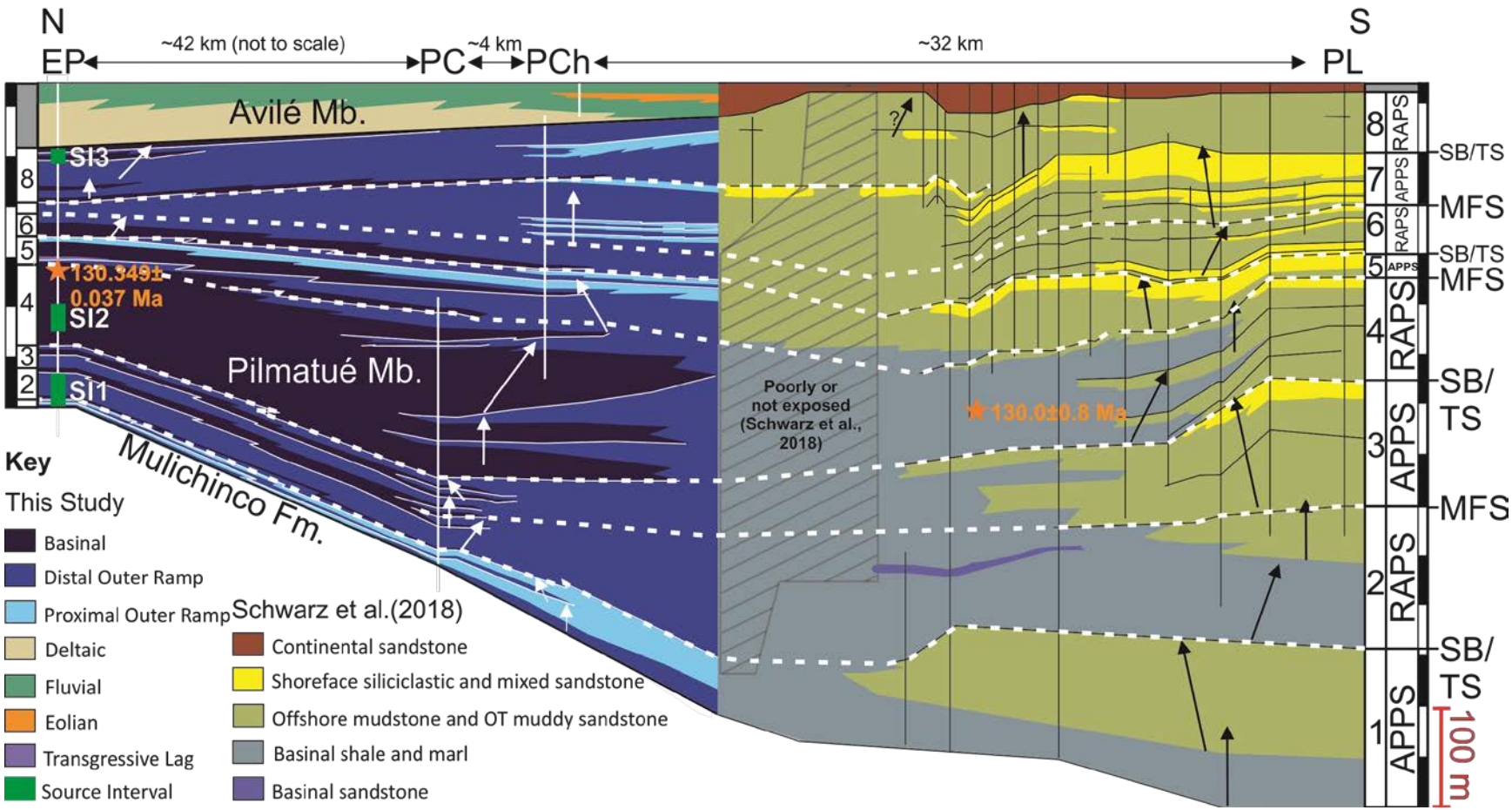
N
S
EP
~42 km (not to scale)
PC
~4 km
PCh
~32 km
PL
Avilé Mb.
Pilmatué Mb.
Mulichinco Fm.
SI3
SI2
SI1
130.349±
0.037 Ma
130.0±0.8 Ma
Poorly or
not exposed
(Schwarz et al.,
2018)
?
8
7
6
5
4
3
2
1
RAPS
APPS
RAPS
APPS
RAPS
APPS
SB/TS
MFS
SB/TS
MFS
SB/
TS
MFS
SB/
TS
100 m
Key
This Study
Basinal
Distal Outer Ramp
Proximal Outer Ramp
Deltaic
Fluvial
Eolian
Transgressive Lag
Source Interval
Schwarz et al.(2018)
Continental sandstone
Shoreface siliciclastic and mixed sandstone
Offshore mudstone and OT muddy sandstone
Basinal shale and marl
Basinal sandstone

SOURCE POTENTIAL

The main programmed pyrolysis proxies of interest for evaluating source potential and thermal maturity in this assessment are TOC, S2, HI, OI, and Tmax. The programmed pyrolysis data from the measured sections in this study allow for a comparison of source potential by facies as well as by locality and stratigraphic interval. This makes possible a north (paleo-updip/ proximal) to south (paleo-downdip/ distal) proxy comparison within the Pilmatué Member, as well as a proxy understanding of the Agua de la Mula Member in the north only.

For several reasons, an evaluation of source potential by facies will focus on facies 1 and 2 only. First, these are the most volumetrically abundant facies by a significant margin (Appendices A, B, C). As such, they are the only facies with a statistically significant number of programmed pyrolysis data points (Table 4). Additionally, these facies are most relevant and comparable to previous literature concerning the source potential of the Agrio, with facies 1 equivalents typically described as the main organic matter bearing facies (Cruz et al. 1996; Tyson et al. 2005). Contrary to this assumption, geochemical analysis of programmed pyrolysis data indicates facies 1, on average, are only slightly TOC enriched (avg. 1.57 wt.%) relative to facies 2 (avg. 1.2 wt.%) and S2 values indicate that facies 2 (avg. 3.97 mg HC/g rock) has a slightly higher source quality that facies 1 (avg. 3.44 mg HC/g rock). Overall there is a high degree of heterogeneity associated with the source of organic material in these samples, particularly

for facies 1 and 2; with HI and OI trends plotting largely along Type II and mixed Type II/III trends (Fig. 8a). Perhaps most significantly, facies 2 displays more marine-dominated organic matter trends than the more mixed terrigenous/marine trends of facies 1 (Fig. 8b). This indicates that facies 2 may be more oil prone in general then facies 1. Because of this weak relationship between source potential and facies, with both of the dominant facies acting as potential source units, identification of source rock intervals herein will focus on identifying temporally or stratigraphically significant intervals.

In this study, high source potential is defined as samples that display the following geochemical characteristics: TOC ≥ 2 wt.%, S2 ≥ 5 mg HC/g rock, and HI ≥ 300 mg HC/g TOC (Peters 1986; Peters and Casa 1994; Pepper and Corvi 1995a, 1995b). Both northern and southern localities display samples that meet the established TOC and S2 value criteria for high source potential (Table 5; Fig. 17a, b). However, HI values are low throughout the southern localities (Table 5; Fig. 17c) with no southern samples meeting the established HI value criteria. HI values and geochemical diagrams of the data indicates the northern locality, El Portón, is dominated by marine to mixed terrigenous and marine organic material, whereas the southern localities, Puerta Curaco and Puesto Chivito, are dominated by terrigenous to inert organic material (Fig. 8, 17c). Tmax values indicate that the Pilmatué Member ranges from early oil mature to peak oil maturity in the north and from peak oil maturity to late oil mature at the southern localities (Fig. 17d). The Agua de la Mula in the north largely ranges from immature to early oil mature (Fig. 17d).

Based on stratigraphic clustering of samples reaching the above established geochemical cutoffs, five source intervals have been established within the Aqua de la

Mula and Pilmatué Members at the northern El Portón locality (Table 6). Source interval one (SI1) is positioned in the basal portion of the Pilmatué member, mostly within stratigraphic interval two, and has a thickness of ~30 m (Fig. 16, 18). Source interval two (SI2) is positioned within stratigraphic interval four of the Pilmatué Member and has a thickness of ~25 m (Fig. 16, 18). Source interval 3 (SI3) is isolated to the upper portion of the Pilmatué Member and is ~20 m thick (Fig. 16, 18). Source intervals 4 and 5 (SI4, SI5) are located within the Agua de la Mula Member and are ~7 m and ~50 m thick, respectively (Fig. 19).

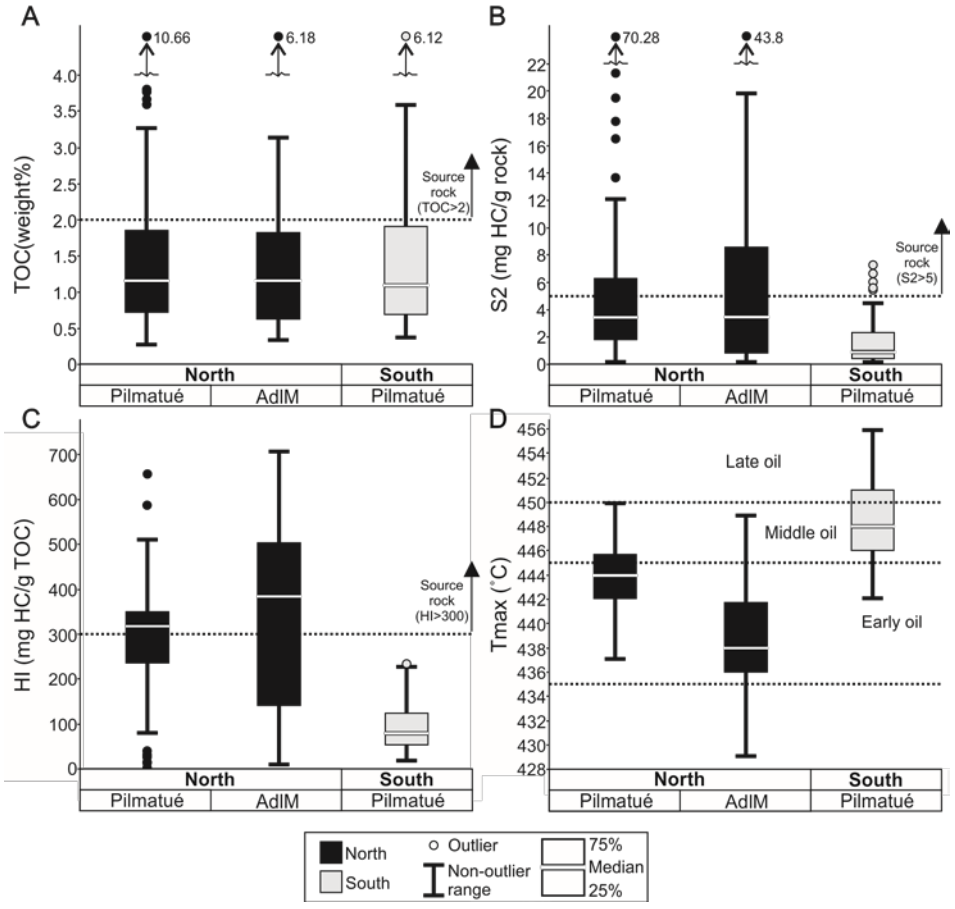

Figure 17. Variations in geochemical properties by location and member based on programmed pyrolysis. Box plots show median, distribution quartile, nonoutlier range, and outliers of each parameter.

Figure 18. Log data for the Pilmatué Member at the northern El Portón locality. Includes lithology, depositional environment interpretations, and XRD and programmed pyrolysis data. Samples with source rock potential are marked with a star. Yellow stars are for samples for which stratigraphic height is precisely known and white stars are for samples for which approximate stratigraphic height is known. Priority source rock intervals are numbered and highlighted in green, with the darker green representing conservative thickness, and the lighter green representing liberal thickness.

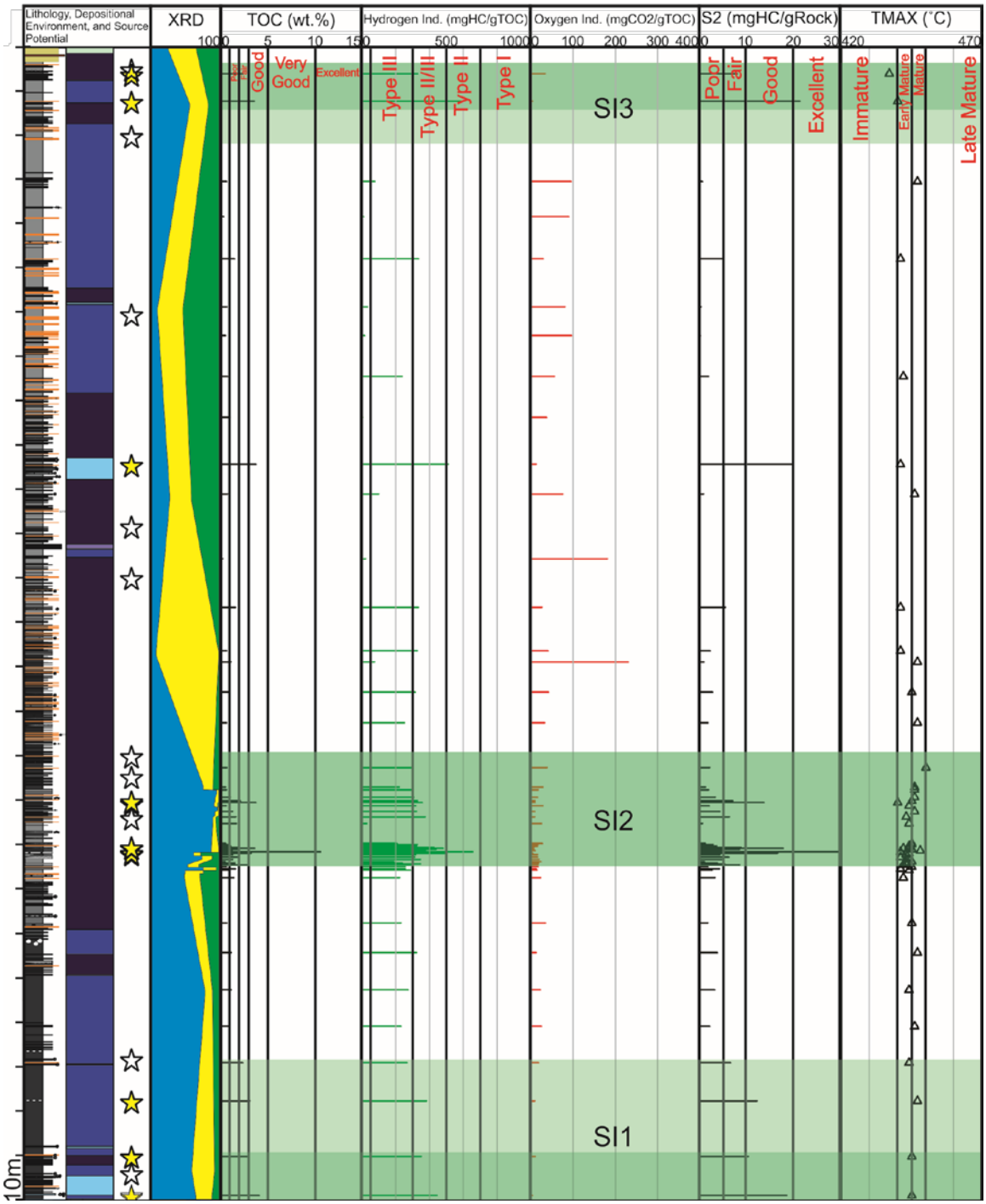
Lithology, Depositional Environment, and Source Potential
XRD
TOC (wt.%)
Hydrogen Ind. (mgHC/gTOC)
Oxygen Ind. (mgCO2/gTOC)
S2 (mgHC/gRock)
TMAX (°C)
Poor
Fair
Good
Very Good
Excellent
Type III
Type II/III
Type II
Type I
Pobr
Fair
Good
Excellent
Immature
Early Mature
Mature
Late Mature
SI3
SI2
SI1
10m

Figure 19. Log data for the Agua de la Mula Member at the northern El Portón locality. Includes lithology, depositional environment interpretations, and XRD and programmed pyrolysis data. Samples with source rock potential are marked with a star. Yellow stars are for samples for which stratigraphic height is precisely known and white stars are for samples for which approximate stratigraphic height is known. Priority source rock intervals are numbered and highlighted in green, with the darker green representing conservative thickness, and the lighter green representing liberal thickness.

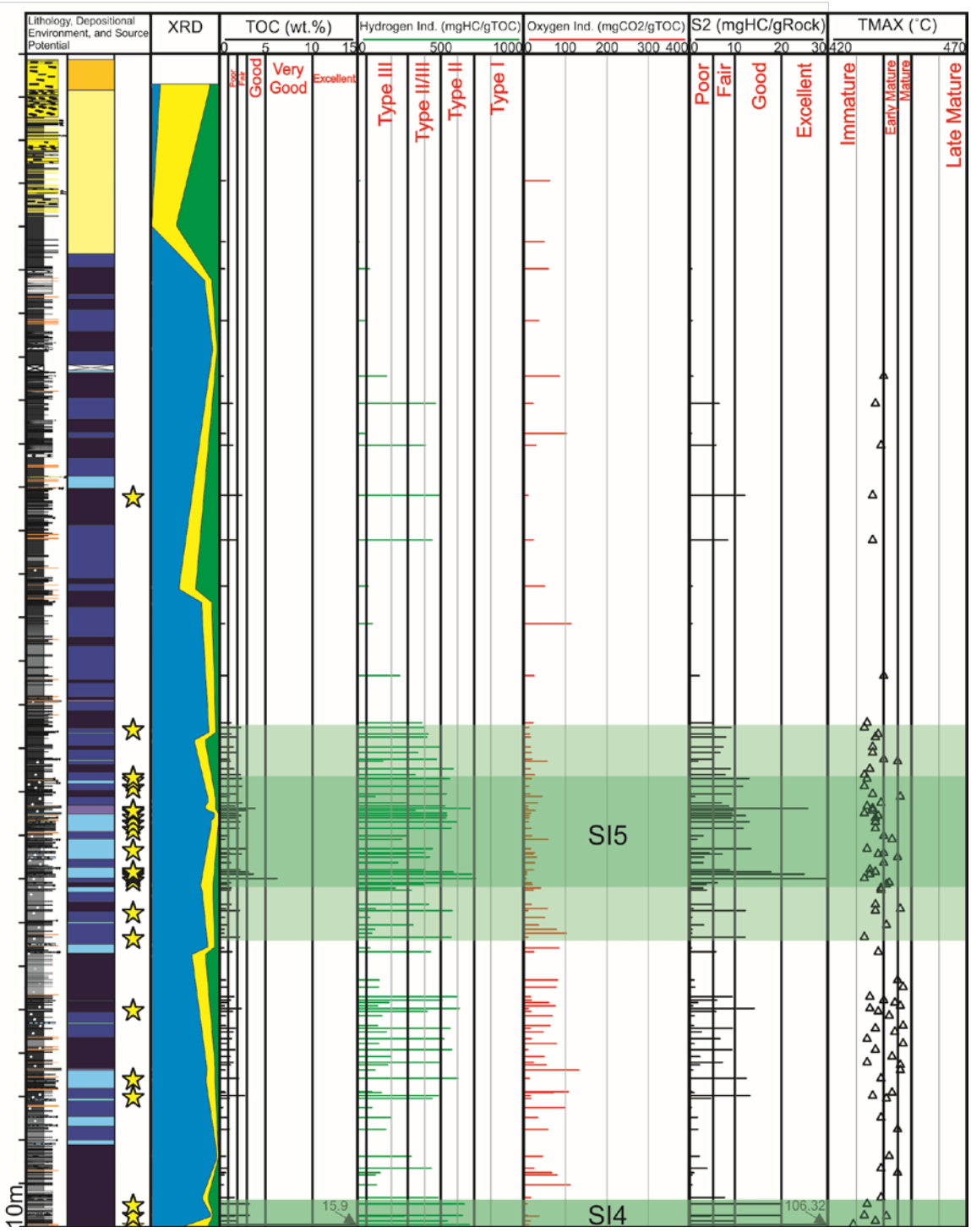
Lithology, Depositional Environment, and Source Potential
XRD
TOC (wt.%)
0
5
10
15
Poor
Fair
Good
Very Good
Excellent
Hydrogen Ind. (mgHC/gTOC)
100
500
1000
Type III
Type II/III
Type II
Type I
Oxygen Ind. (mgCO2/gTOC)
100
200
300
400
S2 (mgHC/gRock)
0
10
20
30
Poor
Fair
Good
Excellent
TMAX (°C)
420
470
Immature
Early Mature
Mature
Late Mature
SI5
SI4
15.9
106.32
10m

Table 5. Programmed pyrolysis data by area and member with averages bolded

Area	Member	TOC (w.t %)	S2 (mg HC/g rock)	HI (mg HC/g TOC)
North	Agua de la Mula (*n=97*)	0.31-15.9 (**1.56**)	0.04-106.32 (**7.14**)	6-709 (**339**)
	Pilmatué (*n=55*)	0.25-10.66 (**1.69**)	0.05-70.28 (**6.38**)	7-695 (**289**)
South	Pilmatué (*n=137*)	0.35-6.12 (**1.37**)	0.06-7.30 (**1.52**)	14-234 (**96**)

Table 6. El Portón source intervals (numbered)

Member	Source interval	Stratigraphic height (m)	Stratigraphic thickness (m)
Agua de la Mula	5	415-463	48
	4	350-357	7
Pilmatué	3	268-285	17
	2	105-130	25
	1	30-62	32

DISCUSSION

Depositional Model

The Agrio Formation displays a bulk mineralogic composition that resembles the carbonate-rich Eagle Ford Group, one of the most significant unconventional plays worldwide (Fig. 20). There are additional similarities in the Agrio and Eagle Ford depositional models. During the deposition of the Eagle Ford, the Cretaceous Western Interior Seaway displayed a fluvial to deltaic siliciclastic shoreline along the eastern margin and a carbonate platform shoreline along the southern margin (Fairbanks et al. 2016). This is similar to the lateral transition from a deltaic shoreline to longshore current-dominated shoreline to shallow marine carbonate platform along the margin of the Neuquén Basin during the deposition of the Agrio Formation. Recent studies on the Eagle Ford have depicted dynamic deposition (Fairbanks et al. 2016; Frébourg et al. 2016; Minisini et al. 2018), where the dominant mechanisms of deposition include variations in primary productivity of planktonic foraminifera and reworking by bottom currents, similar to the shallow water contour currents described in this study. A further similarity is the presence of alternating of mudstone-carbonate beds, at meter scale, related to climate cyclicity (Sagasti 2005; Eldrett et al. 2015).

Even with similar shoreline dynamics and the shared designation as mixed carbonate-siliciclastic systems, the resulting Eagle Ford and Agrio Formation systems vary considerably. The main differences are thickness (Agrio up to ~1,000 m, Eagle Ford

up to 120 m), siliciclastic input (abundant detrital quartz silt in Agrio, lack of detrital quartz in Eagle Ford with illite as the main detrital input), and source of carbonate mud (pelagic and detrital/transported in Agrio, only pelagic in Eagle Ford). When comparing similar time spans, the detrital carbonate mud and the siliciclastic sediment input of the Agrio caused a higher sediment accumulation rate, hence a thicker stratigraphic package than in the Eagle Ford. The Agrio's higher sediment accumulation rate ultimately preserved a succession suitable to study lithologies with higher stratigraphic resolution, in fact. Importantly, no one offshore model can be imposed onto these mixed siliciclastic-carbonate mudstone deposits. Each will behave differently due in part to the complexities of multiple sediment sources and lateral variations in shoreline dynamics.

Though the mudstone facies of the Agrio Formation presented in the study area are dominated by carbonate with minor siliciclastic siltstone content, sedimentologic and stratigraphic studies paleodepositionally updip from our study indicate siliciclastic dominance of the updip shoreline to the south of this study area (Veiga and Schwarz 2017; Schwarz et al. 2018). As such, the Agrio Formation cannot be understood by considering a single point source or 2-dimensional updip-downdip depositional profile, but rather, as a whole, representing a 3-dimensional mixed carbonate-siliciclastic system. Thin sections and XRD analyses distinguish systematic compositional and microfossil variability, allowing the identification of multiple facies, each of them associated with an environment of deposition. Consequently, the high resolution of the dataset allowed for the designation of previously unidentified depositional subenvironments. The depositional system was much more dynamic than previously thought and represents

inputs from both the southern and east/northeastern paleoshorelines of the Neuquén Basin.

Stratigraphic Stacking Patterns

The multiple existing studies on the stratigraphy of the Agrio Formation have focused on stratigraphic packaging rather than on developing a detailed sequence stratigraphic framework. Previous stratigraphic analyses have generally been performed on outcrop localities characterized by the presence of sandstone bodies, where shallowing upwards successions (or parasequences) are more clearly delineated (i.e., Legarreta & Uliana 1991; Spalletti et al. 2001a, 2001b; Lazo 2007a, 2007b). Only a few studies focused on the distal portion of the basin, where it is more difficult to distinguish grain size variations (Spalletti et al. 2001b; Schwarz et al. 2018). For instance, Spalletti et al. (2001a) utilized onlapping and downlapping patterns visible in a laterally extensive outcrop section to define three sequence sets of 3rd order in the Agua de la Mula Member; and Schwarz et al. (2018) strengthened the stratigraphic understanding of the Pilmatué Member northward but admitted the difficulty in identifying sequences in the most distal (sandstone limited) portion of the basin further to the north, the geographic focus area of this study. Deposits that were classified as “basinal” by Schwarz et al. (2018) were further distinguished and subdivided in this study based on the facies criteria outline herein. Through this differentiation, this study was able to relate stratigraphic and paleogeographic variability in the distal realm to updip stratigraphic packages developing a meaningful genetic framework for the organic-rich, mud-dominated portion of the stratigraphy. Recognition of systematic heterogeneity provides a predictive model for the

Agrio Formation as not only a source rock, but also an emerging unconventional hydrocarbon system.

The current model for tectonic phases and large scale depositional controls within the Neuquén Basin dictates that subsidence and accommodation during the deposition of the Agrio Formation was driven by a combination of widespread passive thermal subsidence in a generally extensional setting and eustacy with little to no influence by active tectonism beyond a localized scale (Legarreta and Gulisano 1989; Legarreta and Uliana 1991; Vergani et al. 1995; Ramos and Folguera 2005; Spalletti et al. 2011). However, the combination of eustacy and passive thermal subsidence does not account for the magnitude relative sea-level change documented in the Agrio. In the Agrio, facies deposited in basinal to distal outer ramp (below storm wave base) in the uppermost Pilmatué Member are overlain by deltaic, then fluvial, then eolian facies of the Avilé Member, and thus indicating a relative sea level fall of 20-70 m, based on the average depth of storm wave base in open ramp systems (Immenhauser 2009). Previous studies indicate this may be a conservative estimate and that water depths in the Neuquén Basin during the accumulation of the Pilmatué and Aqua de la Mula Members may have reached up to 200 m (i.e., Sagasti 2005). Similarly, basinal facies overlie the top of the fluvial to eolian facies at the top of the Avilé Member, recording a similar magnitude of relative sea level rise. Because relative sea level change reflects changes in the ratio of sediment supply to accommodation, between 70 and 200 m of relative sea level change requires a large shift in either sediment supply, accommodation, or both. Absolute sea-level fluctuations during the Cretaceous greenhouse, which was free of continental ice-sheets, have an amplitude of ~15-50 m with calculated rates of sea-level change ranging

from ~10-60 m/Ma (Sømme et al. 2009; Kidder and Worsley 2010). Only few authors dispute this ice-free view (e.g., Plint et al. 2009). Therefore, eustasy could only account for 10s of m of sea level change at most. These magnitudes of eustatic shifts paired with thermal subsidence are unlikely to account for not only the shifts in relative sea level apparent in the facies of the Agrio, but also the amount of accommodation necessary to accumulate over 1000 m of sediment in a shallow epeiric, open ramp environment.

Additionally, passive thermal subsidence and general extension is an oversimplification for the tectonic processes occurring in a basin experiencing active subduction along its western margin. Though it can be difficult to separate the effects of various subsidence mechanisms from one another, models predict that depressions of over 500 m occur over subduction slabs due to dynamic topography alone (Allen and Allen 2013). In addition to thermal subsidence and isostatic effects of lithospheric thickness changes due to shortening that occur in the overlying plate Decelles et al. (2009) present a cyclic model, for both North and South American Cordilleran orogenic systems, of dynamic upper-plate processes focused on the growth and removal of dense eclogitic roots. In this model the cyclic arc root growth and removal leads to alternating periods of negative buoyancy with the prevention of further underthrusting and periods of isostatic uplift with rapid renewal of underthrusting respectively. Such tectonic cycles could have been affecting the Neuquén Basin, aiding in the creation of accommodation during the deposition of the Agrio and facilitating the end of marine sedimentation represented by the deposition of the Huitrín Formation. A detailed comparison of the stratigraphy of the Agrio Formation and the timing of high-flux events associated with the formation of eclogite roots would establish if this model was helpful in understanding

accommodation in the Neuquén Basin. To further complicate the basin tectonic history, the emplacement of the Paraná-Etendeka large igneous province (between 133-131 Ma) occurred roughly 400 km east of the Neuquén basin as the time the Agrio Formation was deposited (Renne et al. 1996). Large igneous provinces such as this can cause loading and even crustal doming over distances of up to 700 km (He et al. 2003).

Importantly, the data from this study suggest sea level change during the deposition of the Agrio Formation was driven by tectonics not eustasy alone. Similarly, in the Eagle Ford Group, authors assert regional tectonics drove sea level change (Minisini et al. 2018). In short, tectonic and/or climatic mechanisms for significant changes in the ratio of sediment supply to accommodation in the Neuquén Basin during the Early Cretaceous should be reexamined through a basin-scale analysis. The stratigraphic assessment presented in this study can help to calibrate these types of analyses.

Geochemistry and Source Potential

There have been a number of studies focused on the petroleum system of the Agrio Formation, which utilize geochemical characterization of source potential to various degrees (Legarreta and Uliana 1991; Uliana and Legarreta 1993; Urien and Zambrano 1994; Cruz et al. 1996, 1998; Kozlowsky et al. 1998; Uliana et al. 1999; Tyson et al. 2005; Spalletti et al. 2011). In general, the geochemical analyses of these studies rely on limited data points, focus almost exclusively on the basal section of the Agua de la Mula and Pilmatué Members, and lack more than a very basic integration with stratigraphy and facies characterization. Previous work supports the overall increase in

organic richness from south to north within the Neuquén province that is suggested by S2 and HI values across this study area (Tyson et al. 2005) (Fig. 17). The depositional model presented herein may shed light on this trend, with the more siliciclastic shoreline-proximal southern localities receiving a higher proportion of original terrigenous organic matter (Fig. 2). Additionally, in the southern more proximal portion of the basin, organic matter may have been affected by a higher degree of degradation due to oxic conditions and/or increased bioturbation. Preferential degradation of the more liable marine organic compounds would lead to enrichment of the more molecularly stable terrigenous background organic matter (Hoefs et al. 2002; Sinninghe Damasté et al. 2002; Forster et al. 2008). An alternative explanation for the increase in organic richness from south to north in programmed pyrolysis data could be the effects of maturity overprints based on kerogen conversion behavior (Pepper and Corvi 1995a, 1995b; Pepper and Dodd 1995). The higher thermal maturity in the southern localities could cause increased kerogen conversion behaviors, obscuring the original or depositional source potential within this portion of the basin. Though it is beyond the scope of this work, future studies could explore establishing kinetic models specific to the Agrio Formation to correct the programmed pyrolysis data to original depositional values.

Previous outcrop- and well-based studies largely indicate that the basal sections of the Agua de la Mula Member, informally known as the “Spitidiscus shale,” and the basal and upper sections of the Pilmatué Member in the more northern portion of the basin have the highest source rock potential (Cruz et al. 1996, 1998; Kozlowsky et al. 1998; Tyson 2001). By utilizing a much higher density of sample points collected from entire sections of each member, within the portion of the Neuquén province considered to have

the highest source potential, this study is able to identify additional stratigraphic source intervals with well constrained stratigraphic heights and thicknesses. Furthermore, this study looks beyond TOC, applying filters for organic matter quality and type, and linking geochemistry, facies (depositional), and stratigraphic patterns.

Integrating the proposed facies and depositional model, the sequence stratigraphic framework, and geochemical data, reveals several key insights. Organic richness is not isolated to one facies but is fairly equally distributed across facies types (Fig. 7). Establishing source potential within the two most volumetrically abundant facies (facies 1 and 2) opens up the unconventional Agrio Formation play fairway significantly. Most significantly, this study correlates stratigraphically constrained source intervals within the Pilmatué Member to the three RAPS presented in this study. RAPS are equivalent to transgressive systems tracts, which have commonly been associated with the preservation of organic material in many unconventional systems (e.g., Slatt and Rodriguez 2012). Furthermore, condensed sections of transgressive systems tracts (or RAPS) are prime target zones for horizontal well placement in unconventional systems. Establishing the lateral extent of RAPS through sequence stratigraphy and the internal and lateral variability of these intervals through facies and depositional models are key to developing unconventional petroleum systems like the Agrio Formation. This level of correlative and predictive capability in terms of depositional source potential interval will allow these zones to be established in the subsurface. This sequence stratigraphic framework can be used to predict source intervals, even in the absence of basic organic geochemical data.

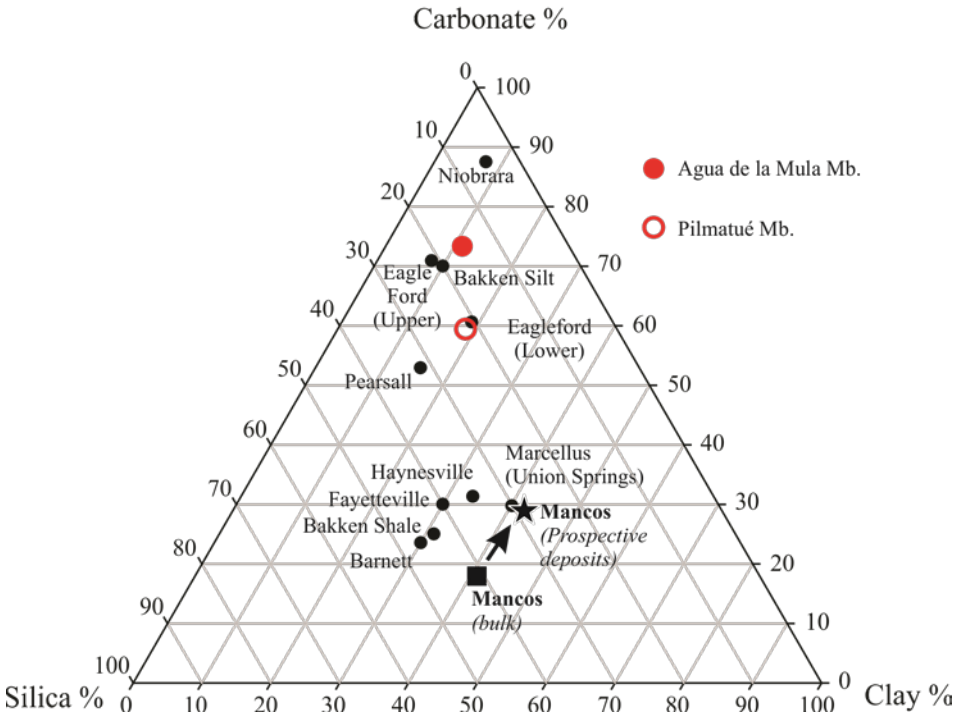

Figure 20. Composition of productive shale plays of North America in comparison to the upper Agua de la Mula Member and lower Pilmatué Member of the Agrio Formation. Based on normalized total quartz, total clay, and total carbonate content. Ternary diagram adapted from Birgenheier et al. (2017).

CONCLUSIONS

In this study area, the majority of the Pilmatué and Agua de la Mula Members of the Agrio Formation consist of seven marine facies (see Table 1). The most volumetrically abundant of which are detrital silt-bearing fMs (facies 1), radiolarian-bearing calcareous fMs (facies 2), detrital silt and shell-bearing calcareous fMs (facies 3), and calcareous wackestone (facies 4).

Based on the facies interpretation and a paleogeographic understanding of the Neuquén Basin, three depositional mechanisms are recognized: 1) Wave and/or current-enhanced sediment gravity flows that delivered updip siliciclastic fluvial and shallow marine sediment to the offshore realm; 2) Along-shore and oblique shallow water contour current-transported carbonate mud, sourced from the shallow marine carbonate platform portion of the shoreline, and 3) Production of pelagic and benthic tests, both calcareous and siliceous (i.e., nanno- and micro-fossils). The interpreted depositional environments with in this study area are basinal ramp, distal outer ramp, and proximal outer ramp.

Eight distinct parasequence sets were identified in the Pilmatué Member: four characterized as aggradational to progradational (APPS) and four as retrogradational to aggradational (RAPS). The parasequence sets define four full composite sequences. Seven key sequence stratigraphic surfaces were also regionally constrained: four combined sequence boundary and transgressive surfaces, and three maximum flooding surfaces. Both the parasequence sets and the key stratigraphic surfaces are linked to, and

support, the stratigraphic framework from a paleo-updip portion of the depositional system presented by Schwarz et al. (2018).

Utilizing previously established geochemical cutoffs, five source rock intervals have been identified within the Agua de la Mula and Pilmatué Members at El Portón. Within the context of the stratigraphic framework established herein for the Pilmatué Member, these source intervals are isolated to RAPS parasequence sets. These stratigraphic packages were correlated over 80 km in this study and can be utilized to correlate into the subsurface. The identification of depositional source intervals and their correlation, with potential to extend to the subsurface, is innovative within the Agrio Formation.

Overall facies variability, dominant dynamic depositional mechanisms, and lateral shoreline variability all played a large role in the Agrio depositional system and have implications for source rock quality, reservoir characterization, and hydraulic fracturing potential. The Agrio Formation is an ideal case study to build upon the growing number of studies on dynamic offshore systems that are of interest as unconventional systems, as it is understudied and found in a basin of international significance for hydrocarbon production. With a new depositional model and source rock evaluation of these distal prospective units, a play concept can be delineated through further investigation focused on reservoir potential and geomechanical analyses in the context of facies to determine prospective unconventional play elements. This study provides a novel integration of sedimentology, stratigraphy, and inorganic and organic geochemical datasets, which is necessary for constructing an unconventional petroleum system model of the Agrio Formation.

APPENDIX A

DRAFTED MEASURED SECTION FROM

THE EL PORTÓN LOCALITY

Appendix A- El Portón- Mulichinco Formation; Pilmatué, Avilé and Agua de la Mula Members

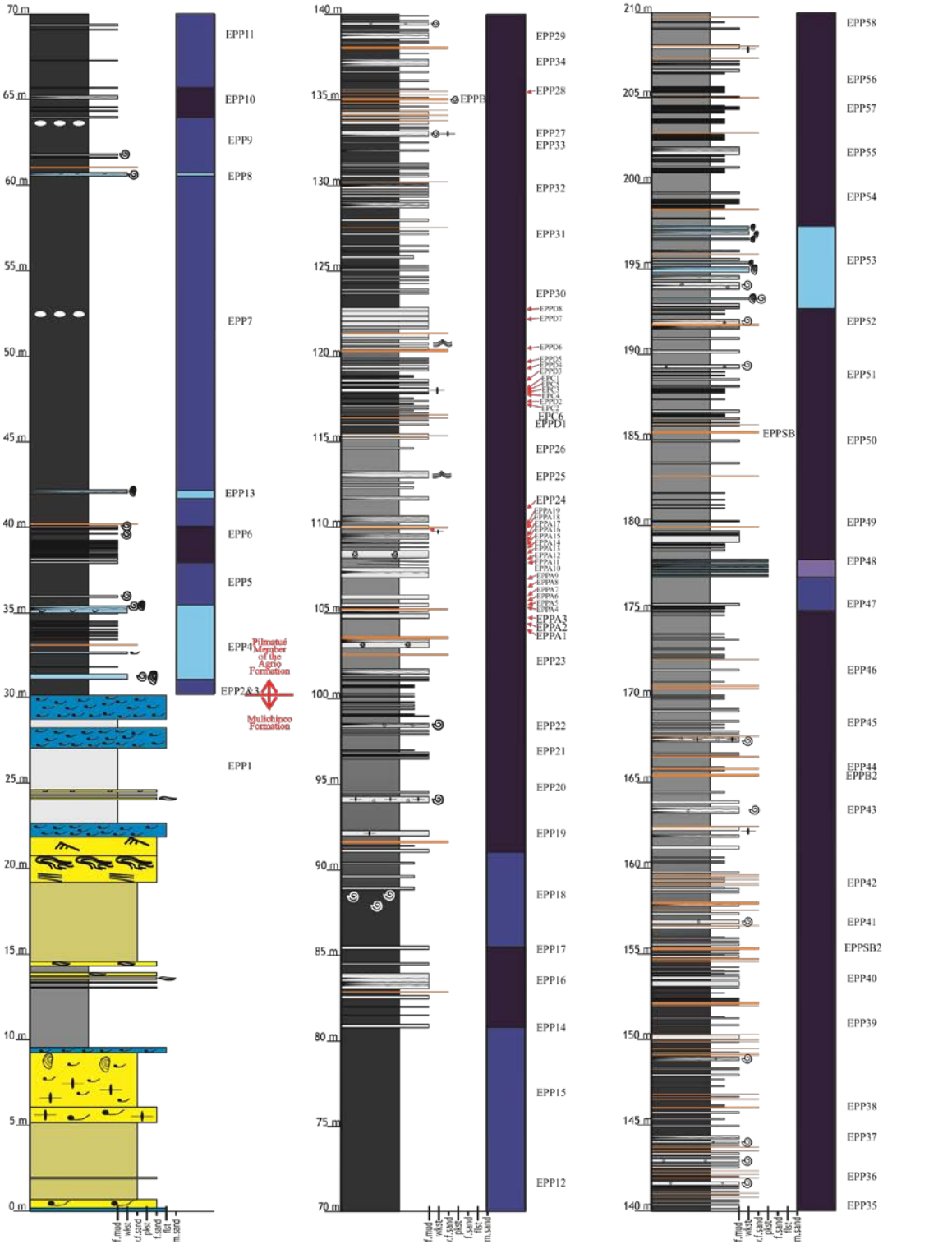

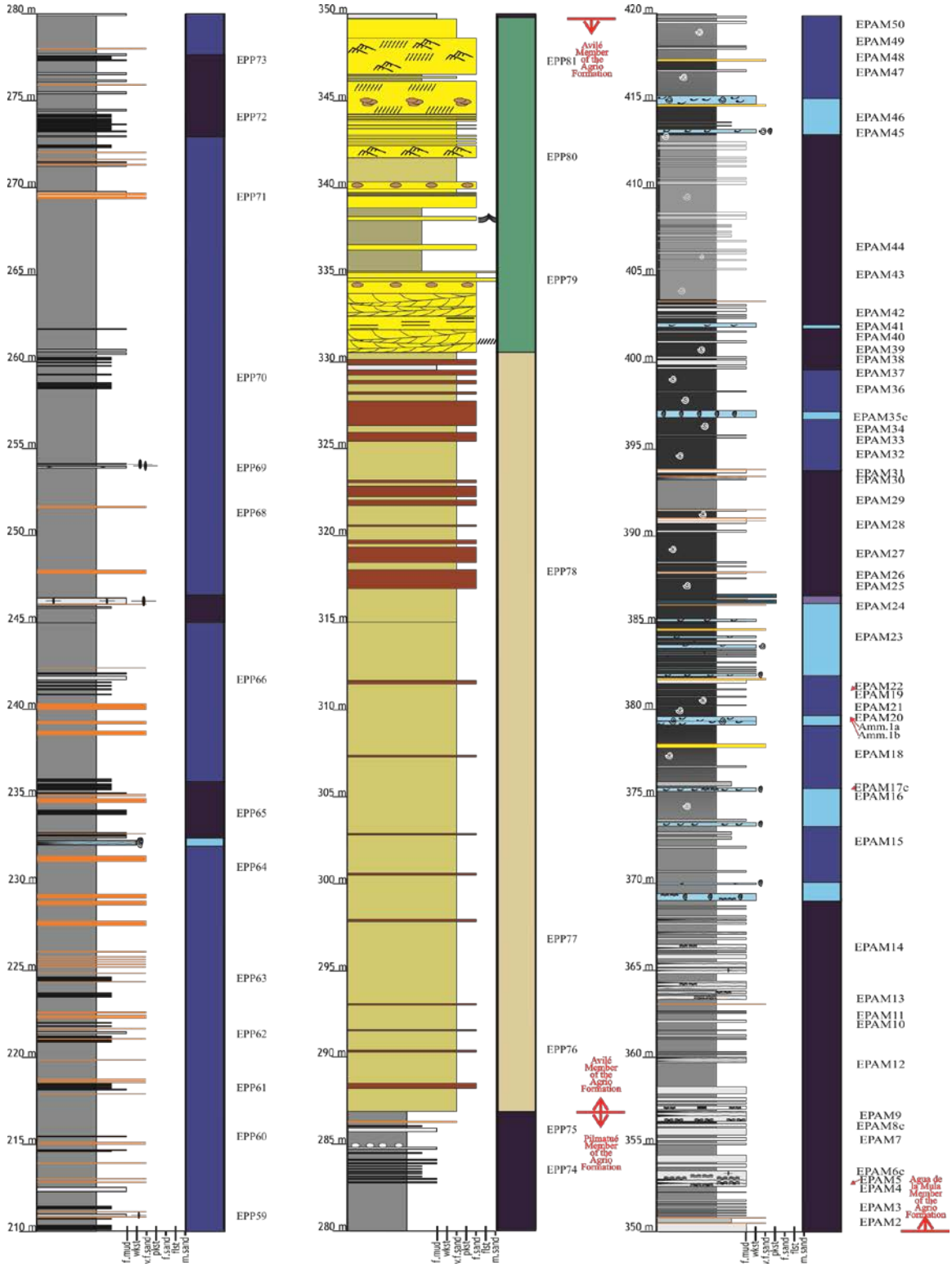
280 m
275 m
270 m
265 m
260 m
255 m
250 m
245 m
240 m
235 m
230 m
225 m
220 m
215 m
210 m
EPP73
EPP72
EPP71
EPP70
EPP69
EPP68
EPP66
EPP65
EPP64
EPP63
EPP62
EPP61
EPP60
EPP59
350 m
345 m
340 m
335 m
330 m
325 m
320 m
315 m
310 m
305 m
300 m
295 m
290 m
285 m
280 m
EPP81
Avilé Member of the Agrio Formation
EPP80
EPP79
EPP78
EPP77
EPP76
Avilé Member of the Agrio Formation
EPP75
Pilmatué Member of the Agrio Formation
EPP74
420 m
415 m
410 m
405 m
400 m
395 m
390 m
385 m
380 m
375 m
370 m
365 m
360 m
355 m
350 m
EPAM50
EPAM49
EPAM48
EPAM47
EPAM46
EPAM45
EPAM44
EPAM43
EPAM42
EPAM41
EPAM40
EPAM39
EPAM38
EPAM37
EPAM36
EPAM35c
EPAM34
EPAM33
EPAM32
EPAM31
EPAM30
EPAM29
EPAM28
EPAM27
EPAM26
EPAM25
EPAM24
EPAM23
EPAM22
EPAM19
EPAM21
EPAM20
Amm.1a
Amm.1b
EPAM18
EPAM17c
EPAM16
EPAM15
EPAM14
EPAM13
EPAM11
EPAM10
EPAM12
EPAM9
EPAM8c
EPAM7
EPAM6c
EPAM5
EPAM4
EPAM3
EPAM2
Agua de la Mula Member of the Agrio Formation
f.mud
wkst
v.f.sand
pkst
f.sand
bfst
m.sand

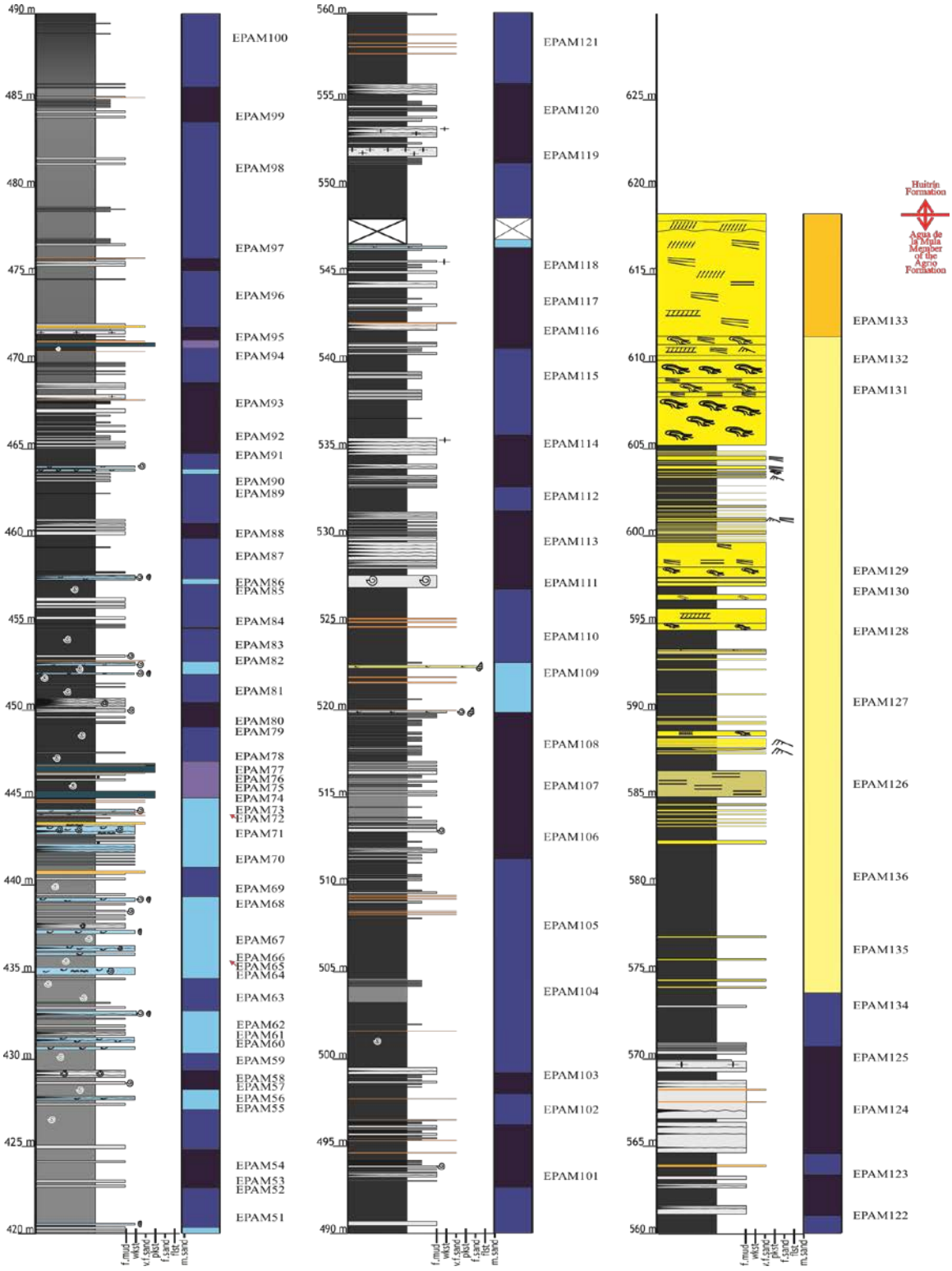
490 m
485 m
480 m
475 m
470 m
465 m
460 m
455 m
450 m
445 m
440 m
435 m
430 m
425 m
420 m
EPAM100
EPAM99
EPAM98
EPAM97
EPAM96
EPAM95
EPAM94
EPAM93
EPAM92
EPAM91
EPAM90
EPAM89
EPAM88
EPAM87
EPAM86
EPAM85
EPAM84
EPAM83
EPAM82
EPAM81
EPAM80
EPAM79
EPAM78
EPAM77
EPAM76
EPAM75
EPAM74
EPAM73
EPAM72
EPAM71
EPAM70
EPAM69
EPAM68
EPAM67
EPAM66
EPAM65
EPAM64
EPAM63
EPAM62
EPAM61
EPAM60
EPAM59
EPAM58
EPAM57
EPAM56
EPAM55
EPAM54
EPAM53
EPAM52
EPAM51
f.mud
wkst
v.f.sand
pkst
f.sand
fgst
m.sand
560 m
555 m
550 m
545 m
540 m
535 m
530 m
525 m
520 m
515 m
510 m
505 m
500 m
495 m
490 m
EPAM121
EPAM120
EPAM119
EPAM118
EPAM117
EPAM116
EPAM115
EPAM114
EPAM112
EPAM113
EPAM111
EPAM110
EPAM109
EPAM108
EPAM107
EPAM106
EPAM105
EPAM104
EPAM103
EPAM102
EPAM101
f.mud
wkst
v.f.sand
pkst
f.sand
fgst
m.sand
625 m
620 m
615 m
610 m
605 m
600 m
595 m
590 m
585 m
580 m
575 m
570 m
565 m
560 m
Huitrín Formation
Agua de la Mula Member of the Agrio Formation
EPAM133
EPAM132
EPAM131
EPAM129
EPAM130
EPAM128
EPAM127
EPAM126
EPAM136
EPAM135
EPAM134
EPAM125
EPAM124
EPAM123
EPAM122
f.mud
wkst
v.f.sand
pkst
f.sand
fgst
m.sand

Appendices Key

Lithology

- black detrital silt-bearing fine mudstone
- gray detrital silt-bearing fine mudstone
- detrital silt and shell-bearing mudstone
- Radiolarian-bearing mudstone
- sandy coarse mudstone
- tuff
- silty very fine sandstone
- silty fine sandstone
- sandstone
- wackestone
- packstone
- floatstone

Depositional Environment

- Basinal
- Distal Outer Ramp
- Proximal Outer Ramp
- Lower Shoreface
- Upper Shoreface
- Prodelta
- Fluvial
- Eolian
- Transgressive Lag

Symbols

- Trough cross-bedding
- Planar cross-bedding
- Hummocky cross-bedding
- Horizontal, planar lamination
- Low angle laminations
- Current Ripple cross-lamination
- Climbing Ripples
- Soft Sediment Deformation
- Discontinuous Wavy Parallel Laminations
- Discontinuous Wavy nonparallel Laminations
- Wave Ripples
- Wavy Ripple Laminations
- Shell Fragments
- Burrows
- Bivalve
- Ammonite
- Gastropod

Sample Codes

EPP- El Portón Pilmatué

EPAM- El Portón Agua de la Mula

PCPA- Puerta Curaco Pilmatué Alter Section

PCC- Puesto Chivito Pilmatué

ACC- Puesto Chivito Avilé

APPENDIX B

DRAFTED MEASURED SECTION FROM

THE PUERTA CURACO LOCALITY

Appendix B- Puerta Curaco- Mulichinco Formation; Pilmatué Member

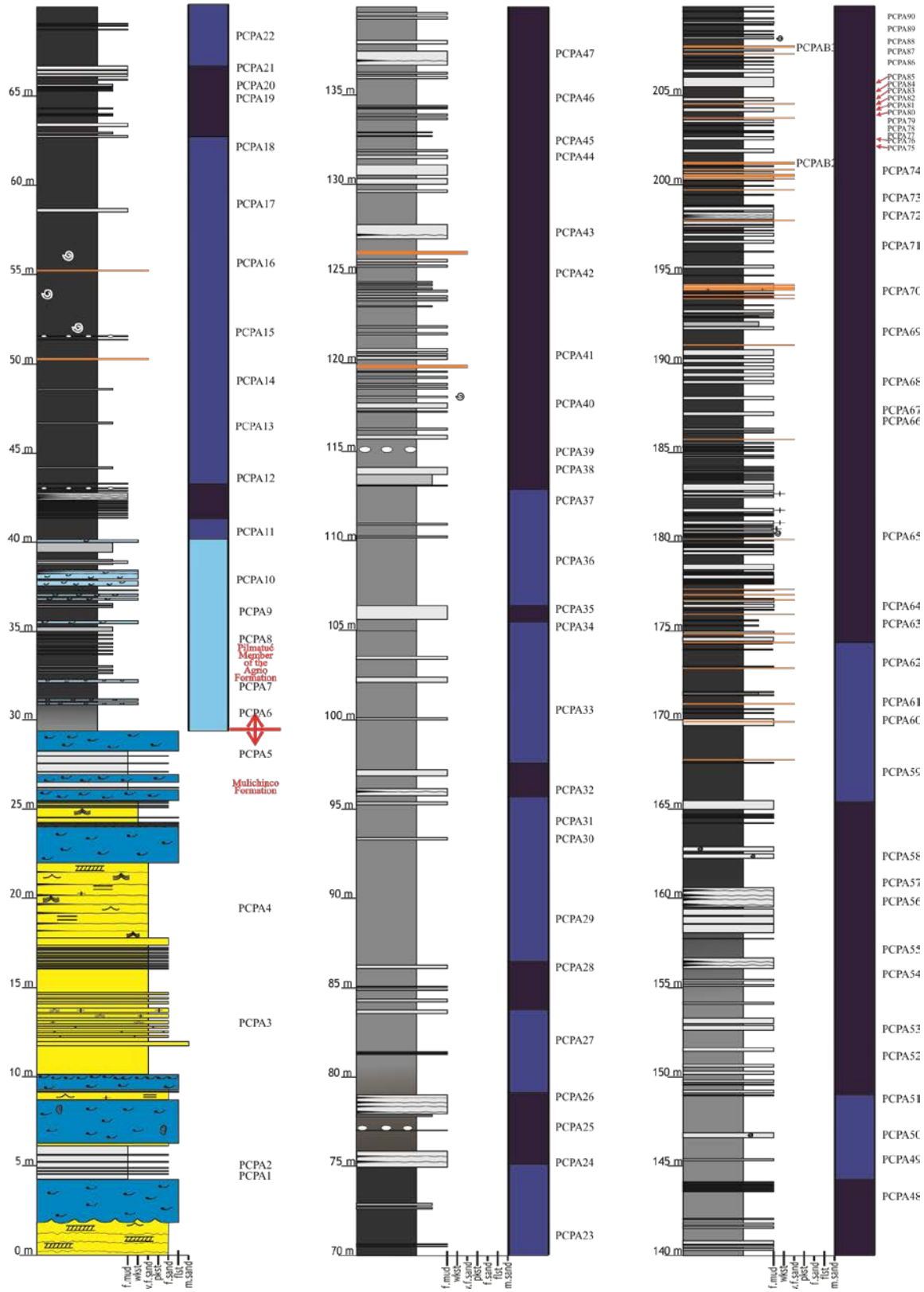

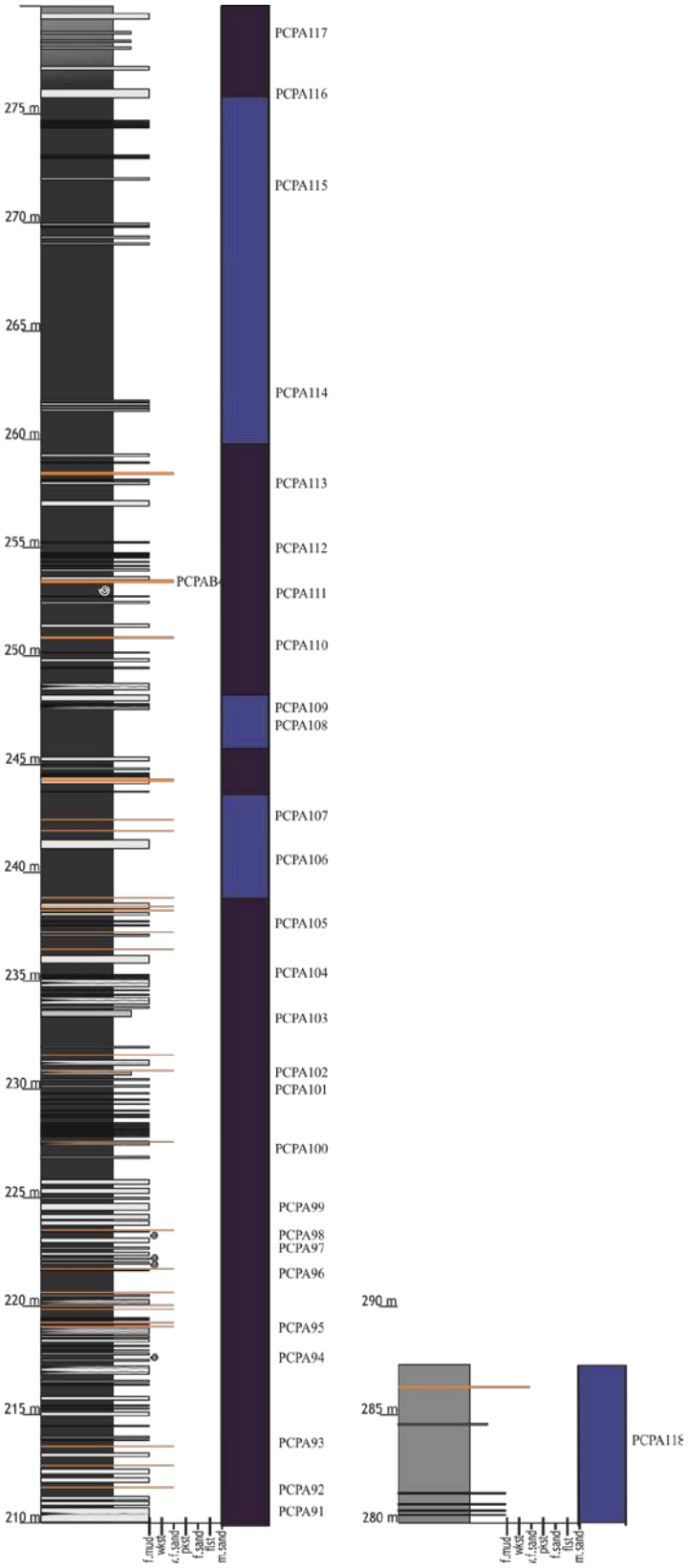
PCPA117
PCPA116
PCPA115
PCPA114
PCPA113
PCPA112
PCPA111
PCPA110
PCPA109
PCPA108
PCPA107
PCPA106
PCPA105
PCPA104
PCPA103
PCPA102
PCPA101
PCPA100
PCPA99
PCPA98
PCPA97
PCPA96
PCPA95
PCPA94
PCPA93
PCPA92
PCPA91
PCPA118
275 m
270 m
265 m
260 m
255 m
250 m
245 m
240 m
235 m
230 m
225 m
220 m
215 m
210 m
290 m
285 m
280 m
f.mud
wkst
f.sand
pkst
f.sand
fist
m.sand

APPENDIX C

DRAFTED MEASURED SECTION FROM

THE PUESTO CHIVITO LOCALITY

Appendix C- Puesto Chivito A - Pilmatué and Avilé Member

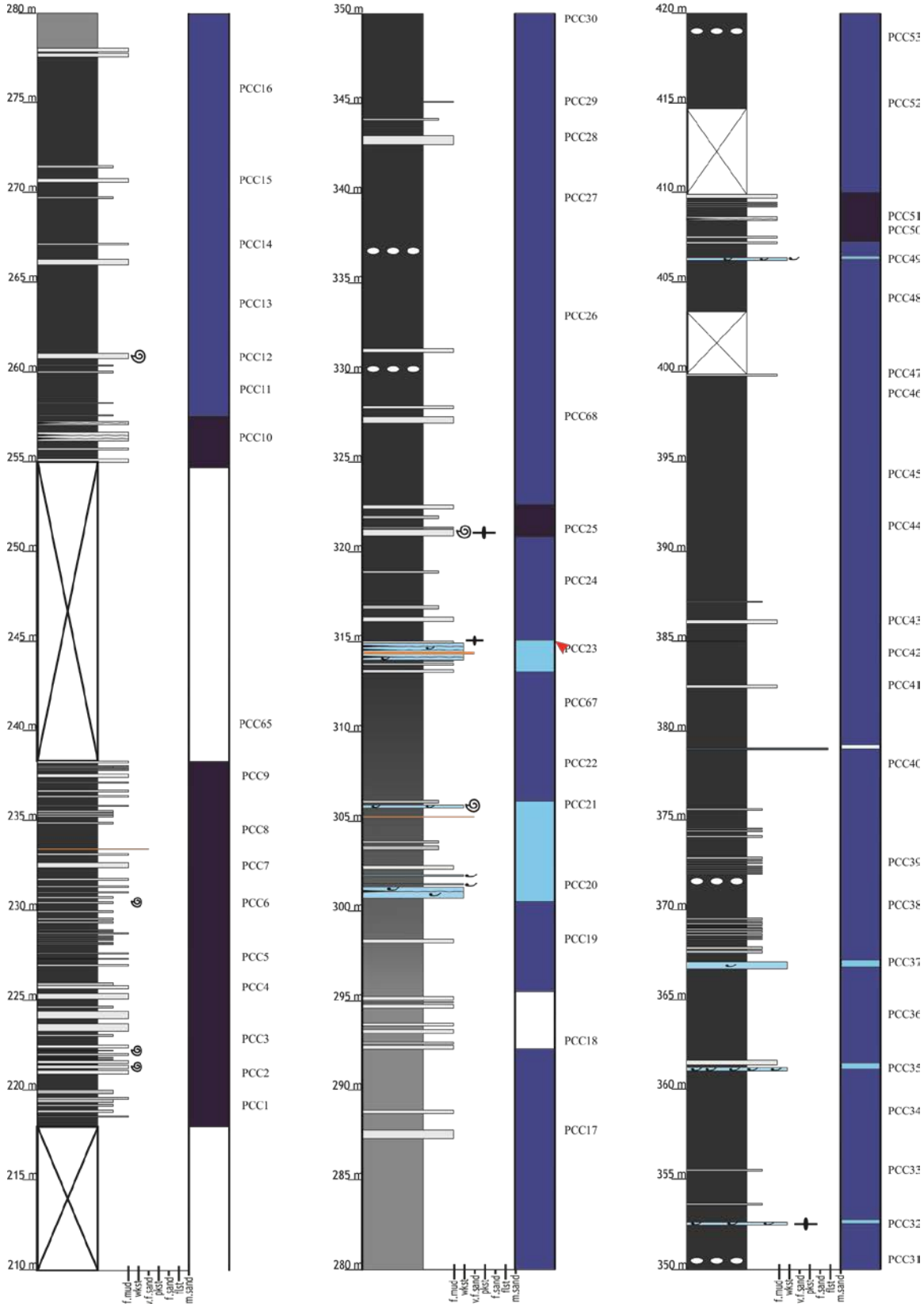

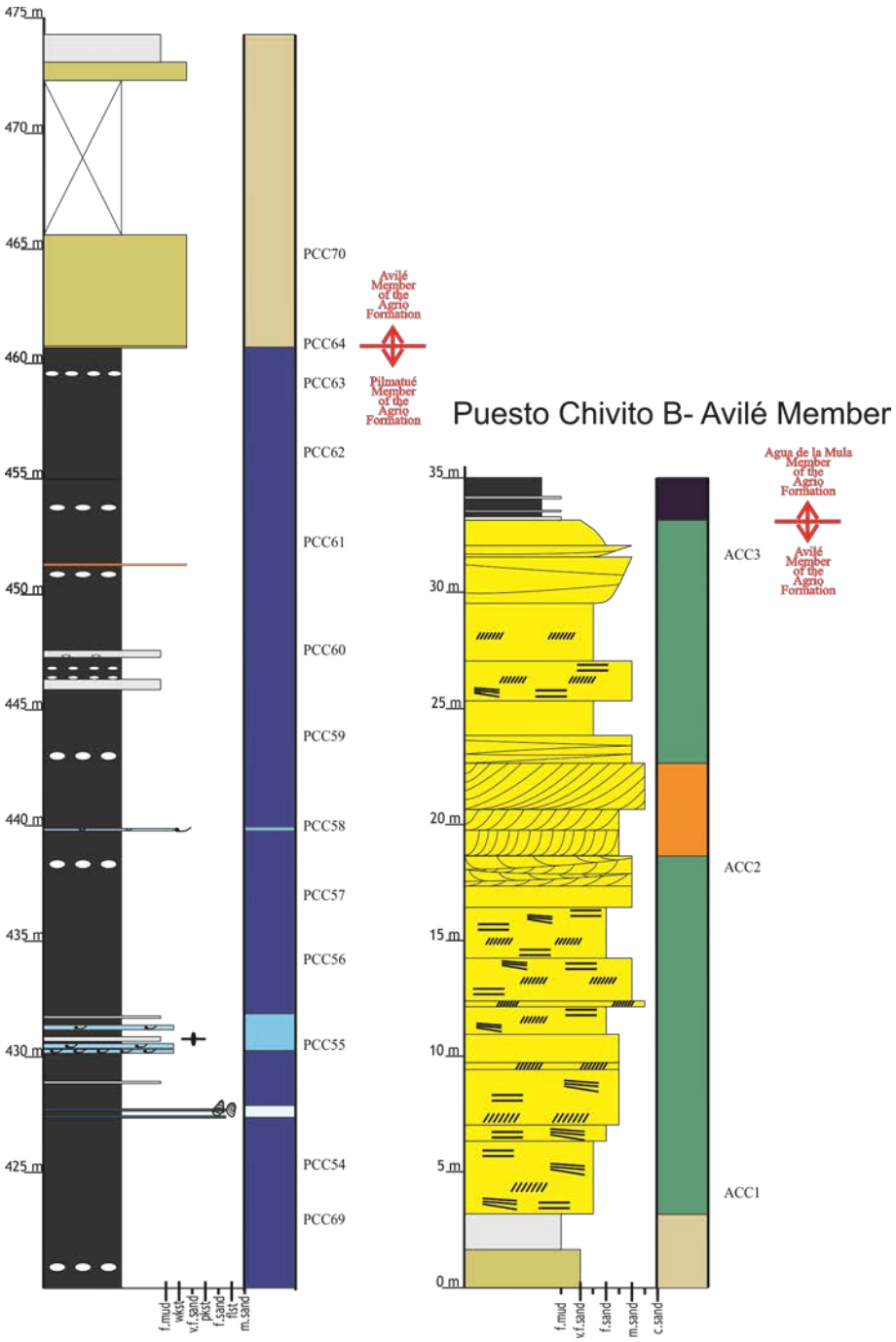
Puesto Chivito B- Avilé Member
475 m
470 m
465 m
460 m
455 m
450 m
445 m
440 m
435 m
430 m
425 m
PCC70
PCC64
PCC63
PCC62
PCC61
PCC60
PCC59
PCC58
PCC57
PCC56
PCC55
PCC54
PCC69
Avilé Member of the Agrio Formation
Pilmatué Member of the Agrio Formation
f.mud
wkst
v.f.sand
pkst
f.sand
flst
m.sand
35 m
30 m
25 m
20 m
15 m
10 m
5 m
0 m
ACC3
ACC2
ACC1
Agua de la Mula Member of the Agrio Formation
Avilé Member of the Agrio Formation
f.mud
v.f.sand
f.sand
m.sand
c.sand

APPENDIX D

SEDIMENTARY FACIES AND PROCESSES CONTINUED

Facies 5: Calcareous Intraclastic Packstone

Calcareous intraclastic packstone, facies 5, is relatively rare and is only observed at El Portón. In outcrop, it is tabular, laterally continuous, and moderately thinly bedded (~0.4 m) with a flaggy laminar appearance (Fig. 21a, b). On the tops of beds round, densely packed sand-sized "grains" are observed. No shell material or trace fossils are visible in outcrop.

Thin section analysis (*n = 2*) indicates that the round "grains" seen in outcrop are micritic intraclasts (Fig. 21c). The intraclastic grain fraction accounts for ~40% of this sample with ~20% of the sample consisting of the nonintraclastic grain fraction. These intraclasts are micritic, without any distinguishable internal grains. Compaction of these grains resulted in a lenticular laminated texture (Lazar et al. 2015) with fine organic rich deformed laminations between intraclasts (Fig. 21c). The nonintraclastic grain fraction is dominated by micro- and macrofossil scale shell material, foraminifera (possibly agglutinated), and to a much lesser degree radiolaria and detrital silt. All bioclastic and biogenic material has been recrystallized or replaced by drusy and/or blocky spar calcite cement, possibly through aggrading neomorphism.

An XRD analysis of three samples of facies 5 indicates that the matrix of this facies is composed primarily of calcite with very minor detrital illite (Fig. 22). On average clay minerals, feldspars and silica account for only ~16 % of facies 5 (Fig. 22). Very minor amounts of dolomite are present (Fig. 22). Programmed pyrolysis results of two samples of facies 5 show an average TOC content of 1.66 wt.%, an average S2 value of 8.73 mg HC/g rock, an average HI value of 526 mg HC/g TOC, and an average OI value of 12 mg CO_2/g TOC. Kerogen type of facies 5 is Type II based on the HI and OI values.

The micritic intraclasts present in facies 5 bear some similarities to shale lithics, as described by Schieber (2016), which can be transported into the offshore marine environment from eroded subaerially exposed lithified mudstone. However, a coupled decrease in both siliciclastic and shell material within the intraclastic packstone facies indicates a decrease in the offshore transport or a distal depositional position. This suggests that the micritic intraclasts are likely basinally derived, which is supported by the high degree of compaction that would not likely occur to fully lithified shale lithics. Intraclasts likely originated from subaqueous erosion and redistribution of rapidly stabilized offshore to basinal carbonate mudstone deposits (Lazar et al. 2015; Schieber 2016). These erosive beds could be related to energetic transgressive events or ravinement surfaces and are likely the distal equivalents of the bioclastic transgressive lags described by Schwarz et al. (2018).

Facies 6: Calcareous Floatstone

Calcareous floatstone, facies 6, is the most minor facies and is only observed as several beds in the upper portion of the Pilmatué Member at Puesto Chivito. In outcrop it is semiresistant, laterally discontinuous over more than 10 m, and thinly bedded (0.05-0.15 m). It contains both abundant shell hash material (mm-5cm scale bivalve and gastropods) and large, in some cases intact, bivalve shells that are both articulated and disarticulated (Fig. 21d, e). Further XRD, programmed pyrolysis and thin section analyses were not conducted due to rare occurrence of this facies.

The rarity and lack of lateral continuity of these beds indicates that they likely represent isolated and localized bioherms. The presence of large invertebrate benthic colonization in the floatstone facies indicates an oxygen rich environment and articulated shells suggest deposition likely occurred at least below fairweather wave base, but perhaps also likely below storm wave base.

Facies 7: Tuff

Very fine grained pyroclastic ash, or tuff, beds occur in varying abundance throughout the Agrio Formation. In outcrop, they are commonly friable, thinly bedded (0.01-0.15 m) with an orange-ish weathering expression (Fig. 21b). They are commonly heavily altered by gypsum. This facies represents distal ash fall from the active magmatic arc to the west and can be found in any depositional environment described herein. No sedimentary structures are viable in outcrop, which may indicate these deposits settled out of suspension, or that diagenesis and compaction have destroyed any evidence of reworking.

Figure 21. Examples of key feature in facies 5 (Intraclastic packstone) and facies 6 (Calcareous floatstone). (A) Outcrop of a rare facies 5 bed. Beds of facies 1 and 2 are also shown for contrast in weathering pattern. Ruler is 1.4 m. (B) Close up view of facies 5 in outcrop. (C) Facies 5 showing compacted intraclasts *(IC)*. (D) Whole shells in an isolated patch of floatstone. (E) Shell fragments and smaller articulated and disarticulated shells.

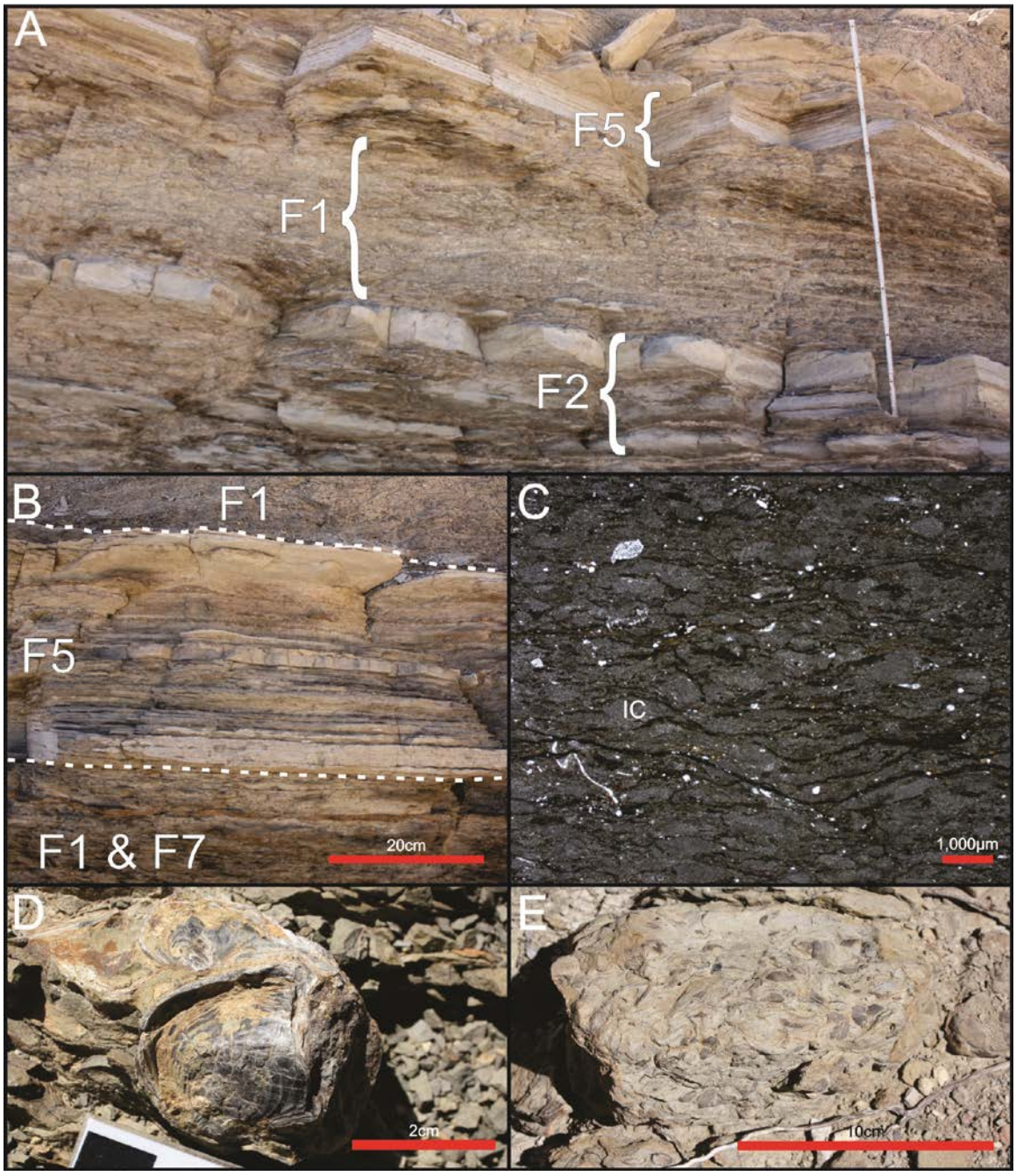
A
F5
F1
F2
B
F1
F5
F1 & F7
20cm
C
IC
1,000µm
D
2cm
E
10cm

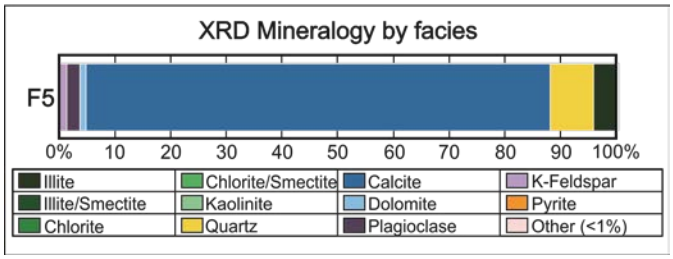

Figure 22. Mineralogy of facies 5 based on X-ray diffraction.

REFERENCES

Aguirre-Urreta, M.B., and Rawson, P.F., 1997, The ammonite sequence in the Agrio Formation (Lower Cretaceous), Neuquén Basin, Argentina: Geological Magazine, v. 134, no. 4, p. 449–458.

Aguirre-Urreta, M.B., Concheyro, A., Lorenzo, M., Ottone, E.G., and Rawson, P.F., 1999, Advances in the biostratigraphy of the Agrio Formation (Lower Cretaceous) of the Neuquén Basin, Argentina: ammonites, palynomorphs, and calcareous nannofossils: Palaeogeography, Palaeoclimatology, Palaeoecology, v. 150, p. 33–47, doi:10.1016/S0031-0182(99)00006-1.

Aguirre-Urreta, M.B., Rawson, P.F., Concheyro, G.A., Bown, P.R., and Ottone, E.G., 2005, Lower Cretaceous (Barriasian-Aptian) biostratigraphy of the Neuquén Basin, *in* Veiga, G.D., Spalletti, L.A., Howell, J.A., and Schwarz, E., eds., The Neuquen Basin , Argentina: A Case Study in Sequence Stratigraphy and Basin Dynamics: Geological Society, London, Special Pubications, 252, p. 57–81.

Aguirre-Urreta, M.B., Price, G.D., Ruffell, A.H., Lazo, D.G., Kalin, R.M., Ogle, N., and Rawson, P.F., 2008, Southern Hemisphere Early Cretaceous (Valanginian-Early Barremian) carbon and oxygen isotope curves from the Neuquén Basin, Argentina: Cretaceous Research, v. 29, p. 87–99.

Aguirre-Urreta, M.B., Lescano, M., Schmitz, M.D., Tunik, M., Concheyro, A., Rawson, P. F., and Ramos, V.A., 2015, Filling the gap: new precise Early Cretaceous radioisotopic ages from the Andes: Geological Magazine, v. 152, no. 3, p. 557–564, doi:10.1017/S001675681400082X.

Aguirre-Urreta, M.B., Schmitz, M., Lescano, M., Tunik, M., Rawson, P.F., Concheyro, A., Buhler, M., and Ramos, V.A., 2017, A high precision U–Pb radioisotopic age for the Agrio Formation, Neuquén Basin, Argentina: implications for the chronology of the Hauterivian Stage: Cretaceous Research, v. 75, p. 193–204, doi:10.1016/j.cretres.2017.03.027.

Allen, P.A., and Allen, J.R., 2013, Basin analaysis: principles and applications to petroleum play assesment: West Sussex, UK, Wiley-Blackwell.

Aplin, A.C., and Macquaker, J.H.S., 2011, Mudstone diversity: origin and implications for source, seal, and reservoir properties in petroleum systems: AAPG Bulletin, v. 95, no. 12, p. 2031–2059, doi:10.1306/03281110162.

Betzler, C., Lüdmann, T., Hübscher, C., and Fürstenau, J., 2013, Current and sea-level signals in periplatform ooze (Neogene, Maldives, Indian Ocean): Sedimentary Geology, v. 290, p. 126–137, doi:10.1016/j.sedgeo.2013.03.011.

Betzler, C., Lindhorst, S., Eberli, G.P., Lüdmann, T., Möbius, J., Ludwig, J., Schutter, I., Wunsch, M., Reijmer,J.J.G., and Hübscher, C., 2014, Periplatform drift: the combined result of contour current and off-bank transport along carbonate platforms: Geology, v. 42, no. 10, p. 871–874, doi:10.1130/G35900.1.

Bhattacharya, J.P., and MacEachern, J.A., 2009, Hyperpycnal rivers and prodeltaic shelves in the Cretaceous Seaway of North America: Journal of Sedimentary Research, v. 79, p. 184–209.

Birgenheier, L.P., Frank, T. D., Fielding, C.R., and Rygel, M.C., 2010, Coupled carbon isotopic and sedimentological records from the Permian system of eastern Australia reveal the response of atmospheric carbon dioxide to glacial growth and decay during the late Palaeozoic Ice Age: Palaeogeography, Palaeoclimatology, Palaeoecology, v. 286, no. 3–4, p. 178–193, doi:10.1016/j.palaeo.2010.01.008.

Birgenheier, L.P., Horton, B., Mccauley, A.D., Johnson, C.L., and Kennedy, A., 2017, A depositional model for offshore deposits of the lower Blue Gate Member, Mancos Shale, Uinta Basin, Utah, USA: Sedimentology, v. 64, p. 1402–1438, doi:10.1111/sed.12359.

Bornemann, A., Aschwer, U., and Mutterlose, J., 2003, The impact of calcareous nannofossils on the pelagic carbonate accumulation across the Jurassic-Cretaceous boundary: Palaeogeography, Palaeoclimatology, Palaeoecology, v. 199, p. 187–228, doi:10.1016/S0031-0182(03)00507-8.

Breyer, J.A., 2016, The Eagle Ford Shale: a renaissance in U.S. oil production: AAPG Memoir, 1-389 p.

Burchette, T.P., and Wright, V.P., 1992, Carbonate ramp depositional systems: Sedimentary Geology, v. 79, p. 3–57.

Calvert, S.E., Bustin, R.M., and Ingall, E.D., 1996, Influence of water column anoxia and sediment supply on the burial and preservation of organic carbon in marine shales: Geochimica et Cosmochimica Acta, v. 60, p. 1577–1593.

Comerio, M., Fernández, D.E., and Pazos, P.J., 2018, Sedimentological and ichnological characterization of muddy storm related deposits: the upper Hauterivian ramp of the Agrio Formation in the Neuquén Basin, Argentina: Cretaceous Research, v. 85, p. 78–94, doi:10.1016/j.cretres.2017.11.024.

Cruz, C.E., Villar, H.J., and Muñoz, G.E., 1996, Los sistemas petroleros del Groupo Mendoza en la fosa de Chos Malal, *in* XII Congreso Geológico Argentino y III Congreso de Exploración de Hidrocarburos, Actas I,: p. 45–60.

Cruz, C.E., Kozlowsky, E., and Villar, H.J., 1998, Agrio (Neocomian) petroleum systems: main target in the Neuquén Bain Thrust Belt, Argentina, *in* Mello, M.R., and Yilmaz, P.O., eds., AAPG International Confrence and Exhibition, Rio de janeiro, November 1998. Extended Abstracts: p. 670–671.

Decelles, P.G., Ducea, M.N., Kapp, P., and Zandt, G., 2009, Cyclicity in Cordilleran orogenic systems: Nature Geoscience, v. 2, no. 4, p. 251–257, doi:10.1038/ngeo469.

Demaison, G.J., and Moore, G.T., 1980, Anoxic environments and oil source bed genesis: AAPG Bulletin, v. 64, p. 1179–1209.

Denommee, K.C., Bentley, S.J., Harazim, D., and Macquaker, J.H.S., 2016, Hydrodynamic controls on muddy sedimentary-fabric development on the sothwest Louisiana subaqueous delta: Marine Geology, v. 382, p. 162–175.

Dunham, R.J., 1962, Classification of carbonate rocks according to depositional texture, *in* W. E. Ham, ed., Classification of Carbonate Rocks: AAPG Memoir, p. 108–121.

Egenhoff, S.O., and Fishman, N.S., 2013, Traces in the dark: sedimentary processes and facies gradients in the upper shale member of the Upper Devonian-Lower Mississippian Nakken Formation, Williston Basin, North Dakota, U.S.A.: Journal of Sedimentary Research, v. 83, p. 803–824.

Eldrett, J.S., Ma, C., Bergman, S.C., Ozkan, A., Minisini, D., Lutz, B., Jackett, S.J., Macaulay, C., and Kelly, A.E., 2015, Origin of limestone-marlstone cycles: astronomic forcing of organic-rich sedimentary rocks from the Cenomanian to Early Coniacian of the Cretaceous Western Interior Seaway, USA: Earth and Planetary Science Letters, v. 423, p. 98–113, doi:10.1016/j.epsl.2015.04.026.

Fairbanks, M.D., Ruppel, S.C., and Rowe, H., 2016, High-resolution stratigraphy and facies architecture of the Upper Cretaceous (Cenomanian–Turonian) Eagle Ford Group, central Texas: AAPG Bulletin, v. 100, no. 3, p. 379–403, doi:10.1306/12071514187.

Forster, A., Kuypers, M.M.M., Turgeon, S.C., Brumsack, H., Rose, M., and Sinninghe Damasté, J. S., 2008, The Cenomanian / Turonian oceanic anoxic event in the South Atlantic : new insights from a geochemical study of DSDP Site 530A: Palaeogeography, Palaeoclimatology, Palaeoecology, v. 267, p. 256–283, doi:10.1016/j.palaeo.2008.07.006.

Frébourg, G., Ruppel, S.C., Loucks, R.G., and Lambert, J., 2016, Depositional controls on sediment body architecture in the Eagle Ford/Boquillas system: insights from outcrops in west Texas, United States: AAPG Bulletin, v. 100, no. 4, p. 657–682, doi:10.1306/12091515101.

Gabbott, S.E., Zalasiewicz, J.A., Aldridge, R.J., and Theron, N., 2010, Eolian input into the Late Ordovician postglacial Soom Shale, South Africa: Geology, v. 38, no. 12, p. 1103–1106.

He, B., Xu, Y.G., Chung, S.L, Xiao, L., and Wang, Y., 2003, Sedimentary evidence for a rapid, kilometer-scale crustal doming prior to the eruption of the Emeishan flood basalts: Earth and Planetary Science Letters, v. 213, no. 3–4, p. 391–405, doi:10.1016/S0012-821X(03)00323-6.

Hoefs, M.J.L., Rijpstra, W.I.C., and Sinninghe Damasté, J.S., 2002, The influence of oxic degradation on the sedimentary biomarker record I: evidence from Madeira Abyssal Plain turbidites: Geochimica et Cosmochimica Acta, v. 66, p. 2719–2735.

Howell, J.A., Schwarz, E., Spalletti, L.A., and Veiga, G.D., 2005, The Neuquén Basin: an overview, *in* Veiga, G.D., Spalletti, L.A., Howell, J.A., and Schwarz, E., eds., The Neuquen Basin , Argentina: A Case Study in Sequence Stratigraphy and Basin Dynamics: Geological Society, London, Special Pubications, 252, p. 1–14.

Immenhauser, A., 2009, Estimating palaeo-water depth from the physical rock record: Earth-Science Reviews, v. 96, no. 1–2, p. 107–139, doi:10.1016/j.earscirev.2009.06.003.

Ingall, E.D., Bustin, R.M., and Van Cappellen, P., 1993, Influence of water column anoxia on the burial and preservation of carbon and phosphorus in marine shales: Geochimica et Cosmochimica Acta, v. 57, p. 303–316.

Kidder, D.L., and Worsley, T.R., 2010, Phanerozoic Large Igneous Provinces (LIPs), HEATT (Haline Euxinic Acidic Thermal Transgression) episodes, and mass extinctions: Palaeogeography, Palaeoclimatology, Palaeoecology, v. 295, no. 1–2, p. 162–191, doi:10.1016/j.palaeo.2010.05.036.

Kietzmann, D.A., Palma, R.M., Riccardi, A.C., Martín-Chivelet, J., and López-Gómez, J., 2014, Sedimentology and sequence stratigraphy of a Tithonian-Valanginian carbonate ramp (Vaca Muerta Formation): a misunderstood exceptional source rock in the Southern Mendoza area of the Neuquén Basin, Argentina: Sedimentary Geology, v. 302, p. 64–86, doi:10.1016/j.sedgeo.2014.01.002.

Kietzmann, D.A., Ambrosio, A.L., Suriano, J., Alonso, S., Gonz, F., Depine, G., and Repol, D., 2016, The Vaca Muerta – Quintuco system (Tithonian – Valanginian) in the Neuquén Basin, Argentina: a view from the outcrops in the Chos Malal fold and thrust belt: AAPG Bulletin, v. 5, no. 5, p. 743–771, doi:10.1306/02101615121.

Kozlowsky, E., Cruz, C.E., and Sylwan, C., 1998, Modelo exploratorio en la faja corrida da la Cuenca Neuqina, Argentina: Boletin de Informaciones Petroleras, v. 55, p. 4–23.

Lazar, O.R., Bohacs, K.M., Macquaker, J.H.S., Schieber, J., and Demko, T.M., 2015, Capturing key attributes of fine-grained sedimentary rocks in outcrops, cores, and thin sections: nomenclature and description guidelines: Journal of Sedimentary Research, v. 85, p. 230–246.

Lazo, D.G., 2004, Análisis de concentraciones fósiles del Cretácico Inferior de la Cuenca Neuquina: Universidad de Buenos Aires.

Lazo, D.G., 2006, Análisis tafonómico e inferencia del grado de mezcla temporal y espacial de la macrofauna del Miembro Pilmatué de la Formación Agrio, Cretácico Inferior de Cuenca Neuquina, Argentina: Ameghiniana, v. 43.

Lazo, D.G., 2007a, Análisis de biofacies y cambios relativos del nivel del mar en el Miembro Pilmatué de la Formación Agrio, Cretácico Inferior de cuenca Neuquina, Argentina: Ameghiniana, v. 44, p. 73–89.

Lazo, D.G., 2007b, Early Cretaceous bivalves of the Neuquén Basin, west-central Argentina: notes on taxonomy, palaeobiogeography and palaeoecology: Geological Journal, v. 42, p. 127–142, doi:10.1002/gj.1080.

Lazo, D.G., Cichowolski, M., Rodríguez, D.L., and Aguirre-Urreta, M.B., 2005, Lithofacies, palaeoecology and palaeoenvironments of the Agrio Formation, Lower Cretaceous of the Neuquén Basin, Argentina, *in* Veiga, G.D., Spalletti, L.A., Howell, J.A., and Schwarz, E., eds., The Neuquen Basin, Argentina: A Case Study in Sequence Stratigraphy and Basin Dynamics: Geological Society, London, Special Pubications, 252, p. 295–315, doi:10.1144/GSL.SP.2005.252.01.15.

Lazo, D.G., Aguirre-Urreta, M.B., Price, G.D., Rawson, P.F., Ruffell, A.H., and Ogle, N., 2008, Palaeosalinity variations in the Early Cretaceous of the Neuquén Basin, Argentina: evidence from oxygen isotopes and palaeoecological analysis: Palaeogeography, Palaeoclimatology, Palaeoecology, v. 260, p. 477–493, doi:10.1016/j.palaeo.2007.12.008.

Leanza, H.A., Hugo, C.A., and Repol, D., 2001, Hoja Geológica 3969- I, Zapala, provincia del Neuquén: 128 p.

Legarreta, L., and Gulisano, C.A., 1989, Análisis estratigráfico secuencial de la Cuenca Neuquina (Triásico superior-Terciario inferior), *in* Chebli, G., and Spalletti, L.A., eds., Cuencas Sedimentarias Argentinas: Serie Correlación Geológica 6, p. 221–243.

Legarreta, L., and Uliana, M.A., 1991, Jurassic-Cretaceous marine oscillations and geometry of back-arc basin fill, central Argentine Andes: Spec. Pubis. int. Ass. Sediment, v. 12, p. 429–450.

Legarreta, L., and Uliana, M.A., 1999, El Jurásico y Cretácico de la Cordillera Principal y la Cuenca Neuquina., *in* R. Caminos, ed., Geología Argentina. Instituto de Geología y Recursos Minerales, Servicio Geológico Minero Argentino, Anales 29: Buenos Aires, Instituto de Geología y Recursos Minerales, Servicio Geológico Minero Argentino, Anales 29, p. 399–416.

Legarreta, L., and Villar, H.J., 2012, Las facies generadoras de hidrocarburos de la cuenca Neuquina: Petrotecnica, no. Agosto, p. 14–37.

Legarreta, L., Kozlowsky, E., and Bol, A., 1981, Esquema estratigráfico y distribución de facies del Grupo Mendoza en el ámbito surmendocino de la Cuenca Neuquina., *in* VIII Congr. Geol. Argentino III: p. 389–409.

Legarreta, L., Villar, H.J., Laffitte, G.A., Cruz, C.E., and Vergani, G., 2005, Cuenca Neuquina: balance de masa enfocado a la evaluación del potencial exploratorio de los distritos productivos y de las zonas no productivas, *in* VI Congreso de Exploración y Desarrollo de Hidrocarburos: Instituto Argentino del Petróleo y del Gas.

MacEachern, J.A., Pemberton, S.G., Gringras, M.K., and Bann, K.L., 2010, Ichnology and facies models, *in* James, N.P., and Dalrymple, R.W., eds., Facies Models 4: Geological Society of Canada, p. 19–58.

Macquaker, J.H.S., Taylor, K.G., and Gawthorpe, R.L., 2007, High-resolution facies analyses of mudstones: implications for paleoenvironmental and sequence stratigraphic interpretations of offshore ancient mud-dominated successions: Journal of Sedimentary Research, v. 77, p. 324–339, doi:10.2110/jsr.2007.029.

Macquaker, J.H.S., Bentley, S.J., and Bohacs, K.M., 2010a, Wave-enhanced sediment-gravity flows and mud dispersal across continental shelves: reappraising sediment transport processes operating in ancient mudstone successions: Geology, v. 38, no. 10, p. 947–950.

Macquaker, J.H.S., Keller, M.A., and Davies, S.J., 2010b, Algal blooms and “marine snow”: mechanisms that enhance preservation of organic carbon in ancient fine-grained sediments: Journal of Sedimentary Research, v. 80, p. 934–942, doi:http://doi.org/10.2110/jsr.2010.085.

Martinez, M., Pellenard, P., Deconinck, J.F., Monna, F., Riquier, L., Boulila, S., Moiroud, M., and Company, M., 2013, An orbital floating time scale of the Hauterivian/Barremian GSSP from a magnetic susceptibility signal (Río Argos, Spain): Cretaceous Research, v. 36, p. 106–115, doi:10.1016/j.cretres.2012.02.015.

Martinez, M., Deconinck, J.F., Pellenard, P., Riquier, L., Company, M., Reboulet, S., and Moiroud, M., 2015, Astrochronology of the Valanginian-Hauterivian stages (Early Cretaceous): chronological relationships between the Paraná-Etendeka large igneous province and the Weissert and the Faraoni events: Global and Planetary Change, v. 131, p. 158–173, doi:10.1016/j.gloplacha.2015.06.001.

McNeill, D.F., 2005, Accumulation rates from well-dated late Neogene carbonate platforms and margins: Sedimentary Geology, v. 175, no. 1–4 SPEC. ISS., p. 73–87, doi:10.1016/j.sedgeo.2004.12.032.

Minisini, D., Eldrett, J.S., Bergman, S.C., and Forkner, R., 2018, Chronostratigraphic framework and depositional environments in the organic-rich, mudstone dominated Eagle Ford Group, Texas, USA: Sedimentology, doi:10.1111/ijlh.12426.

Morris, J.E., Hampson, G.J., and Johnson, H.D., 2006, A sequence stratigraphic model for an intensely bioturbated shallow-marine sandstone: the Bridport Sand Formation, Wessex Basin, UK: Sedimentology, v. 53, p. 1229–1263.

Nawratil, A., Gomez, H., and Larriestra, C., 2012, Key tools for black shale evaluation: geostatistics and inorganic geochemistry applied to Vaca Muerta Formation, Neuquén Basin, Argentina, *in* Neuquen Basin, Argentina: AAPG Search and Discovery Article.

Neal, J., and Abreu, V., 2009, Sequence stratigraphy hierarchy and the accommodation succession method: Geology, v. 37, no. 9, p. 779–782, doi:10.1130/G25722A.1.

Nichols, G., 2009, Sedimentology and Stratigraphy: London, Blackwell Publishing Ltd., 419 p.

Pedersen, T.F., and Calvert, S.E., 1990, Anoxia vs. productivity: what controls the formation of organic-carbon-rich sediments and sedimentary rocks? AAPG Bulletin, v. 74, p. 454–466.

Pepper, A.S., and Corvi, P.J., 1995a, Simple kinetic models of petroleum formation. Part I: oil and gas generation from kerogen: Marine and Petroleum Geology, v. 12, no. 3, p. 291–319, doi:10.1016/0264-8172(95)98381-E.

Pepper, A.S., and Corvi, P.J., 1995b, Simple kinetic models of petroleum formation. Part III: modelling an open system: Marine and Petroleum Geology, v. 12, no. 4, p. 417–452, doi:10.1016/0264-8172(95)96904-5.

Pepper, A.S., and Dodd, T.A., 1995, Simple kinetic models of petroleum formation. Part II: oil-gas cracking: Marine and Petroleum Geology, v. 12, no. 3, p. 321–340, doi:10.1016/0264-8172(95)98382-F.

Peters, K.E., 1986, Guidelines for evaluating petroleum source rock using programmed pyrolysis: AAPG Bulletin, v. 70, p. 318–329.

Peters, K.E., and Casa, M.R., 1994, Applied source rock geochemistry, *in* Magoon, L.B., and Dow, W.G., eds., The Petroleum System – from Source to Trap: AAPG Memoir, p. 93–120.

Phelps, R.M., Kerans, C., Da-Gama, R.O.B.P., Jeremiah, J., Hull, D., and Loucks, R.G., 2015, Response and recovery of the Comanche carbonate platform surrounding multiple Cretaceous oceanic anoxic events, northern Gulf of Mexico: Cretaceous Research, v. 54, p. 117–144, doi:10.1016/j.cretres.2014.09.002.

Plint, A.G., Tyagi, A., Hay, M.J., Varban, B.L., Zhang, H., and Roca, X., 2009, Clinoforms, paleobathymetry, and mud dispersal across the Western Canada Cretaceous Foreland Basin: evidence from the Cenomanian Dunvegan Formation and Contiguous Strata: Journal of Sedimentary Research, v. 79, no. 3, p. 144–161, doi:10.2110/jsr.2009.020.

Ramos, V.A., and Folguera, A., 2005, Tectonic evolution of the Andes of Neuquén: constraints derived from the magmatic arc and foreland deformation, *in* Veiga, G.D., Spalletti, L.A., Howell, J.A., and Schwarz, E., eds., The Neuquen Basin, Argentina: A Case Study in Sequence Stratigraphy and Basin Dynamics: Geological Society, London, Special Pubications, 252, p. 15–35, doi:10.1144/GSL.SP.2005.252.01.02.

Rebesco, M., Hernández-molina, F.J., Van Rooij, D., and Wåhlin, A., 2014, Contourites and associated sediments controlled by deep-water circulation processes: state-of-the-art and future considerations: Marine Geology, v. 352, p. 111–154, doi:10.1016/j.margeo.2014.03.011.

Renne, P.R., Glen, J.M., Milner, S.C., and Duncan, A.R., 1996, Age of Etendeka flood volcanism and associated intrusions in southwestern Africa: Geology, v. 24, no. 7, p. 659–662, doi:10.1130/0091-7613(1996)024<0659:AOEFVA>2.3.CO;2.

Rossi, G.R., 2001, Arenisca Avilé: facies, ambientes sedimentarios y estratigrafía de una regresión forzada del Hauteriviano inferior de la Cuenca Neuquina: Universidad Nacional de La Plata.

Sagasti, G., 2002, Estudio sedimentológico y de estratigrafía secuencial de las sedimentitas carbonáticas de la Formación Agrio (Cretácico inferior), en el sector surmendocino de la cuenca Neuquina, República Argentina: Universidad Nacional de La Plata.

Sagasti, G., 2005, Hemipelagic record of orbitally-induced dilution cycles in Lower Cretaceous sediments of the Neuquén Basin, *in* Veiga, G.D., Spalletti, L.A., Howell, J.A., and Schwarz, E., eds., The Neuquén Basin, Argentina: A Case Study in Sequence Stratigraphy and Basin Dynamics: p. 231–250.

Sagasti, G., and Ballent, S., 2002, Caracterización microfaunística de una transgresión marina: Formatión Agrio (Cretácico Inferior), Cuenca Neuquina, Argentina: Geobios, v. 35, p. 721–734.

Sageman, B.B., Murphy, A.E., Werne, J.P., Ver Straeten, C.A., Hollander, D.J., and Lyons, T.W., 2003, A tale of shales: the relative roles of production, decomposition, and dilution in the accumulation of organic-rich strata, Middle-Upper Devonian, Appalachian basin: Chemical Geology, v. 195, p. 229–273, doi:10.1016/S0009-2541(02)00397-2.

Schieber, J., 2016, Mud re-distribution in epicontinental basins - exploring likely processes: Marine and Petroleum Geology, v. 71, p. 119–133.

Schieber, J., and Yawar, Z., 2009, New twist on mud deposition - mud ripples in experiment and rock record: The Sedimentary Record, v. 7, no. 2, p. 4–8, doi:10.1306/D4268AB8-2B26-11D7-8648000102C1865D.

Schieber, J., Southard, J., and Thaisen, K., 2007, Accretion migrating of mudstone floccule beds from ripples: v. 318, no. 5857, p. 1760–1763.

Schwarz, E., Spalletti, L.A., Veiga, G.D., and Fanning, C.M., 2016, First U-Pb SHRIMP age for the Pilmatué Member (Agrio Formation) of the Neuquén Basin, Argentina: implications for the Hauterivian lower boundary: Cretaceous Research, v. 58, p. 223–233, doi:10.1016/j.cretres.2015.10.003.

Schwarz, E., Veiga, G.D., Álvarez Trentini, G., Isla, M.F., and Spalletti, L.A., 2018, Expanding the spectrum of shallow-marine, mixed carbonate–siliciclastic systems: processes, facies distribution and depositional controls of a siliciclastic-dominated example: Sedimentology, doi:10.1111/sed.12438.

Sinninghe Damasté, J.S., Rijpstra, W.I.C., and Reichart, G.J., 2002, The influence of oxic degradation on the sedimentary biomarker record II. Evidence from Arabian Sea sediments: Geochimica et Cosmochimica Acta, v. 66, p. 2737–2754.

Slatt, R.M., and Rodriguez, N.D., 2012, Comparative sequence stratigraphy and organic geochemistry of gas shales: commonality or coincidence? Journal of Natural Gas Science and Engineering, v. 8, p. 68–84, doi:10.1016/j.jngse.2012.01.008.

Sømme, T.O., Helland-Hansen, W., and Granjeon, D., 2009, Impact of eustatic amplitude variations on shelf morphology, sediment dispersal, and sequence stratigraphic interpretation: icehouse versus greenhouse systems: Geology, v. 37, no. 7, p. 587–590, doi:10.1130/G25511A.1.

Sonnenberg, S.A., 2011, The Niobrara petroleum system: a new resource play in the Rocky Mountain Region, *in* Estes-Jackson, J.E., and Anderson, D.S., eds., Revisiting and Revitalizing the Niobrara in the Central Rockies: Denver Co, The Rocky Mountain Association of Geologists, p. 13–32.

Spalletti, L., Poiré, D.G., Pirrie, D., Matheos, S., and Doyle, P., 2001a, Respuesta sedimentológica a cambios de nivel de base en una secuencia mixta clástica – carbonática del Cretácico de la Cuenca Neuquina, Argentina: Revista de la Sociedad Geológica de España, v. 14, p. 57–74.

Spalletti, L.A., Poiré, D.G., Schwarz, E., and Veiga, G.D., 2001b, Sedimentologic and sequence stratigraphic model of a Neocomian marine carbonate-siliciclastic ramp: Neuquén Basin, Argentina: Journal of South American Earth Sciences, v. 14, no. 6, p. 609–624, doi:10.1016/S0895-9811(01)00039-6.

Spalletti, L.A., Veiga, G.D., and Schwarz, E., 2011, La Formación Agrio (Cretácico Temprano) en la Cuenca Neuquina, *in* Leanza, H.A., Arregui, C., Carbone, O., Danieli, J.C., and Vallés, J.M., eds., Geología y Recursos Naturales de la Provincia del Neuquén: Relatorio del XVIII Congreso Geológico Argentino, p. 145–160.

Stinco, L.P., and Barredo, S., 2014, Vaca Muerta Formation: an example of shale heterogeneities controlling hydrocarbon accumulations: Society of Petroleum Engineers, doi:10.15530/urtec-2014-1922563.

Stow, D.A., Faugéres, J.C., Howe, J.A., Pudsey, C.J., and Viana, A.R., 2002, Bottom currents, contourites and deep-sea sediment drifts: current state-of-the-art, *in* Stow, D.A., Pudsey, C.J., Howe, J.A., Faugéres, J.C., and Viana, A.R., eds., Deep-water Contourite Systems: Modern Drifts and Ancient Series, Seismic and Sedimentary Characteristics: Geological Society of London Memoirs, p. 7–20.

Taylor, A.M., and Goldring, R., 1993, Description and analysis of bioturbation and ichnofabric: Journal of the Geological Society, v. 150, p. 141–148.

Taylor, J., and Sonnenberg, S.A., 2013, Reservoir characterization of the Niobrara Formation, southern Powder River Basin, Wyoming: The Mountain Geologist, v. 51, no. 1, p. 83–108.

Tunik, M.A., Pazos, P.J., Impiccini, A., Lazo, D.G., and Aguirre-Urreta, M.B., 2009, Dolomitized tidal cycles in the Agua de la Mula Member of the Agrio Formation (Lower Cretaceous), Neuquén Basin, Argentina: Latin American Journal of Sedimentology and Basin Analysis, v. 16, p. 29–43.

Tyson, R.V., 2001, Sedimentation rate, dilution, preservation and total organic carbon: some results of a modeling study: Organic Geochemistry, v. 32, p. 333–339.

Tyson, R.V., and Pearson, T.H., 1991, Modern and ancient continental shelf anoxia: an overview, *in* Tyson, R.V., and Pearson, T.H., eds., Modern and Ancient Continental Shelf Anoxia: Geological Society Special Publication, p. 1–24.

Tyson, R.V., Esherwood, P., and Pattison, K.A., 2005, Organic facies variations in the Valanginian--Mid-Hauterivian interval of the Agrio Formation (Chos Malal area, Neuquén, Argentina): local significance and global context, *in* Veiga, G.D., Spalletti, L.A., Howell, J.A., and Schwarz, E., eds., The Neuquén Basin: a Case Study in Sequence Stratigraphy and Basin Dynamics: Geological Society of London, Special Publications, p. 251–266.

Uliana, M.A., and Legarreta, L., 1993, Hydrocarbons habitat in a Triassic-to-Cretaceous sub-Andean setting: Neuquén Basin, Argentina: Journal of Petroleum Geology, v. 16, no. 4, p. 397–420.

Uliana, M.A., Legarreta, L., Laffitte, G.A., and Villar, H.J., 1999, Estratigrafía y geoquímica de las facies generadoras de hidrocarburos en las cuencas petrolíferas de Argentina, *in* IV Congreso de Exploración y Desarollo de Hidrocarburos: p. 1–61.

Urien, C.M., and Zambrano, J.J., 1994, Petroleum systems in the Neuquén Basin, Argentina, *in* Magoon, L.B., and Dow, W.G., eds., The Petroleum System–from Source to Trap: AAPG Memoir 60, p. 513–535.

Urien, C.M., Zambrano, J.J., and Yrigoyen, M.R., 1995, Petroleum basins of southern South America: an overview, *in* Tankard. A.J., Suárez R.S., and Welsink, H.J, eds., Petroleum Basins of South America: AAPG Memoir 62, p. 63–77.

U.S. Energy Information Administration (EIA), 2017, Annual Energy Outlook 2017, U.S. Energy Information Administration: Washington, DC, https://www.eia.gov/outlooks/aeo/, 11/13/2017.

Van Dongen, B.E., Schouten, S., and Sinninghe Damasté, J.S., 2006, Preservation of carbohydrates through sulfurization in a Jurassic euxinic shelf sea: examination of the Blackstone Band TOC cycle in the Kimmeridge Clay Formation, UK: Organic Geochemistry, v. 37, p. 1052–1073.

Veiga, G.D., and Vergani, G.D., 1993, Depósitos de nivel bajo: nuevo enfoque sedimentológico y estratigráfico del Miembro Avilé en el Norte del Neuquén, Argentina, *in* V. A. Ramos, ed., XII Congreso Geológico Argentino y II Congreso de Exploración de Hidrocarburos, Actas I,: p. 55–65

Veiga, G. D., and E. Schwarz, 2017, Facies characterization and sequential evolution of an ancient offshore dunefield in a semi-enclosed sea: Neuquén Basin, Argentina: Geo-Marine Letters, no. 37, p. 411–426, doi:10.1007/s00367-016-0467-1.

Veiga, G.D., Spalletti, L.A., and Flint, S., 2002, Aeolian/fluvial interactions and high-resolution sequence stratigraphy of a non-marine lowstand wedge: the Avilé Member of the Agrio Formation (Lower Cretaceous), central Neuquén Basin, Argentina: Sedimentology, v. 49, p. 1001–1019.

Veiga, G.D., Howell, J.A., and Strömbäck, A., 2005, Anatomy of a mixed marine/non-marine lowstand wedge in a ramp setting. The record of a Barremian/Aptian complex relative sea-level fall in Central Neuquén Basin, Argentina, *in* Veiga, G.D., Spalletti, L.A., Howell, J.A., and Schwarz, E., eds., The Neuquén Basin: a Case Study in Sequence Stratigraphy and Basin Dynamics: Geological Society of London, Special Publications, p. 139–162.

Veiga, G.D., Spalletti, L.A., and Flint, S.S., 2007, Anatomy of a fluvial lowstand wedge: the Avilé Member of the Agrio Formation (Hauterivian) in central Neuquén Basin (NW Neuquén province), Argentina, *in* Nichols, G., Williams, E., and Paola, C., eds., Sedimentary Environments, Processes and Basins. A tribute to Peter Friend: Special Publication International Association of Sedimentologists, p. 341–365.

Veiga, G.D., Spalletti, L.A., and Schwarz, E., 2011, El Miembro Avilé de la Formación Agrio (Cretácico Temprano), *in* Leanza, H.A., Arregui, C., Carbone, O., Danieli, J.C., and Vallés, J.M., eds., Geología y Recursos Naturales de la Provincia del Neuquén: Relatorio del XVIII Congreso Geológico Argentino, p. 161–173.

Vergani, G.D., Tankard, A.J., Belotti, H.J., and Welsink, H.J., 1995, Tectonic evolution and paleogeography of the Neuquén Basin, Argentina, *in* Tankard. A.J., Suárez R.S., and Welsink, H.J, eds., Petroleum Basins of South America: AAPG Memoir 62, p. 383–402.

Villar, H.J., Laffitte, G.A., and Legarreta, L., 1998, The source rocks of the Mesozoic petroleum systems of Argentina: a comparative overview on their geochemistry,

paleoenvironments and hydrocarbon generation patterns (abs.): International Congress and Exhibition of the AAPG and the Brazilian Association of Petroleum Geologists, p. 186–187.

Weaver, C.E., 1931, Paleontology of the Jurassic and Cretaceous of west central Argentina: Seattle, University of Washington, 1-469 p.

Werne, J.P., Sageman, B.B., Lyons, T.W., and Hollander, D.J., 2002, An integrated assessment of a “type euxinic” deposit: evidence for multiple controls on black shale deposition in the middle Devonian Oatka Creek Formation: American Journal of Science, v. 302, p. 110–143.

Wilson, R.D., and Schieber, J., 2014, Muddy prodeltaic hyperpycnites in the Lower Genesee Group of Central New York, USA: implications for mud transport in epicontinental seas: Journal of Sedimentary Research, v. 84, no. 10, p. 866–874, doi:10.2110/jsr.2014.70.

Zeller, M., Reid, S.B., Eberli, G.P., Weger, R.J., and Luis, J., 2015, Sequence architecture and heterogeneities of a field Scale Vaca Muerta analog (Neuquén Basin, Argentina)- from outcrop to synthetic seismic: Marine and Petroleum Geology, v. 66, p. 829–847, doi:10.1016/j.marpetgeo.2015.07.021.